Università degli Studi di Palermo

Dottorato di Ricerca in Scienze della Terra e del Mare
Dipartimento di Scienze della Terra e del Mare (DiSTeM)
Settore Scientifico Disciplinare CHIM/01

STUDY OF ACTIONS OF BIOPLASTIC MATERIALS ON MARINE MICROBIAL COMMUNITIES AND EFFECTS ON MARINE INVERTEBRATE ORGANISMS

LA DOTTORESSA
NICOLETTA TORREGROSSA

IL COORDINATORE
PROF. ALESSANDRO AIUPPA

LA TUTOR
PROF.SSA SALVATRICE VIZZINI

CO TUTOR
PROF.SSA DANIELA PIAZZESE
DOTT. DAVID GIRALDI
DOTT.SSA VALENTINA CATANIA

CICLO XXXVI
ANNO CONSEGUIMENTO TITOLO 2023

A me,
perché, guardandomi indietro,
osservo ammirata fin dove sono arrivata.
Guardando avanti, invece, vedo strade da
prendere e scelte da compiere.
Forse con fatica, come finora è stato,
o forse con un passo più leggero,
ma andrà bene.

N. Torregrossa

ABSTRACT

Bioplastics are nowadays widely considered as an alternative to conventional plastics of petrochemical origin. Considering the high growth rates estimated for their production in the coming years, we want to evaluate whether the environmental problem linked to conventional plastics is not shifting to bioplastics. To do this, we focused on the factors involved in the biodegradation processes of the latter within marine ecosystems, analyzing the two most widespread bio-based and biodegradable biopolymers today: polyhydroxyalkanoates (PHAs) and polylactic acids (PLA). The study of these bioplastics was carried out through the analysis of the bacterial communities constituting a biofilm known as Plastisphere, developed on the surfaces of the biopolymeric materials exposed in marine environment for different times, The research and identification of bacterial degradation products was performed by mass spectrometry analysis (MS). Morover, the possible interactions that the presence of biopolymer micro- and nanoparticles can determine on marine organisms was evaluated on bioindicator model organism *Mytilus galloprovincialis* by *in vitro* and *in vivo* exposure tests. To study the Plastisphere of biopolymers, porous bioplastic scaffolds produced by Thermally Induced Phase reversal process, were exposed in marine environment for 60 and 120 days. The composition of plastispheres was detected by Next Generation Sequencing of V3 and V4 hypervariable region of the 16S rDNA gene. The composition of bacterial communities was related to biodegradable biopolymer and the bacterial diversity was affected by exposition times. In general, the bacterial biomass decreases as time increases and was higher in Poly(DL-lactic Acid)/Poly(L-lactic Acid) (PDLLA/PLLA) scaffold. A high abundance of Proteobacteria was detected in all biopolymers, with Alpha and Gamma Proteobacteria dominant. High abundance of sequences assigned to hydrocarbon-degrading bacteria (i.e. *Oleibacter*, *Labrenzia Alcanivorax*) and genera associated with biopolymers was observed (*Maricaulis*, *Oceanicaulis*). The genus *Vibrio* was first detected associated with PLA bioplastic.

Tests carried out using minimal mineral media with biopolymer overlays allowed the identification of 5 potentially degrading bacterial strains, capable of growing in the presence of polyhydroxyalkanoate/polyhydroxybutyrate (PHA/PHB) as the sole carbon source, isolated from the plastisphere of scaffolds exposed in a marine habitat. The sequences were assigned to *Alcanivorax sp.* and *Labrenzia sp.* genera, suggesting a possible role in degradation of biopolymers. The products of bacterial biodegradation were studied by MS analysis and revealed the presence of products resulting from bacterial degradation of PLA, suggesting an active role of the marine plastisphere in PLA biodegradation. The presence of family and genera know to degrade PLA (belonging to the phyla Actinobacteria,

Proteobacteria, Bacteriodetes) detected by sequencing, confirms this hypothesis. The immunobiological investigations, applied here for the first time for the evaluation of the possible effects produced by bioplastics on marine organisms, have highlighted effects determined by exposure to PLA particles. In fact, the haemocytes showed reduced phagocytic activity, compared to an increase in enzymatic activities compared to the control both in the digestive gland sample and in the haemolymph sample. Furthermore, histological analysis of the digestive glands highlighted tissue damage and atrophy with enlargement of the glandular lumens and thinning of the epithelium lining them.

The work described here has highlighted actual critical points for the promising environmental compatibility of bioplastics for natural aquatic systems, since they appear to be similar in terms of behavior to plastics of fossil origin and lays the methodological foundations for an in-depth study of the bioplastics problem.

SUMMARY

LIST OF ABBREVIATIONS AND ACRONYMS

16S rRNA	16S Ribosomal ribonucleic acid
3HB	3-hydroxybutyrate
3HD	3-hydroxydecanoate
3HDD	3-hydroxydodecanoate
3HHx	3-hydroxyhexanoate
3HO	3-hydroxyoctanoate
3HV	3-hydroxyvalerate
4HB	4-hydroxybutyrate
ALP	Alkaline phosphatase assay
ANOVA	Analysis of Variance
AO	Acridine Orange Hydrochloride
ATR-FTIR	Attenuated total reflection- Fourier transform infrared spectroscopy
BSA	Bovine Serum Albumin
CFU	Colony forming units
CI	Crystallinity Index
CNT	Total cells counted
COSY NMR	Correlated Spectroscopy Nuclear magnetic resonance
CP	Protein concentration
DG	Digestive gland
DLA	Double-layer plaque assay technique
DMSO	Dimethyl sulfoxide
DNase	Deoxyribonuclease
DO	Dissolved oxygen
DSC	Differential scanning calorimetry
EDTA	Ethylenediaminetetraacetic acid
EPS	Extracellular Polysaccharide Substances
EST	Esterase assay
EU	European Union
FDA	Food and Drug Administration
GPx	Glutathione peroxidase assay

H&E	Haematoxylin–eosin
HDPE	High Density Polyethylene
HPLC	High-performance liquid chromatography
HSQC NMR	Heteronuclear Single Quantum Coherence Nuclear magnetic resonance
IUPAC	International Union of Pure and Applied Chemistry
L-Dopa	3,4 dihydroxy-L-phenylalanine
LDPE	Low-density polyethylene
LYS	Lysozyme assay
MAS	Magic angle spin
MBTH	3-methyl-2 benzothiazolinone hydrazone hydrochloride
MP	Microplastics
MS	Mass spectrometry
NGS	Next Generation Sequencing
NMR	Nuclear magnetic resonance
NP	Nanoplastics
nr/nt	Non-redundant nucleotide
OTU	Operational taxonomic unit
PBAT	Poly(butylene adipate terephthalate)
PBS	Poly(butylene succinate)
PCL	Poly(caprolactone)
PCR	Polymerase chain reaction
PDLA	Poly(D-lactic Acid)
PDLLA	Poly(DL-lactic Acid)
PE	Poly(ethylene)
PET	Poly(ethylene terephthalate)
PGA	Poly(glycolic acid)
PHA	Poly(hydroxyalkanoates)
PhaC	Polyhydroxyalkanoates synthase (enzyme)
PHB	Poly(3-hydroxybutyrate)
PHB_GF	Poly(3-hydroxybutyrate) – Good Fellow
PHBH	Poly(3-Hydroxybutyrate -co-3-Hydroxyhexanoate)

PHBV	Poly(3-hydroxybutyrate-co-3-hydroxyvalerate) (copolymer)
PHBV_GF	Poly(3-hydroxybutyrate-co-3-hydroxyvalerate) – Good Fellow
PHV	Poly(3-hydroxyvalerate)
PLA	Poly(lactic acid)
PLLA	Poly(L-lactic Acid)
PO	Phenoloxidase assay
PP	Poly(propylene)
PS	Poly(styrene)
PTT	Polytrimethylene terephthalate
rDNA	Ribosomal Deoxyribonucleic acid
RNase	Ribonuclease
ROS	Reactive oxygen species
SBS	Sequencing by synthesis
SDGs	Sustainable Development Goals
SEM	Scanning electron microscope
SUP	Single Use Plastic (Directive)
TBS	Tris-buffered saline
TGA	Thermogravimetric analysis
TG-DSC	Thermogravimetric - Differential scanning calorimetry analyses
TIPS	Thermally Induced Phase reversal process
TPC-ET	Thermoplastic copolyester elastomers
U	Units
UHPLC-ESI-HRMS	Ultra-Performance Liquid Chromatography–Electrospray ionization - High-Resolution Mass Spectrometry
UNEP	United Nations Development Programme
UV	Ultraviolet
WF	Wood flour
Xc	Percentage of crystallinity of the polymer
ΔH_{100}	Theoretical enthalpy of 100% crystalline PHB
ΔH_m	Melting enthalpy of the polymer

LIST OF MATERIALS

Poly (R) -3-hydroxybutyric acid (PHB, Sigma Aldrich, 363502)	Pure powder
Poly-DL-lactic acid (PDLLA, Sigma Aldrich, 38534)	Pellet
Polyhydroxyalkanoate (PHBV_GF, Merck, GF11943604)	Pellet
Poly-L-lactic acid (PLLA, NatureWorks, 2002D Ingeo)	Flakes
High Density Polyethylene (HDPE, MP94 by Versalis)	Pellet

PREPARATION AND COMPOSITION OF CULTURE MEDIA

Marine Agar

Marine Agar is a medium used to isolate and enumerate heterotrophic marine bacteria. It was prepared by adding 40 g of Marine Broth product (Conda) to 1L of distilled H_2O. For the solid Marine Broth, 15 g/L of Technical Agar (OXOID) was added. The medium was sterilized in an autoclave at 121°C at 1 atm for 20 minutes. Below is the composition of the Marine Broth.

Components	g/L
NaCl	19.4
$MgCl_2$	8.8
Bacteriological Peptone	5
Na_2SO_4	3.24
$CaCl_2$	1.8
Yeast Extract	1
KCl	0.55
$NaHCO_3$	0.16
Fe(III)	0.1
KBr	0.08
$SrCl_2$	0.034
H_3BO_3	0.022
Na_2HPO_4	0.008
Sodium Silicate	0.004
NaF	0.0024
NH_4NO_3	0.0016

ONR7a

ONR7a mineral medium was prepared by combining three separately prepared solutions.

- **Solution 1 (Final Volume 500 mL):**

Components	g/L
NaCl	22.79
Na_2SO_4	3.98
KCl	0.72
NaBr	0.083
$NaHCO_3$	0.031
H_3BO_3	0.027
NaF	0.0026
NH_4Cl	0.27
Na_2HPO_4 x ($7H_2O$)	0.089
TAPSO	30

The pH was brought to 7.6 with NaOH. To obtain the solid medium, 15 g/L of Bacto agar was added. The solution was sterilized in an autoclave at 121°C at 1 atm for 20 minutes.

- **Solution 2 (Final Volume 300 mL):**

Components	g/L
$MgCl_2$ x 6 H_2O	11.18
$CaCl_2$ x 2 H_2O	1.46
$SrCl_2$ x 6 H_2O	0.024

The solution was sterilized in an autoclave at 121°C at 1 atm for 20 minutes.

- **Solution 3 (Final Volume 200 mL):**

Component	g/L
$FeCl_2$ x 4 H_2O	0.002

Solution 3 was sterilized by filtration.

The solutions were mixed at a temperature of around 50° s.

LIST OF SAMPLES

List of scaffolds of biopolymeric materials used for field tests:

Bioplastic (Scaffold)	Contact medium	Contact time (days)	Sample name
PDLLA/PLLA	Sea	60	A60
PDLLA/PLLA	Sea	120	A120
PLLA	Sea	60	B60
PLLA	Sea	120	B120
PHA/PHB	Sea	60	-
PHB	Sea	60	-

List of scaffolds in biopolymeric material used for tests in microcosms:

Bioplastic (Scaffold)	Contact medium	Sample name
PDLLA/PLLA	Sterilized seawater + Inoculum (A60)	Ai60
PDLLA/PLLA	Sterilized seawater + Inoculum (A120)	Ai120
PLLA	Sterilized seawater + Inoculum (B60)	Bi60
PLLA	Sterilized seawater + Inoculum (B120)	Bi120
PHA/PHB	Unsterilized seawater	C60
PHB	Unsterilized seawater	D60

List of controls used for tests in microcosms:

Bioplastic (Scaffold)	Contact medium	Sample name
PDLLA/PLLA	Sterilized seawater	C_A60
No polymer	Sterilized seawater + Inoculum (A60)	C_Ai60
PDLLA/PLLA	Sterilized seawater	C_A120
No polymer	Sterilized seawater + Inoculum (A120)	C_Ai120
PLLA	Sterilized seawater	C_B60
No polymer	Sterilized seawater + Inoculum (B60)	C_Bi60
PLLA	Sterilized seawater	C_B120
No polymer	Sterilized seawater + Inoculum (B120)	C_Bi120
PHA/PHB	Sterilized seawater	C_C60
PHB	Sterilized seawater	C_D60
No polymer	Unsterilized seawater	C

1 – INTRODUCTION

1.1 Bio-based Plastics

In the last decade, the economy has delivered new sustainable materials mainly based on polymers biologically or chemically synthesized starting from renewable sources (Döhler et al., 2022). These materials defined as "Bioplastics", are functionally like classical plastics and are considered environmentally sustainable throughout their life cycle (Atiwesh et al., 2021). Three different types of bioplastics can be distinguished according to their origin and their biodegradability (**Figure 1**).
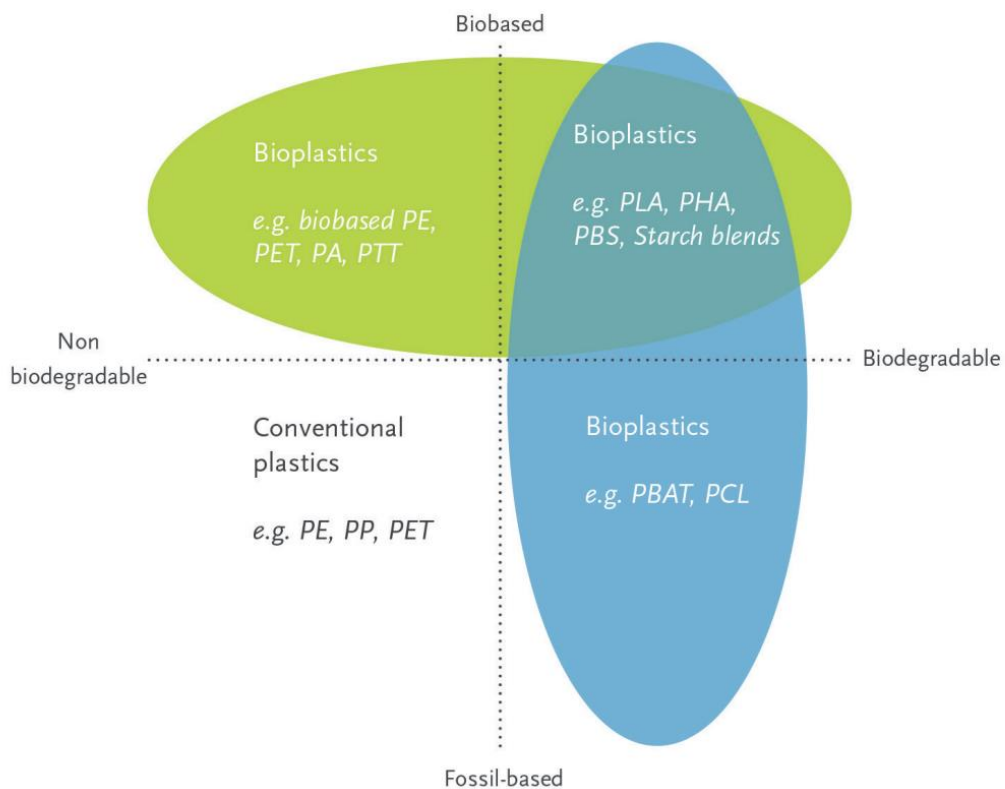
Figure 1 - Coordinated system of bioplastic

(Source: European Bioplastics; Ottoni et al., 2018)

The first group includes biodegradable plastics of fossil origin, such as polybutylene adipate terephthalate (PBAT) and polycaprolactone (PCL). A second group consists of non-biodegradable bio-based plastics, such as bio-based polyethylene (PE), polypropylene (PP), or polyethylene terephthalate (PET), and bio-based technical performance polymers such as polytrimethylene terephthalate (PTT) or thermoplastic copolyester elastomers (TPC-ET).

A final type of bioplastics is represented by polymers that are both bio-based and biodegradable, such as polyhydroxyalkanoates (PHA) and polylactic acid (PLA). These biopolymers are aliphatic polyesters and can be degradable due to the presence of ester

groups in their backbone chains which are cleaved through hydrolysis processes or by enzymatic activity.

The biodegradation process of bioplastics depends on biotic and abiotic factors, such as oxygen, temperature, humidity, specific microorganisms (Emedian et al., 2017) and strongly depends on the complexity, chemical structure, and crystallinity of the biopolymers themselves (Shen et al. al. al., 2020). These conditions are guaranteed within special disposal plants in which the polymers are appropriately disposed of once their life cycle has ended. On the contrary, dispersion in the natural environment may not place these materials in adequate conditions to favor the degradation process. It must also be said that information regarding degradation processes and their implications on ecosystems and organisms in the natural environment is still limited and fragmented.

Bioplastics are used in an increasing number of sectors involving everyday life (**Figure 2**), consequently, the bio-based polymer industry is growing rapidly. In 2019 the total production volume of bio-based polymers reached 2.22 Mt (million tons) corresponding to 1% of the total production volume of a bio-based plastics oil base (Naser et al., 2021), and to date, it is estimated that their growth rates could increase to reach a value of about 30% by 2025 (Coppola et al., 2021).
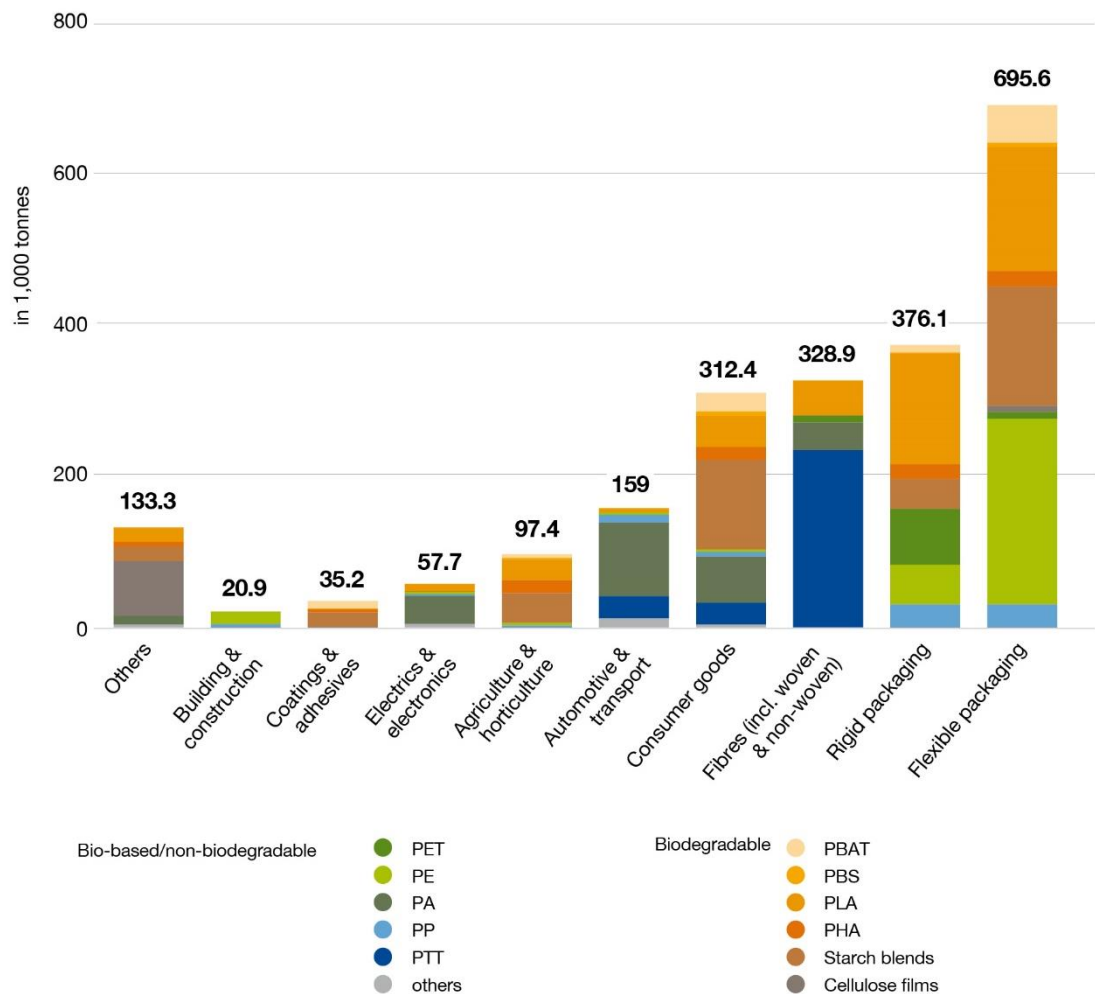
Figure 2 - Global production capacities of bioplastic in 2022 (by market segment)

(Graph developed by European Bioplastics, nova-Institute, 2022

https://www.european-bioplastics.org/market/).

The growing interest in bioplastics is mainly due to the serious environmental pollution generated by petroleum-based plastics which is affecting all ecosystems on the planet (Banaderakhshan et al., 2022; Manfra et al., 2021; Miller et al., 2020; Shruti & Kutralam-Muniasamy, 2019; Raza et al., 2018; Minguez-Alarcon et al., 2016; Otero et al., 2015).

An important drive towards the conversion to bioplastics is also given by recent political strategies. Starting from January 2018, with the adoption by the EU Commission of the "European Strategy for Plastics in a Circular Economy" (European Union, 2018), the European Community has launched a process of regulation of single-use plastic materials both on their production and consumption by promoting more sustainable models, and on their disposal. This regulation materialized on 2 July 2019 with the entry into force of Directive (EU) 2019/904, known as the "SUP Directive - Single Use Plastic", implemented in Italy with Legislative Decree n.196/2021 (Gazzetta Ufficiale - Italy, 2021). To these is added the European Green Deal (European Commission, 2019), an action plan outlined by

the European Commission aimed to "*supports the transformation of the EU into a fair and prosperous society with a modern and competitive economy and to set the EU on the path to a green transition, with the ultimate goal of reaching climate neutrality by 2050*". The objectives of the SUP Directive, as well as of the Green Deal, are intimately linked to the principles of the Circular Economy, according to which it is necessary not only to prevent the production of waste through the reuse and recycling of plastic materials but also starting from the origin of the product, adopting alternative raw materials of biological origin as a replacement for materials of petrochemical origin. (Johansen et al., 2022; European Parliament, 2022). Furthermore, the development of new types of bioplastic materials is one of the objectives of the 2030 Agenda for Sustainable Development Goals (SDGs) of the United Nations Development Programme (UNEP, 2016).

Although bioplastics are considered the best alternative to conventional plastics, they still have disadvantages. The first disadvantage is related to the high production costs: current process costs are 3-10 times those of conventional PP and PE (Shen et al., 2020; Singh et al., 2019; Kourmentza et al., 2017). Further negative effects, indirectly caused by the production of bioplastics, concern the use of intensive monocultures (such as sugar, starch, oil, or natural rubber) (Kabasci, 2013), with consequent high consumption of water, fertilizers, and increased eutrophication phenomena (Pellis et al., 2021). A recent study carried out by European Bioplastics showed that the production of bio-based polymers in 2022 amounted to 2.22 million tonnes resulting in the use of 0.8 million hectares of land and predicted global production will rise to 6.3 million tonnes corresponding to the exploitations of 2.9 million hectares, about 0.06% of the global agricultural area in 2027 (European Bioplastics, 2023, https://www.european-bioplastics.org/market/).

Among the disadvantages, it is also worth mentioning that they lack mechanical properties comparable to conventional plastics (Emadian et al., 2017). Therefore, to be able to obtain higher performance and other properties, additives such as plasticizers, dyes, light stabilizers and pro-oxidants are mixed with pure polymers during production. These chemical additives, following the fragmentation and degradation processes of the bioplastic, are more easily released into the environment (Fan et al., 2022). Despite all these concerns, on the global market are currently available different kinds of bioplastics (**Table 1**) (Shruti & Kutralam-Muniasamy, 2019). Considering that knowledge of the possible environmental interactions that these bioplastics can potentially cause at the end of their life cycle is still limited, it is appropriate to also explore these important aspects.

Table 1 - General characteristics of commonly available bioplastics

Bioplastics	Group	Backbone	Types and examples	Consumer products
Polylactic acid	Bio-based homo-polymer	Lactic acid	Racemic PLLA (Poly-L-lactic Acid), Regular PLLA (Poly-L-lactic Acid), PDLLA (Poly-DL-lactic Acid), copolymer (e.g., P(LA-HB)), blends (e.g., PLA/starch)	Plastic films, bottles, and biodegradable medical devices (e.g., screws, pins, rods) and plates metal and paint coatings
Polyhydroxy alkanoates (PHA)	Bio-based polymer	3-Hydroxy-fatty acids, 2-hydroxy-fatty acids, 4-hydro-fatty acids and 5-hydroxy-fatty acids	Copolymer (e.g., PHBV, P(3-hydroxybutyrate-3-hydroxyvalerate); P(3HB-co-3HHx), P(3-hydroxybutyrate-3-hydroxyhexanoate)); blends (e.g. PLA/PHB), composites (e.g. wood-PHA)	Bags, bottles, disposable items, items of personal hygiene, degradable diapers, films, coatings on paper, encapsulation of fertilizers and food packaging
Polybutylene succinate (PBS)	Fossil based co-polymer	Succinic acid Butanediol	Copolymer (e.g., P(BS-LA), P(BS-BAT)), blends (e.g. PBS/PCL)	Food packaging, coffee capsules, disposables, agriculture fibres, nonwovens industrial/automotive, mulch film, plant pots, hygiene products (e.g., diapers), fishing nets and lines, wood-plastic composites, composites with natural fibres
Polyethylene succinate (PES)	Fossil based co-polymer	Succinic acid Ethylene glycol	Blends (e.g., PES/polyethylene oxide (PEO))	
Polybutylene succinate adipate (PBSA)	Fossil based random co-polymer	Succinic acid Butanediol Adipate	Blends (e.g., PBSA/PLA)	
Polyglycolic acid (PGA)	Fossil based homo-polymer	α-hydroxyacetic acid	Copolymer (e.g., P(GA-LA), P(GA-CL), P(GA-HB))	Subcutaneous sutures, intracutaneous closures, abdominal and thoracic surgeries, implantable medical devices (anastomosis rings, pins, rods, plates and screws)
Polycaprolactone (PCL)	Fossil based homo-polymer	ε-Caprolactone	Copolymer (e.g., P(GA-CL)), blends (e.g. PLA/PCL, PBS/PCL)	Food packaging, medical devices

1.2 Bio-based bioplastics used in this study

The manufacturing industry placed great interest in the category of biobased and biodegradable materials and the most widespread are polyhydroxyalkanoates (PHAs) and polylactic acid (PLA) (Manfra et al. 2021) therefore we focus on the study of these polymers. PHAs are straight-chain aliphatic polyesters, synthesized by microorganisms through fermentation processes of organic substrates (Raza et al., 2018). PHAs is a class of polymers formed by repeating monomeric units (**Figure 3**) that produce chiral, optically active molecules and all in the R configuration due to the stereospecificity of the biosynthetic enzyme, PHA synthase (PhaC) (Sudesh et al., 2000). Observing the structure of a generic PHA monomer (**Figure 3**), the presence of an R group in the β position is observed. This is an alkyl group with a number of carbon atoms between 1 and 15, which can be branched or linear, saturated or unsaturated, with aromatic or halogenated substituents. PHAs are defined as short chain when the R-side chain is composed of 1 to 5 carbon atoms, while they are defined as medium chain when the R-side chain is made up of between 6 and 14 carbon atoms (Tan et al., 2014). Today over 150 variants of PHA monomers are known, with the most common being 3-hydroxybutyrate (3HB or C_4), 3-hydroxyvalerate (3HV or C_5), 3-hydroxyhexanoate (3HHx or C_6), 3-hydroxyoctanoate (3HO or C_8), 3-hydroxydecanoate (3HD or C_{10}) and 3-hydroxydodecanoate (3HDD or C_{12}) and 4-hydroxybutyrate (4HB) (Wang et al., 2014).

Poly(3-hydroxyalkanoate)
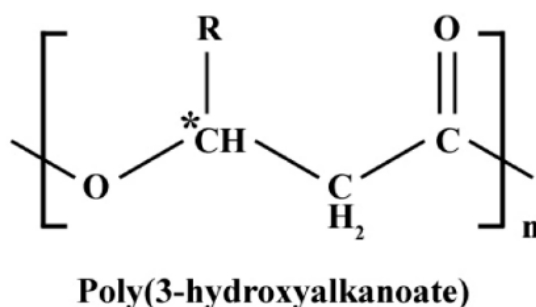
Figure 3 - Polyhydroxyalkanoate (PHA) chemical structure. The nomenclature and carbon number for PHA compounds are determined by the functional alkyl R group. The asterisk denotes the chiral center of PHA-building block. (Tan et al., 2014)

The synthesis of the different PHA monomers depends both on the microorganism and on the growth conditions, as well as on the type of starting organic substrate. Furthermore, PHAs can be modulated by combination with other biopolymers, enzymes, organic and inorganic materials, and others suitable to improve mechanical properties and increase biocompatibility (Chan et al., 2018). In particular, a common form of PHAs is the copolymer of PHB with PHV, a low molecular weight straight chain carboxylic acid that can be

degraded, which showed better processability and greater simplification of recycling processes. Furthermore, an improvement in the biodegradation process was observed in the case of mixtures consisting of PHB-covalerate with wood flour (up to 50% by weight) as a composite (Hubbe et al., 2021; Chan et al., 2018). PHAs, both in homo- and hetero-polymer form or blended with other materials, find applications in many sectors such as packaging, medicine and pharmacology, agriculture, and food, as raw materials for the synthesis of enantiomerically pure chemicals and the production of paints (Rehm & Steinbüchel, 1999).

Polylactic acid (PLA) is an aliphatic, naturally occurring, biocompatible, and biodegradable thermoplastic polyester, with stiffness and clarity comparable to polystyrene (PS) or poly(ethylene-terephthalate) (PET) (Auras et al., 2011). The monomer units of lactic acid are derived from the fermentation of substrates such as starch, glucose, lactose, and maltose, products from corn and potatoes, and other abundant natural resources by microorganisms (particularly of the genus Lactobacillus) endowed with high resistance to low pH values. Once the lactic acid monomers have been produced, the polymerization phase can subsequently take place, following two distinct types of process: by direct condensation of the lactic acid monomer (IUPAC name: 2-hydroxypropanoic acid) and/or by the opening of the lactic acid ring (ROP – Ring-Opening Polymerization) (IUPAC name: 3,6-dimethyl-1,4-dioxane-2,5-dione) catalyzed by an Sn(II)-based catalyst (**Figure 4**) (Nofar et al., 2019; Kabashi, 2013). Then monomers can be connected by ester bonds.
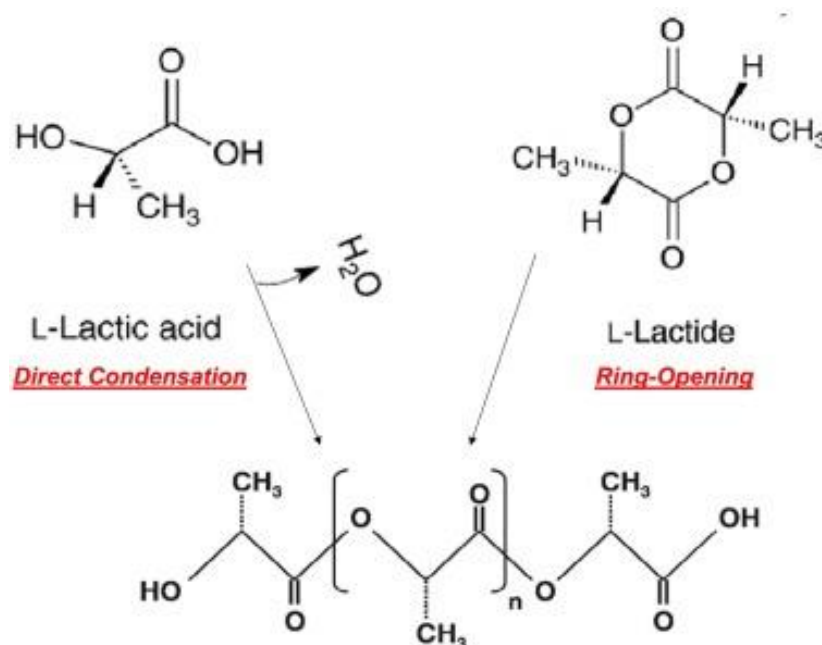
Figure 4 - Synthesis of PLA by direct condensation and ring-opening polymerizations.

Lactic acid is the simplest hydroxy acid with an asymmetric carbon atom. Because it is a chiral molecule, three forms of polylactic acid are formed: poly-L-lactic acid (PLLA), poly-D-lactic acid (PDLA), and poly-D,L-lactic acid (PDLLA) (**Figure 5**) (Chan et al., 2018).
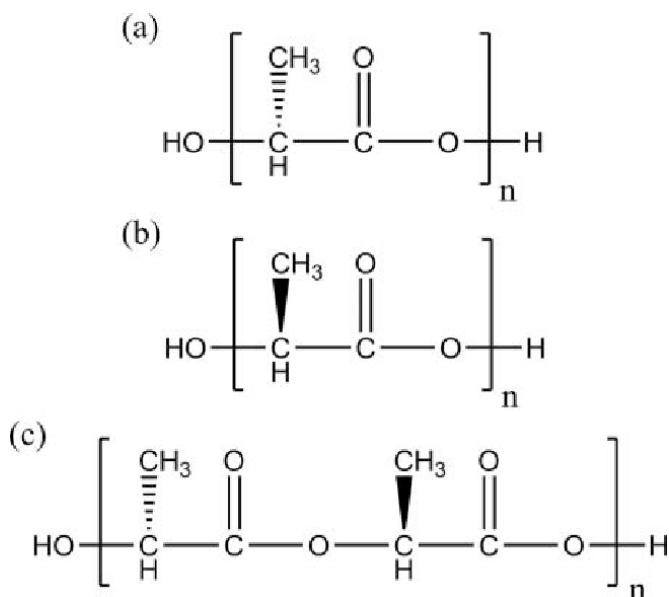

Figure 5 - Chemical structure of (a) poly(L-lactide) (PLLA); (b) poly(D-lactide) (PDLA); (c) poly(D, L-lactide)(PDLLA).

PLLA (poly-L-lactide) and PDLA (poly-D-lactide) forms are two isomers of the polylactic acid (PLA) polymer. These forms are optically active, which means they can interact with polarized light and can crystallize, forming an ordered and crystalline structure. However, unmodified PLLA and PDLA polymers have some limitations in practical applications. They are brittle and exhibit relatively poor resistance when exposed to oxygen. (Nandy et al., 2022). This makes them less suitable for applications that require durability and mechanical strength, especially in environments with oxygen presence. Furthermore, another characteristic that can affect the use of PLLA and PDLA is their slow degradation rate at room temperature. Due to their hydrophobic nature, and the presence of a methyl group that creates steric hindrance in the ester linkage, the process of hydrolysis of the ester linkage through water, occurs at a very slow rate. (Ilyas et al., 2022). Since the properties of PLA are strongly influenced by the stereoisomeric L/D ratio of the lactate units, PDLLA (which is an amorphous form of the polymer) is commonly adopted in manufacturing, at which the L/D ratio is varied using appropriate additions of PLLA to more effectively control the crystallization, morphology, and nature of the hydrolysis of the polymer (Hong & Park, 2021; Carfì et al., 2011; La Carrubba et al., 2008). This type of biopolymers is very widespread in the biomedical sector, the use of which began in the 1960s - both in

homopolymeric form and as mixtures - for the slow release of drugs and proteins and applications in the surgical field (Li et al., 2020). Today the fields of application of PLA are multiple as it is a material that can be used for packaging, to produce disposable tableware, in clothing, the production of bottles, for injection moulded products, for extrusion coatings, and so on (Auras et al., 2011). In agriculture, PLA is used in the form of mulch films to allow the slow release of pesticides and fertilizers (Gupta & Kumar, 2007). Since PHAs and PLA biopolymers often find application in the form of mixtures, it seems appropriate to deepen the study of degradative processes also considering the different compositions that the finished products can assume.

Both PHAs and PLA are defined as biodegradable bioplastics. Furthermore, the biodegradation processes of these biopolymers occur more slowly in the natural environment, thus making them incapable of bringing substantial benefits to ecosystems and organisms or advantages in the management of bioplastic waste. (Fan et al., 2022; Shen et al., 2020). Literature data reported that PLA mass does not significantly decrease (in terms of mass loss) after 400 days of marine immersion. (Bagheri et al., 2017). A study on the degradation of PHAs in the marine environment was instead carried out by Deroiné et al. (2015): the experiments conducted on a 200 µm thick PHBV film, showed a complete degradation after 9 months of immersion. Therefore, although the average lifetimes of bioplastics in the environment are considerably lower than those of petroleum-derived plastic materials (Ward & Reddy, 2020), it is still necessary to evaluate the possible effects on marine organisms and ecosystems that these bio-materials can generate before their complete degradation.

A fundamental role in degradation processes is that played by the microbial communities that adhere to the surfaces of polymeric materials. In the marine environment (**Figure 6**), immersed or floating plastic is rapidly colonized by pioneer microbial species, leading to the formation of a microbial biofilm attached to plastic and distinct from the surroundings (Syranidou et al. 2017), which has been defined "Plastisphere" (Zettler et al., 2013).
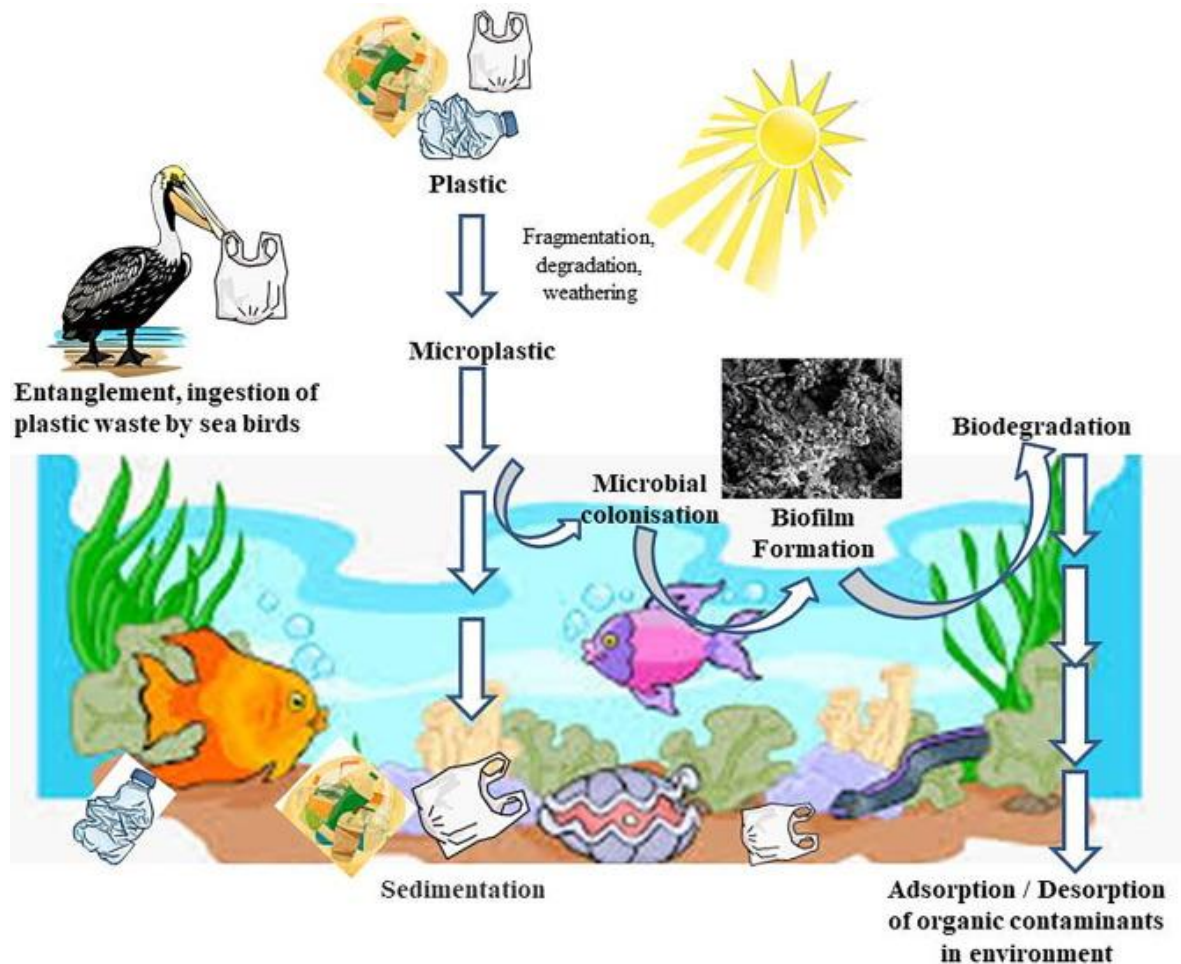
Figure 6 - Schematic representation of plastic deterioration
by abiotic and biotic factors in the marine environment (Basak & Meena, 2022).

Figure 7 graphically shows the sequence of events that occur in the process of biofilm formation in a marine environment on a polymer surface. Microbial communities adhere to polymeric surfaces thanks to extracellular polysaccharide substances (EPS) released by the microorganisms themselves (Basak & Meena, 2022; Carrasco-Acosta et al., 2022). This matrix, in addition to promoting the adhesion and development of the microbial community (Carrasco-Acosta et al., 2022). Subsequently, colonization by other organisms takes place, starting with unicellular algae and protozoa (Dang & Lovell, 2016), up to algae and invertebrate organisms, such as cnidarians, porifera, molluscs, polychaetes, etc. The composition of the biofilm depends on the season, the place, and the type of plastic material on which it forms (Syranidou et al. 2017). It is important to underline that have been attributed to the biota associated with plastic debris (both bio-based and conventional) changes in the surface topography such as the presence of cracks and fissures, which cause the fragmentation of the polymer into micro and nanoparticles (Syranidou et al., 2017). Finally, the biodegradation process ends with mineralization, i.e., with the assimilation by

the biomass of the useful components coming from the polymeric substrate and the release of CO_2 and water (**Figure 7**) (Kumar et al., 2021; Syranidou et al., 2017).

Initial attachment of microbes on the plastic surface

Polymeric material

Microbial Biofilm formation

Biodetoriation: Secretion of extracellular enzymes and EPS

Biofragmentation: Formation of oligomers, dimers, monomers

Mineralization: Microbial biomass, CO_2, H_2O
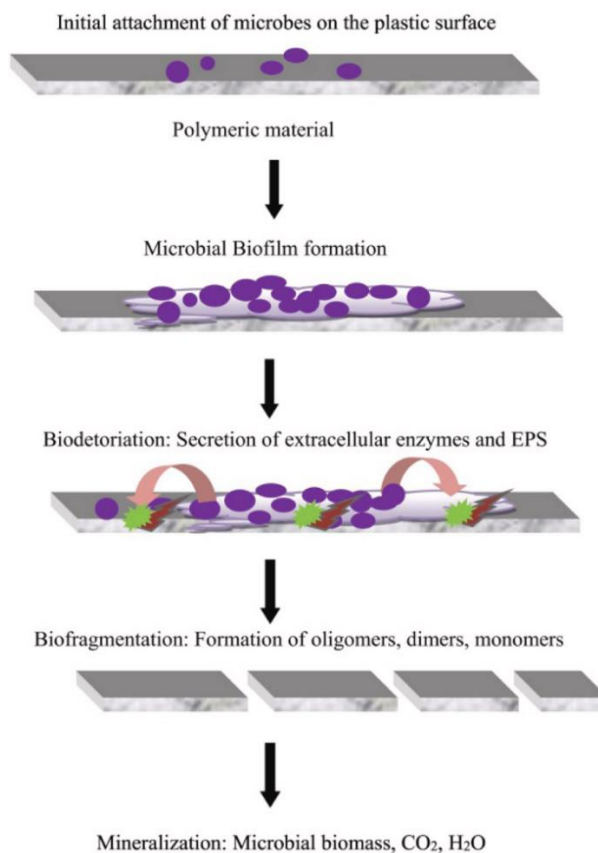
Figure 7 - Schematic illustration of plastic fragmentation by microorganisms (Kumar et al., 2020). This scheme, presented in general for conventional plastics, is also valid for describing the processes that lead to the fragmentation of plastics of biological origin.

As part of the evaluation of the possible impacts produced by these bioplastic materials, it is important to consider that, during the process that leads to the complete degradation of these biopolymers by microbial communities, there is a crucial intermediate step represented by fragmentation. Bioplastics exposed to erosion can more easily shrink in size, transforming into microplastics (MP) and nanoplastics (NP), leading to environmental impact as the conventional plastics (Arpia et al., 2021). This determines more frequent bioaccumulation and biomagnification events which can produce damage not only at the level of the individual organism (Manfra et al., 2021) but also to ecosystems as they introduce various environmental chemical contaminants and potentially pathogenic microorganisms into all food webs adhered to biofilms (Manzoor et al., 2022; Shruti et al., 2019; Mülhaupt, 2013). Several studies, conducted on marine indicator organisms aimed at evaluating the effects given by exposure to conventional micro and nanoplastics, have reported histological alterations, impairment of lysosomal integrity, nuclear anomalies and genotoxicity,

oxidative stress and up-regulation of related genes to immune response and apoptosis, measurements of clearance, respiration and byssus production rates (Détrée & Gallardo-Escarate, 2017; Ribeiro et al., 2017; Paul-Pont et al., 2016; Avio et al., 2015; Von Moos et al., 2012). Since bio-based microplastics tend to migrate deeper due to the fouling phenomenon (Eich et al., 2015), a variation of the vertical distribution of the species involved in the ingestion of bioplastics has been observed and this could represent a problem for the structure and functioning of ecosystems (Rodríguez et al., 2023). Therefore, a fundamental aspect is the evaluation of the damage potentially generated by bioplastics on living organisms. To carry out these assessments, model organisms that can be used as toxicological bioindicators (Curpan et al, 2022) such as *M. galloprovincialis* are adopted. From studies reported in the literature, for the evaluation of the effects caused by exposure to micro and nanoplastics of petrochemical origin, emerges that among the effects observed in *M. galloprovincialis* there are an altered immune response (Pittura et al., 2018), oxidative stress (Paul-Pont et al., 2016), neurotransmission dysfunction (Avio et al., 2015) and increased granulocytoma formation (Von Moos et al., 2012). Preliminary results have shown that bioplastic particles behave very similarly to fossil plastic (Hoellein et al. 2021; Zhang et al. 2020; Foley 2018; Rochman et al., 2015), triggering the immune system and activating the elimination of non-self particles through cellular response. *Mytilus spp.* it is one of the genera that is most often used as an environmental bioindicator (Caricato et al. 2019; Gornati et al. 2019; Beyer et al. 2017) as, in addition to their filtration activity (~ 4 - 5 L H_2O/h), they are also widely available, are easy to sample and to grow in laboratory conditions, have a high tolerance for pollutants and extreme environmental conditions, and have a well-known reactivity to anthropogenic stressors (Curpan et al., 2022; Gedik & Eryaşar, 2020; Parisi et al., 2017). In the wild, *Mytilus galloprovincialis* finds a wide distribution globally. Although in fact, it is a sessile mollusk native to the areas of the Mediterranean Sea, the Black Sea, and the coastal strip of the eastern Atlantic, during the last century it was introduced and naturalized also along the western coast of North America and the coastal regions of East Asia and South Africa, thus becoming an invasive species (Han et al., 2020; Parisi et al., 2017). In addition, these organisms are also consumed by humans and, therefore, represent an important vector for the transfer of pathogens and pollutants within the food chain (Cappello et al., 2021; Gedik & Eryaşar, 2020). In Europe alone, more than 300,000 tons/year of *M. galloprovincialis* are produced by aquaculture for human consumption (Figueras et al., 2019).

Considering the above and the high growth rates estimated for the production in the coming years of bio-based biodegradable bioplastics (Döhler et al., 2022), and in particular

those specifically made with PHAs (Saravanan et al., 2022) and PLA (Ilyas et al., 2022) biopolymers, there's a real possibility that the problem of pollution produced by petroleum-based plastics could soon simply be shifted to bio-based plastics. This study aims to delve into the dynamics linked to the biodegradation process of bioplastics in the marine environment, to be able to evaluate the implications that these materials can have on model organisms and, consequently, also on humans.

2 – AIMS OF THE THESIS

The objective of this doctoral project was the study of the most widespread plastics typologies of biological origin currently on the market, such as PHAs and PLA, considering aspects that can potentially influence their behavior in the environment (**Figure 8**). We chose to focus on what concerns the degradation process of these materials within marine ecosystems.

The study of these bioplastics was carried out considering three points of view:

- microbiological: through the study of the bacterial communities constituting the biofilm developed on the surfaces of the biopolymeric materials;
- chemical: through the research and identification of degradation products obtained by action of microorganisms;
- immunobiological: through the study of the possible interactions that the presence of biopolymer micro- and nanoparticles can determine on marine organisms.

During the first semester of the first year, we carried out the structural and thermal preliminary investigations of the commercial bio-polymers through different techniques [infra-red spectroscopy (ATR - FTIR), nuclear magnetic resonance (^{1}H and ^{13}C NMR), scanning electron microscope (SEM), differential scanning calorimetry (DSC) and thermogravimetry (TGA)]. Furthermore, during the following semester, solubility tests were conducted by placing the biopolymers in several different organic solvents in order to study the behavior of the biopolymers and to better plan the creation of PHAs and PLA scaffolds necessary to recruit biomass in the marine environment with the aim of studying the microorganisms potentially capable of carrying out the degradation of these biopolymers. Plastisphere adhered to scaffolds polymeric materials PHAs and PLA exposed to marine environment was characterized through Next Generation Sequencing (NGS) analysis. In the second year of the project, microcosms were set up in the laboratory in which the biopolymers were placed in contact with a biofilm inoculum recruited from the surface of the bioplastics exposed at sea. From the microcosms, were isolated and taxonomic identified bacteria capable of growing on PHAs and PLA as the sole carbon source. To obtain a realistic assessment of the impact on ecosystems of the diffusion of bioplastics, for the third year of the project we planned to study the degradation of bioplastics in simulated marine conditions and the possible impacts on the marine ecosystem with different approaches: I) analysis of hydrolysis products resulting from the bacterial activity; II) evaluation of the effects generated by exposure to micro and nanoplastics in filter-feeding marine organisms. We started from the concept that the degradation process has, as an intermediate process, the

fragmentation of the bioplastic material into micro and nanoparticles by both the abiotic components (such as oxygen, temperature, humidity, UV rays, wave motion, etc.) and the adhering microbial communities. For these studies, it was decided to adopt the bioindicator *Mytilus galloprovincialis*, as it has high filtering capacity and sessile behavior (Caricato et al., 2019; Gornati et al., 2019; Beyer et al., 2017): *in vitro* and *in vivo* tests were conducted on directly exposed biopolymeric microparticles to observe the immunobiological responses produced by the organisms.
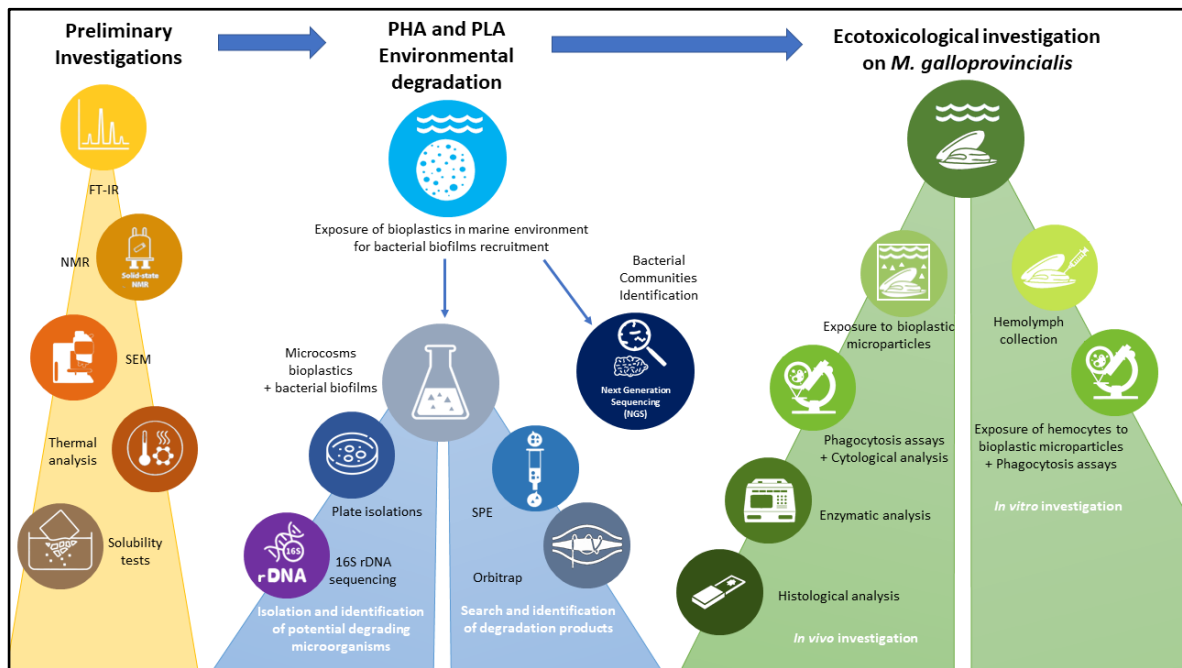
Figure 8 − Graphical abstract of the Ph.D project.

3 – OVERVIEW OF THE MAIN TECHNIQUES USED IN THIS STUDY

3.1 Methods of study of the Plastisphere

Unlike most conventional plastics, bioplastics represent a substrate that is more easily colonized by the microorganisms that make up the Plastisphere. In this study the Plastisphere was analysed by culture-dependent and culture-indipendent methods. The cultural methods were performed to isolate, grow and characterize bacterial strain able to utilize biopolyerms as unique carbon source. The culture-independent techniques, based on Next-Generation Sequencing of metagenomic DNA, were performed to obtained information on diversity and composition of plastisphere.

to better understand the functional and ecological biodiversity of the biofilms recovered from the surfaces of the bioplastics (Shokralla et al., 2012). Furthermore, through this analysis technique, it was possible compare the composition of the microbial communities of different plastic samples.

Through the "Next-Generation Sequencing" (NGS) technique, it is possible to simultaneously sequence hundreds of genomic fragments from a single sample and subsequently analyze the sequences with the aid of bioinformatics software to reconstruct the genomes present (Simon & Daniel, 2010). Currently, the most widely used NGS platforms are (Mardis, 2008):

- Roche 454/FLX
- Illumina/ Solexa Genome Analyzer
- MiSeq Sequencing System-Illumina
- Applied Biosystems SOLID System
- Helicos Heliscope
- Ion Torrent

It is possible to sequence a whole genome or the hypervariable regions of the 16S rRNA gene (Shokralla et al., 2012). From an operational point of view, once the metagenomic DNA has been extracted from the sample of interest, the nucleotide sequences are sequenced by synthesis (SBS), using specific primers, the DNA-polymerase enzyme for the synthesis of the filaments, and nucleotides labelled with a fluorescent substance that bind to the complementary sequences of the DNA to be analysed. Subsequently, the samples are irradiated by a laser beam which causes the excitation of the fluorochromes of the labelled nucleotides, with consequent emission of their fluorescence.

The fluorescence emitted is thus detected and analysed by a special software, which reconstructs the sequence of the sample, aligns it with reference sequences present in the database, and allows to obtain both qualitative and quantitative genomic information relating to the abundance of individual microbial species identified with respect to the whole microbial community analysed (Voelkerding et al., 2009).

3.2 UHPLC-ESI-HRMS

This technique involves the use of high-performance liquid chromatography (HPLC) coupled with high resolution mass spectrometry (HRMS) through an Electrospray type source interfacing system (ESI), used for the chromatographic separation and analysis, in complex matrices, of analytes with medium-high polarity and ionizable characteristics. HPLC exploits the different affinities of the molecules of interest between a stationary phase (column) and a mobile phase (eluent). Commonly we operate in reverse phase, i.e. using a non-polar stationary phase and a polar mobile phase. There are various types of stationary phases having various polarity and affinity characteristics depending on the characteristics of the analytes to be separated, while the mobile phase is normally made up of polar solvents such as water, methanol, or acetonitrile, often used in binary or tertiary mixtures. Thanks to the different affinities of the analytes towards the stationary phase and the mobile phase these will move at different speeds within the chromatographic column with the result of obtaining a separation of the analytes over time thus allowing separate entry into the mass determination system.

At the output of the HPLC system there is the interfacing system ESI with HRMS. Because the HRMS system cannot manage the flow of liquid exiting by the HPLC system, the ESI has the task of "vaporizing" the analytes in ionized form through the formation of an "ionized spray" suitable to be managed by HRMS. The high-resolution mass spectrometer represents the detector of the entire instrumental apparatus that identifies and quantifies the analytes separated during the chromatographic run. In particular, a high-resolution mass spectrometer, such as the Orbitrap, has a very high-resolution capacity which allows it to discriminate masses even to the fourth decimal digit, effectively working on exact monoisotopic masses, allowing for high sensitivity and accuracy analytical. All this is possible because of the Orbitrap mass analyzer, which utilizes a combination of electrostatic fields and radiofrequency trapping to accurately determine the mass-to-charge ratio (m/z) of ions. Orbitrap mass analyzer consists of a central spindle electrode surrounded by an outer barrel-like electrode. The operating principle involves several steps: first, ions are injected into the analyzer and guided into a trapping region between the central spindle electrode and

the outer barrel electrode. In this region, ions orbit around the central electrode due to the influence of a static electric field. As the ions orbit, their motion generates a frequency signal that is detected by the system. Subsequently, the trapped ions are subjected to a perturbing radiofrequency voltage, causing their motion to become unstable. This instability leads to the ions moving out of their stable orbits and oscillating along the central electrode. During this oscillation, the system detects the image current generated by the moving ions. As a result, an interferogram is obtained which is converted, via the Fourier Transform, into a mass spectrum showing the intensity of the signals obtained as a function of their m/z ratio. The Orbitrap's ability to work at high resolution makes it the ideal instrument for all those particularly complex matrices, as in the case of biological or environmental ones, in which it is necessary to discriminate molecules in trace and ultratrace concentrations.

3.4 Methods of study of the immunobiological responses of *Mytilus galloprovincialis*

The impacts of biopolymer particles on the marine environment have been explored, by evaluating *in vitro* the cellular response of *Mytilus galloprovincialis* haemocytes referred to their phagocytic and/or encapsulation activity (Parrinello et al. 2017; Parisi et al. 2014; Falleiros et al. 2003). Considering that not all bio-based materials are biodegradable or biodegradable in a very short time, further the in vitro investigation on cellular recognition, we investigated the fate of the particles in aquatic environments and the interaction with the filter-feeding mussels.

Investigation methodologies include both *in vivo* and *in vitro* tests, the latter performed following the collection of haemolymph from the organisms (Parisi et al., 2021).
Haemolymph is the body fluid of organisms such as mollusks, arthropods, and insects which, similarly to the blood of mammals, is also responsible for the transport of oxygen, metabolites, and other components essential for the life of mollusks. It is an aqueous solution that contains inorganic ions (such as Na^+, K^+, Mg^{2+}, Ca^{2+}, Cl^-, and HCO_3^-), hormones, enzymes and proteins, respiratory agents (hemocyanin), carbohydrates and lipids, and known free cells in suspension (Machałowski & Jesionowski, 2021). The latter, known as haemocytes, are responsible for the innate immune response of organisms (Parisi et al., 2021). The presence of foreign and potentially toxic elements in the body causes the haemocytes to activate cell-mediated responses, such as phagocytic activity and various cytotoxic reactions, such as, for example, the release of lysosomal enzymes, antimicrobial peptides, and the production of oxy radicals (Canesi et al., 2012). In *Mytilus spp.* granular haemocytes represent the dominant cell type, characterized by a diameter of about 7 - 10 µm (depending on the subpopulation considered), a low nucleus/cytoplasm ratio, and the ability

to extend into pseudopodia. *In vitro* assays aim to evaluate the cellular response of mollusks precisely based on the analysis of the functionality, cellular vitality, and morphology of haemocytes following direct exposure to polluting factors (Parisi et al., 2021). Considering that the basic cellular processes of innate immunity are conserved at an evolutionary level from invertebrates to mammals, carrying out the studies described in *M. galloprovincialis* allows us to evaluate the common biological responses generated by environmental exposure to micro and nanoplastics.

If on the one hand the *in vitro* tests allow rapid immunobiological screening, the *in vivo* tests allow for the evaluation of longer-term effects and considering not only the haemocytic response but also the effects on the whole organism. On the basis of *in vivo* tests, it is found that the feeding and respiration processes allow the entry of particles, whether they are food or pollutants, which can be accumulated and concentrated inside the organisms. This characteristic has led to the definition of bivalves as a "Model of Biological Sieve" (Ringwood, 2021) (**Figure 9**), which allows us to characterize the exposure and risks of polluting particles, such as plastic, in time and space.
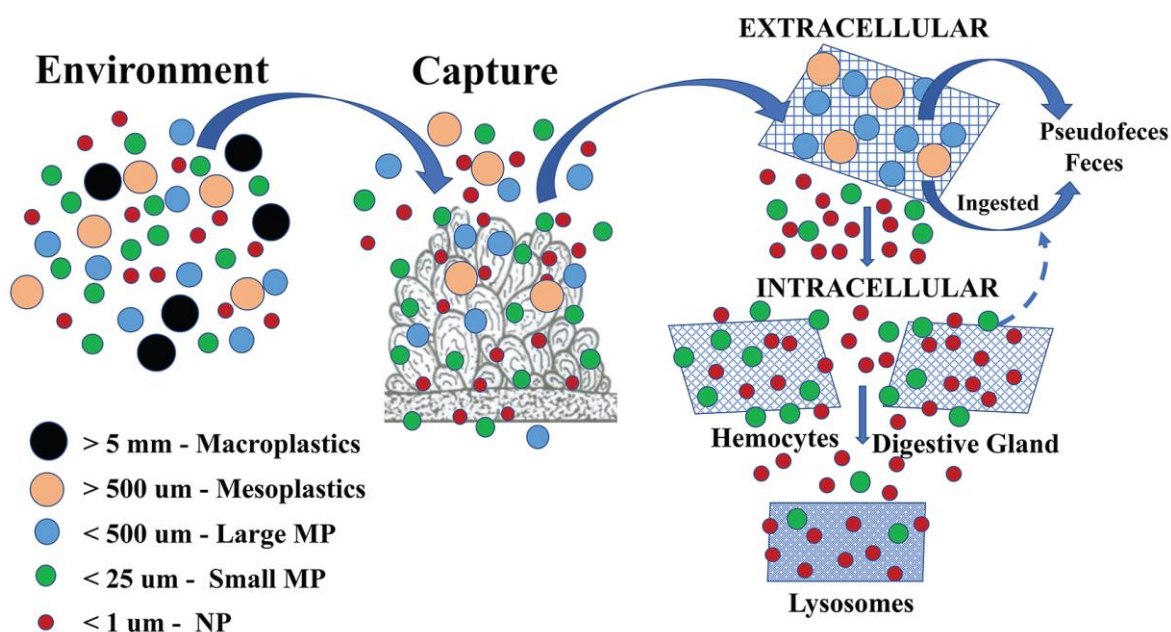
Figure 9 – Schematic representation of the "Biological Sieve Model" (Ringwood, 2021)

The feeding and breathing processes, in fact, cause the water to be pushed through the siphons whose tentacles, together with those of the mantle, act as the first sieve of the organism, capable of preventing the entry of particles larger than 5mm. What overcomes this first barrier is processed by the gills, through which particles smaller than 300 µm pass. The plastic particles which, together with food and organic substances, pass the gill barrier, move inside the digestive tract mixed with mucus, and from there will be transferred into the

digestive diverticula (also known as the digestive gland, DG, or hepatopancreas). Since plastic particles are unlikely to be altered by the action of digestive enzymes, elimination of larger particles in the form of pseudofeces ($< 25 \mu m$) will result, while smaller particles can potentially accumulate in tissues (such as gills, stomach, and intestine, hepatopancreas and adductor muscle), with the possible consequence of cell and tissue death, or inside the lysosomes with consequent alteration in the morphology and functionality of these (Sendra et al., 2019). Histopathological analyzes and lysosomal assays following *in vivo* exposure tests are therefore important evaluations to be considered in order to obtain a more complete view of the potential effects on mussels produced by the ingestion of plastic materials. Since there are numerous studies conducted on the effects produced by microplastics of petrochemical origin, but the number of works carried out considering the use of bioplastics is reduced, in the context of this doctoral project we wanted to pay attention to this aspect. Furthermore, it should be considered that, compared to conventional plastics, bioplastics are much faster reduced into micro and nanoplastics thanks to the action of the microorganisms constituting the biofilm, as they carry out a physical fragmentation prior to the actual degradation understood as the use of the substrate for their own processes metabolic. Therefore, small fractions of these materials will be more easily dispersed in the environment, to the detriment of organisms such as filter feeders such as *Mytilus galloprovincialis*. To evaluate the effect of bioplastic on living eating organisms, in addition to *in vitro* tests, we also carried out an *in vivo* exploration through an intensive test, placing the organisms in the presence of microplastics resuspended in the same water that hosts the mussels and exposing them for a short period of a few hours. The purpose of this test was to determine the acute effects generated by micro- and biopolymeric nanoparticles on these marine filter-feeding and bioindicator organisms. This was done by evaluating possible variations in the number of free haemocytes circulating in the haemolymph, in their phagocytic activity, potential histological variations in the morphology of the digestive glands as well as in the activity of several immune-related enzymes in the digestive gland and in the haemolymph of the mussels (for example phenol oxidase, glutathione peroxidase, lysozyme, alkaline phosphatase, and esterase). These markers were chosen, firstly, because bivalve haemocytes are easily influenced by exogenous factors, as they regulate functional cell-mediated immune responses (Gagnaire et al. 2006; Paillard et al. 2004). Furthermore, enzymes produced in the digestive gland are well known to assist, modulate, and accelerate immunological processes in haemocytes. The digestive gland is a source of innate immune molecules (Smith 2001) and is involved in pathogen clearance, antigen processing, and infection-induced metabolic changes (Alday-Sanz et al. 2002; Luchtel et al. 1997). In detail,

hydrolase enzymes, normally involved in detoxification, inflammatory and digestive processes, the phenoloxidase cascade and reactive oxygen species (ROS) scavenging, are recognized as immune parameters potentially influenced by environmental factors (Parisi et al., 2021; Hellio et al. 2006). Lysozyme activity is a phylogenetically conserved humoral response and has been studied in the mucus, tissues, and haemolymph of many invertebrate species. It corresponds to the primary and rapid defence of organisms against pathogens and is a bactericidal hydrolytic enzyme which hydrolyses the β-1,4-glycosidic bonds of peptidoglycan (an important component of the cell wall of Gram-negative bacteria), resulting in the rupture of bacterial walls due to destabilization of the membrane (Li et al., 2008).

4 – MATERIALS AND METHODS

4.1 Biopolymeric materials

The following biopolymers were used for this study: poly [(R) -3-hydroxybutyric acid in pure powder (PHB, Sigma Aldrich, 363502), polyhydroxyalkanoate (pellet PHBV_GF, Merck, GF11943604), and polylactic acid (PDLLA pellet, Sigma Aldrich, 38534 and PLLA flakes, NatureWorks, 2002D Ingeo). PHBV_GF is a biopolymer composed of two monomers, specifically butyric and valeric acid, and has been prepared as a wood flour composite (WF).

4.2 Preliminary investigations: polymer characterization

4.2.1 Fourier Transform Infrared Spectroscopy - Attenuated total reflection (ATR-FTIR)

ATR-FTIR absorption spectra were acquired using a Spectrum Two spectrophotometer with KBr optics and ATR diamond cell (Perkin-Elmer Inc., Wellesley, MA, USA). The analyses were performed at room temperature, using a scan range between 4000 and 400 cm^{-1}, with a resolution of 4 cm^{-1} and 32 scans. The spectra obtained were then processed using Spectrum 10 software (Perkin-Elmer Inc., Wellesley, MA, USA).

4.2.2 Scanning Electron Microscopy (SEM)

Samples PHB_GF and PHBV_GF in pellet form and PHB in powder form were observed with a Phenom Pharos benchtop scanning electron microscope (Thermo Fischer Scientific, USA). The samples were coated with a metallic Au film deposited by electrovaporization. For metallization purposes, the sample was placed under vacuum. The surface was sprayed by introducing a flow of gaseous Ar to induce the release of any molecules of H_2O and CO_2 adhering to the surface of the sample. The reaction chamber was again emptied to 10^{-2} Torr and then metallization took place. For each sample in pellet format, two pellets were used for observations: one to visualize the section and one to visualize the cut at magnifications ranging from 250x to 15000x and working at a distance of 2 mm. The first micrographs were made at an initial power of 15kV. Despite the metallization, the samples still showed irradiation effects, so the following micrographs were conducted at 10kV and 5kV. Image visualization was performed using Phenomenon Pro Suite software (Thermo Fischer Scientific, USA).

4.2.3 Thermal investigations

Thermal analyses were carried out on ground samples of PHBV_GF, PHB_GF and on PHB powder, in quantities equal to about 14 - 17 mg. These samples were not subjected to any preliminary treatment.

Differential Scanning Calorimetry (DSC) was performed using a DSC 131 EVO (Setaram Instrumentation, France). The thermal program was carried out starting with an initial stabilization phase, during which the constant temperature of 25°C was maintained for 10 minutes. This was followed by a melting phase, with a passage from 25°C to 250°C by means of a thermal increase of 10°C min^{-1}. Finally, the cooling phase took place, with an isotherm at 250°C lasting one minute followed by a temperature drop ramp down to 30°C, with a thermal decrease of 10°C min^{-1} (Pillai et al., 2017; Tan et al., 2014).

Thermogravimetric Analyses (TGA) were performed using the LabSys EVO TG-DSC instrument (Setaram Instrumentation, France). The program was then set up to start with a stabilization phase during which an isothermal condition is maintained at 30°C for 10 minutes. Subsequently, during the melting phase, the temperature ranges from 30°C to 550°C, with a thermal increase of 10°C min^{-1}. The last step is cooling, consisting of a first phase of stabilization at 550°C for one minute, and then proceeding with the gradual decrease in temperature until reaching 30°C, proceeding with temperature gradients of -10°C min^{-1} (Tan et al., 2014).

Both thermal analyses were managed and recorded using Callisto software (Setaram Instrumentation, France).

4.2.4 Crystallinity Index and Degree of Crystallinity

The Crystallinity Index (CI) was calculated for each type of polymer object of this study according to a relationship of inverse proportionality that can be deduced between the solubility and the degree of crystallinity of the polymer (Panaitescu et al., 2017; Valappil et al., 2007). This value is obtained from the ratio between the intensities of the bands of the FT-IR spectra of each polymer at 1382 cm^{-1} (-CH$_3$), which is indicative of the crystallinity of the molecule, to that at 1185 cm^{-1} (-C-O-C-), which is indicative of the amorphous state (Galego et al., 2002). Furthermore, the percentage of crystallinity of the polymer (Xc) was also calculated using the **Equation (1)**:

$$X_c = \frac{\Delta H_m}{\Delta H_{100}} \times 100 \qquad \text{(1)}$$

where ΔH_m is the melting enthalpy of the polymer, obtained from the value of the area under the melting curve of its DSC thermogram, while ΔH_{100} represents the theoretical enthalpy of

100% crystalline PHB, equal to 146.6 J g^{-1} (Aramvash et al., 2015; Kolahchi et al., 2015; Wei & McDonald, 2015; Barham et al., 1984).

4.2.5 Nuclear magnetic resonance spectroscopy (NMR)

Solid-state ^{13}C NMR analyses were performed on ground PHBV_GF and PHB powder samples, at 100.65 MHz on a Bruker Avance II 400 Ultra Shield digital NMR (Bruker Bio Spin Corporation, Woodland, TX, USA), configured for solids investigations using a magic angle probe rotating (MAS) with the following acquisition and processing parameters: rotation speed 6 kHz, number of acquisitions 1024, recycle delay 3 s and contact time 1.5 ms. In addition, ^{1}H and ^{13}C NMR spectra and two-dimensional heteronuclear (^{1}H-^{13}C HSQC NMR) and homonuclear (^{1}H-^{1}H COSY NMR) spectra of ground PHAs solubilized in deuterated chloroform (CDCl$_3$) were recorded.

4.2.6 Solubility tests

Since various studies on the solubility and recovery of polyhydroxyalkanoate polymers from microorganisms agree in attributing the best results to the use of chlorinated solvents (Jacquel et al., 2007; Hahn et al., 1994; Vanleutem, 1982), solubility tests were conducted on samples of ground PHBV_GF and PHB powder using chloroform (CHCl$_3$). In addition, further tests were also conducted in solvents of increasing polarity, such as ethyl acetate (CH$_3$COOC$_2$H$_5$) (Aramvash et al., 2015) and dimethyl sulfoxide (DMSO - C$_2$H$_6$OS) as a polar aprotic solvent. Other solubility tests were conducted using samples pre-solubilized in CHCl$_3$, dried and subsequently redissolved in acetonitrile (CH$_3$CN) and ethanol (C$_2$H$_5$OH). Since the biopolymers object of this study are insoluble in water, it was decided to conduct the solubility tests with these two solvents given their lower polarity compared to water.

All tests were conducted on accurately weighed quantities (0.0500-0.2000 g) of each biopolymer which were placed in contact with appropriate quantities (3-8 mL) of each solvent, under different experimental conditions. In particular, the tests which provided for a preliminary pre-solubilization in CHCl$_3$ were carried out by placing the test tubes containing the polymer/solvent systems in a thermostatic bath at a temperature of 50°C for 72h. The choice of the temperature adopted was made taking into consideration the boiling temperatures of the two solvents CH$_3$CN and C$_2$H$_5$OH used to redissolve the biopolymers (78°C and 82°C respectively). Due to the low boiling point of methanol, the same tests could not be performed in this solvent. The tests in CHCl$_3$, CH$_3$COOC$_2$H$_5$ and DMSO, on the other hand, were carried out at room temperature for 24 hours under constant stirring. At the end of each test, the residues, separated from the solutions by centrifugation at 7000 rpm for 15 min, were then brought to dryness by placing them in an oven at 50°C for 3 days and

subsequently weighed. The solubilized amount of each biopolymer was determined from the difference in the starting amount. Infrared and mass spectrometry investigations were performed on the solubilized and insolubilized fractions.

Finally, solubilization tests were carried out on PHBV_GF in $CHCl_3$ which allowed the wood flour to be separated at room temperature from the polymeric residues of valerate and butyrate. A first solubilization in 10 mL of $CHCl_3$ was carried out by placing the test tube containing the polymer/solvent system on a stirrer set at 200 rpm for 24 h at room temperature. At the end of the contact time, the non-solubilized fraction was separated from the solubilized fraction by centrifugation at 4000 rpm for 10 minutes. Then the supernatant was recovered and another 10 mL of $CHCl_3$ was added to the non-solubilized fraction. The operation was repeated a second time, once again placing the test tube on the stirrer under the same operating conditions previously adopted. Filtration of the residual chloroform solution was carried out with a nylon fiber filter with a porosity of 0.22 µm (Whatman, UK) using a vacuum pump. Finally, the solubilized fraction and the fraction insoluble in $CHCl_3$, both settled by centrifugation and recovered on the filter, were placed in an oven at 55°C until dry.

4.3 Scaffolds preparation

Four different types of scaffolds were made for these studies. The proportions described below were adopted because of manufacturing tests which allowed us to determine the best composition of polymeric material and dioxane solution in terms of stability of the scaffold structure. The manufacturing tests were conducted using both the more crystalline biopolymers (such as PLLA and PHB) and the more amorphous polymers (such as PDLLA and PHA). The first type was made using only the PLLA biopolymer at a concentration of 4% in a solution consisting of dioxane and water in an 87:13 ratio. A second type was made using only PHB powder at a concentration of 6% in dioxane. A third type was made with a mixture consisting of an equal part of the biopolymers PHBV_GF pellet and PHB powder at an overall biopolymer concentration of 10% in a solution of dioxane.

The last type was made with a mixture consisting of 25% of PDLLA pellets (PLA, 38534) and 75% of PLLA flakes at an overall biopolymer concentration of 10% in a solution of dioxane. The scaffolds consisting of mixtures of PHA/PHB and PDLLA/PLLA biopolymers were made with an overall polymer concentration of 10% in a dioxane solution.

The scaffolds were made using a process known as the Thermally Induced Phase reversal process – TIPS (Lopresti et al., 2022). This method was chosen for the transformation of materials for this study because, in addition to being a widely used method for the actual

production of scaffolds applied in tissue engineering, it allows to obtain porous structures, with a greater surface area available for biomass recruitment such as able to resist at exposure in a marine environment. Following the TIPS method, the solutions for the realization of the scaffolds were prepared by dissolving the selected biopolymers in dioxane at the reflux for a time between 30 minutes and 2h. After this time, the dispersion was cooled to 60 °C, poured into an aluminium disc-shaped sample holder with a diameter of 60 mm and a thickness of 2.5 mm, and immediately immersed in ethylene glycol at -20 °C for 10 minutes. At the end of the freezing time, the scaffold made was placed for 24 hours in a washing system with a continuous flow of distilled water and finally transferred into a vacuum oven for drying at 37° C for 24h. After drying, the scaffolds shrink by about 10%.

4.3.1 Preliminary analysis on scaffolds

4.3.1.1 Spectroscopic investigations

ATR-FTIR analyses were conducted using a spectrophotometer Spectrum Two with KBr optics and ATR diamond cell (Perkin-Elmer Inc., Wellesley, MA, USA) to investigate the scaffold's chemical surface properties and to verify if the TIPS process resulted in alterations of the functional groups.

4.3.1.2 Morphological Analysis

To evaluate microstructure and porosity on the scaffolds immediately after their realization, observations were made with the scanning electron microscope (SEM).

To be able to observe the sections of the samples without altering their structure, a brittle fracturing was carried out by immersing the samples in liquid nitrogen. The resulting fragments were subsequently subjected to metallization, with a 10 nm thick deposition of metallic Au deposited by electro-vaporization. Micrographs were made in a magnification range between 540x and 6100x, at a working distance of 2 mm and at a voltage power of 10-15 kV.

4.4 Recruitment of the Plastisphere associated with PHAs and PLA biopolymers

Single scaffold of PHA/PHB, PDLLA/PLLA and PLLA, were positioned in nylon pouches (**Figure 10a**) and positioned inside a support system consisting of a semi-rigid grid tube closed at both ends (**Figure 10b**).
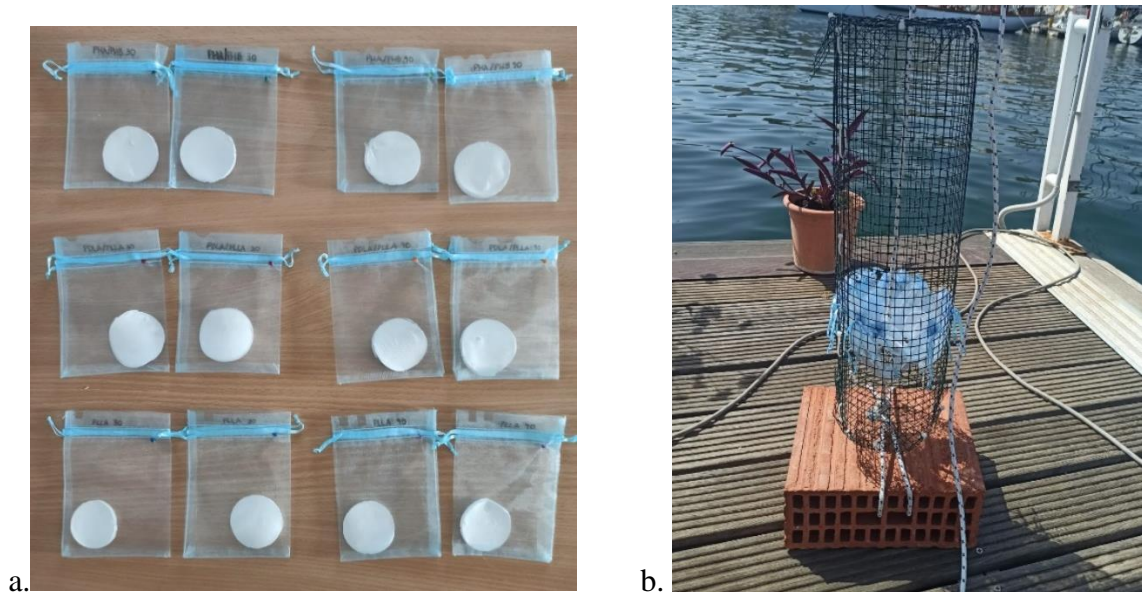
Figure 10 – scaffold of PHA/PHB, PDLLA/PLLA and PLLA (a) and support structure (b) for field tests

The support systems with the PHA/PHB, PDLLA/PLLA and PLLA scaffolds was immersed in a marine anthropized site within the basin Cala of Palermo, at the head of pier D of the establishment Si.Ti.Mar. (38° 07'17.6 "N 13° 22'11.4" E) (**Figure 11**). Samples were placed in the sea at a depth of about 9 meters and left there for 60 (t_1) and 120 (t_2) days. In this way we, therefore, wanted to simulate, from the start of the experimental tests, the effects given by the biofouling process, i.e., by the accumulation of organic and inorganic matter on the surfaces, which makes the materials exposed to different abiotic components compared to those to which they would have been subject floating on the surface (Eich et al., 2015).
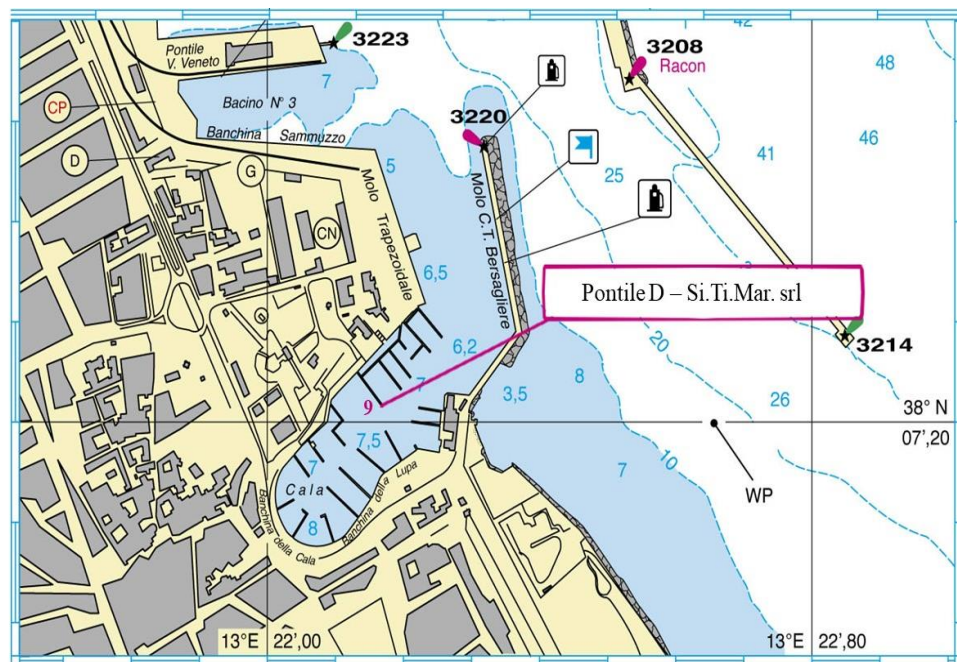
Figure 11 - "La Cala" Basin of Palermo (Italy); the image highlights the site chosen for positioning the samples of PHA/PHB, PDLLA/PLLA and PLLA within the study area, at a depth of 9 meters

Two scaffolds were placed in the field for each type of composition and for each sampling time: one scaffold was destined for the characterization of bacterial biofilm by NGS sequencing, and the other one was destinated for isolation and identification of potential bioplastic degrading bacteria. At the end of 60 (t_1) and 120 (t_1) days of exposition, the scaffolds were recovered and transported to the laboratory, immersed in sea water taken from the same site, in order to avoid the desiccation of the biofilms, and, after removal from seawater, stored at -20°C for molecular analysis or treated immediately.

4.5 Estimation of bacterial biomass on PDLLA/PLLA and PLLA scaffolds

The viable count method was used to determine the number of viable cells forming biofilm on PDLLA/PLLA and PLLA scaffolds surface after 60 and 120 days of incubation. The biofilm was recovered using a sterile scalpel (Syranidou et al., 2017). Therefore, the scaffolds were cut into small pieces and placed in 3 mL of sterile seawater. The samples were vortexed for about one minute and sonicated for 3 minutes to favor the detachment of the residual bacterial biofilm from the scaffold surface. 1 mL of bacterial suspension was utilized for the bacterial count. Briefly, the bacterial suspension was diluted in NaCl (0.9% w/v solution), six sets of decimal dilutions were performed, and 100 µL aliquots of dilution 10^{-2}, 10^{-4}, and 10^{-6} were plated onto Marine broth Agar plates, followed by incubation at 30°C for 48h. To quantify the number of viable bacteria in each scaffold, the value of CFU/mL was determined. The bacterial cell count data was reported in the surface area unit of the plastic films (CFU/cm^2) and used to estimate the bacterial biomass associated with the plastics.

4.6 Characterization of bacterial communities in plastisphere

4.6.1 DNA extraction from bacterial biofilm

Bacterial DNA extraction was performed from biofilm formed on PDLLA/PLLA and PLLA scaffold after 60 and 120 days of exposure to the marine environment and from PHA/PHB and PHB scaffolds, after 60 days of incubation in microcosm using QIAamp® DNA STOOL HANDBOOK kit (Qiagen, Hilden, Germany). The DNA extraction was performed according to the manufacturer's instructions, except in the first and last step. In the first step, 2 mL of Buffer ASL (Stool lysis buffer) were distributed over the entire surface of the plastic covered by the biofilm. To facilitate the detachment of the biofilm from the plastic and bring it into solution, the surface of the plastic was scraped with a sterile scalpel until all the biofilm was removed. The buffer and suspended biofilm were collected and

transferred to a 15 mL tube. With tweezers and a sterile scalpel, the plastic was cut into small pieces and then transferred into the same tube with the tweezers. Then the whole was vortexed for 1 minute and the suspension thus obtained was collected and transferred into 2 mL tubes and then heated for 5 min at 95°C. The solution was briefly vortexed and then centrifuged at 14,000 rpm for 1 min to separate the supernatant from the pellet. The supernatant was transferred and then recovered in new 2 mL microcentrifuge tubes. To elute the DNA, 30 μL of ultrapure water RNase Free and DNase Free was added directly to the membrane of the QIAamp column. After incubation for 1 min at room temperature they were centrifuged at 14,000 rpm for 1 min. Then another 20 μL of H_2O RNase Free and DNase Free were added and then centrifuged for 1 minute at 14000rpm. A second elution as described above was performed for each sample. The NanoDrop ND-1000 Spectrophotometer (NanoDrop Technologies) was used to verify the concentration and quality of the DNA and DNAs were stored at -20 °C until further analysis.

4.6.2 Sequencing of bacterial biofilm

The DNA extracted by the method described in section 4.6.1 was used to amplify the V3-V4 hypervariable region of the 16S rRNA gene of bacteria and archaea by PCR (**Figure 12**).

Amplification was performed using the primers modified with universal tails:

- ❖ Pro341F (5′-CCTACGGGNBGCASCAG-3′)
- ❖ Pro805R (Rev 5′-GACTACNVGGGTATCTAATCC-3′)

(Takahashi et al., 2014)
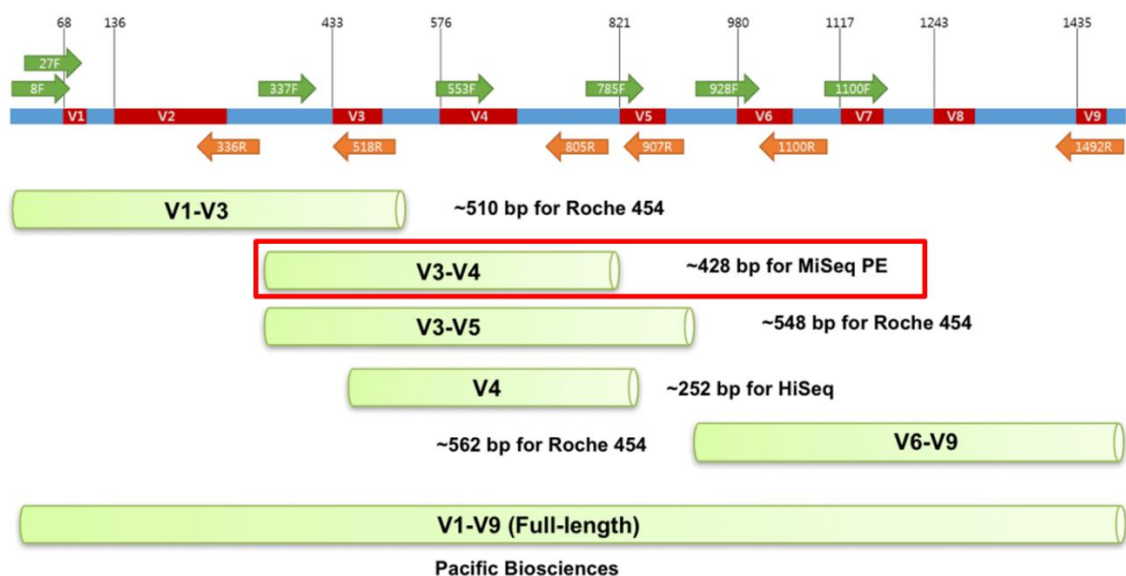
Figure 12 – Primer sets for amplification of V3-V4 region of bacteria and archaea (EZBioCloud, 2019)

PCR amplification was performed in 20 μl reaction volume with 0.1μl of "One Taq" Taq polymerase (Biolabs), 1X One Taq Buffer standard, 0.2 μM of each primer, 0.2 mM of dNTPs and 10 ng of template DNA.

The PCR procedure was as follows:

❖ an initial denaturation at 94°C for 30 s;

❖ 30 cycles of denaturation 94°C for 30s, annealing 55°C for 1min, and extension 68°C for 30s;

❖ a final extension at 68 °C for 5 min.

The 16S-PCR amplification products were separated by electrophoresis on a 1.5% agarose gel. 30 µL of each sample having a minimum concentration of 5 ng/µL were sent to BMR Genomics (Padova, Italy) for sequencing, performed using the Illumine MiSeq PE300 platform. The quality of the sequences was verified using the FastQC software. Furthermore, through the tools of the Qiime2 bioinformatics platform (Bolyen et al., 2019) version 2021.4.0 the following were performed:

❖ The removal of adapter sequences, primers, poly-A tails, and other types of unwanted sequences from high-throughput sequencing reads (Cutadapt tool).

❖ Read denoising, including read quality filtering and trimming, error rate estimation, dereplication, read merging, and chimera detection (DADA2 tool).

❖ Features filtering (0.01%) and singletons discarding.

❖ Taxonomy assessment using trained sequences (99% OTUs) from Silva database version 138.

❖ Definition of the taxonomic table.

4.7 Microcosms set up

Two different types of microcosms were prepared: the first was prepared inoculating the bacterial biofilm recovered from the surface of the PDLLA/PLLA and PLLA scaffold after the exposure period of 60 and 120 days in a marine environment, into 100 mL of sterile natural seawater containing sterile PDLLA/PLLA or PLLA scaffolds. The second type of microcosms, , was prepared by placing sterile scaffolds of PHA/PHB or PHB in sterile PHA/PHB in 100 mL of non-sterilized natural seawater.

Negative controls were carried out both by placing sterile fractions of the different types of scaffolds in sterilized seawater without bacterial inoculum (C^{-bio}), and by inoculating the biofilm biomass recruited from the marine environment in sterilized seawater, but without

placing any biopolymer (C^{-pol}). The microcosms, and their respective negative controls, were incubated at 30°C for 60 days. At the end of the exposure time in the microcosm, the biofilm recovered from the biopolymer fractions was used for the isolation and identification of potential biodegraders bacteria. The residual liquid medium of the microcosms was stored at -20°C for subsequent chemical analyses.

4.7.1 Isolation of potential PHAs and PLA degrading bacteria

After 60 days in microcosms, bacterial biofilm was recovered from surface of the scaffolds to isolate and identify bacteria able to growth in presence of plastic as unique carbon source. The biofilm was recovered using the same procedure described in 4.4 paragraph.Serial dilutions were made (10^{-2} and 10^{-3})and aliquot of 100 μL of each dilution was cultured in a solid ONR7a mineral medium (Dyksterhouse et al., 1995), containing PLA and PHA/PHB polymers as unique carbon source. Solid ONR7a medium with polymer were performed using the Double-layer plaque assay technique (DLA) (Tavares da Silva et al., 2021). According to this technique, the plates are made with a support bottom layer of ONR7a medium (about 20 mL), and an overlying layer (about 5 mL) is added above it, at a biopolymer concentration of 0.2% w/v, as reported in **Figure 13**.
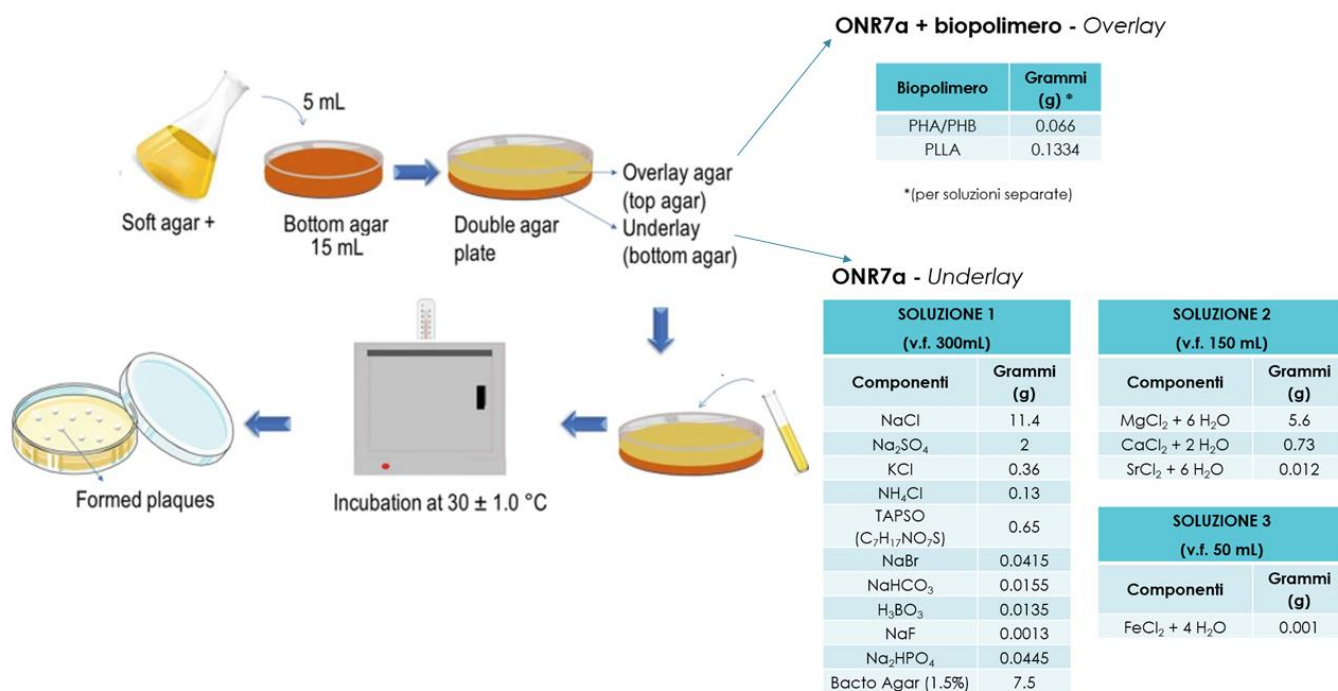
Figure 13 - Double-layer plaque assay technique (DLA) used to prepare ONR7a medium and biopolymers (Tavares da Silva et al., 2021)

As a negative control, the dilutions were grown on ONR7a medium devoid of any carbon source. The plates were incubated at 30°C for about 5-7 days. The possible presence of

degradation halos on the overlayer was an indication of the presence of potential microorganisms that degrade the biopolymeric materials. From the observation of the plates, the different phenotypes were identified (based on the color, shape, size, edges, and appearance of the colonies). Two single colonies for each phenotype were collected and smeared onto a fresh ONR7a medium to obtain a pure culture.

4.7.2 Identification of potential PHAs and PLA degrading bacteria

The isolates identified as degraders of bioplastic materials were identified by amplification and sequencing of 16S rDNA. Each colony was taken from ONR7a plates in which they were isolated in pure culture by the colony picking method and transferred into 25μL of TE Buffer. The colonies were then subjected to cell lysis by thermal shock (5 minutes at 100°C, 5 minutes on ice, and 5 minutes of centrifugation at 14,000 rpm). The bacterial lysate was used as a template for the 16S rDNA amplification reaction using primers 27F and 1492R (Frank et al., 2008). Amplification was performed in 30 μL final volume, using 1X Buffer Standard One Taq (Biolabs, New England), 200mM dNTPs, 0.2 μM primers 27F and 1492R, One Taq polymerase 1 U and 1μl bacterial lysate.
DNA was amplified under the following conditions:

- ❖ an initial denaturation at 94°C for 30 s;
- ❖ 30 cycles of denaturation 94°C for 30s, annealing 50°C for 60s, and extension 68°C for 90s;
- ❖ a final extension at 68 °C for 5 min.

The amplification products of the 16S rDNA gene were analyzed by 1% agarose gel electrophoresis and sent to BMR Genomics (Padova, Italy) for sequencing. The 16S rDNA products of PCR were prepared following the company's instructions: 20 ng/μl of amplified with 10 pmol/μl of primer 1492R. The nucleotide sequences obtained were processed using the NCBI program Nucleotide-BLAST and MEGABLAST ("Highly similar sequences") and compared with those present in the NCBI GenBank database: "Nucleotide Collection (non-redundant nucleotide - nr/nt)" and "16S ribosomal RNA sequences".

4.8 Chemical Analysis

4.8.1 Sample preparation: SPE extraction and purification

All SPE cartridges were conditioned with a volume of methanol and then equilibrated with a volume of water. The seawater samples were acidified with 0.1% v/v formic acid (20

µL in 20 mL of seawater sample). Each sample was automatically transferred to the top of the cartridge. After the sample passed through, each cartridge was rinsed several times with ultrapure water to remove salts naturally present in seawater. In the final step, the sample was eluted in methanol with a final volume of 6 mL, and the eluate was stored in the freezer at -20°C until mass spectrometry analysis.

4.8.2 Identification of degradation products in microcosms using mass spectrometry: A comprehensive analysis

The analysis was performed using an UHPLC separation module coupled with a Q-Exactive Orbitrap MS model via an ESI probe for electrospray ionization set in negative ion mode. The ion source and interface conditions were as follows: spray voltage -3.0 kV, sheath gas flow rate 30, auxiliary gas flow rate 15, and heater and capillary temperature 300 °C. A Luna Omega Polar C18 column (100 x 2.1 mm, 3 µm) was employed for separation at a flow rate of 0.3 mL/min. The eluents used were 0.01% HCOOH in Milli-Q water (solvent A) and CH_3OH (solvent B). The samples were separated by UHPLC using the following elution gradient: 0% B for 4 min, 0–15% B in 6 min, 15–20% B in 5 min, 20% for 13 min, and then returning to initial conditions in 1 min. The column and samples were maintained at 30 °C. The UHPLC eluate was subjected to full scan MS analysis in the range of m/z -50 to 400 u. The MS data were processed using Xcalibur software.

4.9 Immunobiological investigations

Immunobiological investigations on the effects caused by exposure to micro and nanoparticles of bioplastic material on *Mytilus galloprovincialis* were conducted through *in vitro* and *in vivo* analyses (**Figure 14).**
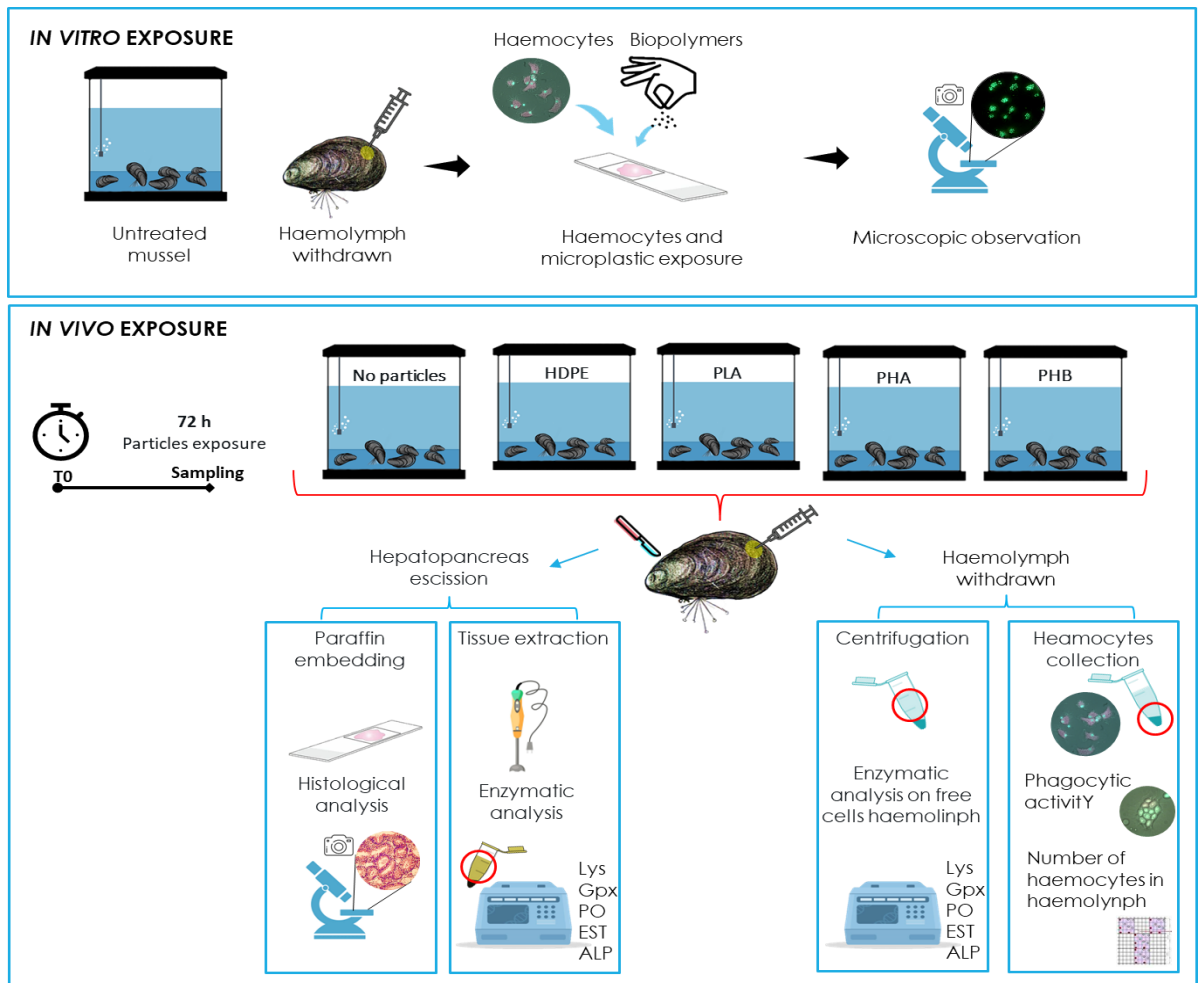
Figure 14 - Schematic representation of the experimental design on the part of the project concerning ecotoxicological investigations.

4.9.1 Mussels in vitro particles exposures

4.9.1.1 Haemolymph collection

Mussels (5-6 cm long) were kept in tanks with water [dissolved oxygen (DO) 8 mg L^{-1}; salinity 28‰; temperature 18 ± 2 °C]. Following the procedure described by Parisi et al. (2021), the haemolymph, containing the haemocytes, was drawn (800 µL for each mussel) from the posterior adductor muscle with a 1 mL sterilized syringe containing Alsever solution anticoagulant (200µl; $Na_3C_6H_5O_7$, 27 mM, d-Glucose 115 mM, NaCl 336 mM, EDTA 9 mM) and placed in plastic tubes. Haemocyte count was carried out using the Neubauer chamber and adjusted to 1×10^6 cells/mL for each sample. After centrifugation (1000×g; 10min; 4 °C), the haemocytes were resuspended in the same volume of synthetic marine solution (MS) (12 mM $CaCl_2$; 11 mM KCl; 26 mM $MgCl_2$; 45 mM Tris(hydroxymethyl)aminomethane; 38 mM HCl; 0.45 M NaCl; pH 7.4) (Parisi et al., 2021).

45

4.9.1.2 Polymer microplastic suspension

Microparticles have been sieved to have a maximum dimension of 150 μm, and successively suspensions were prepared in synthetic marine solution (MS) at the concentration of PHB at 1.25 mg mL^{-1}, PLA at 16.66 mg mL^{-1} and PHBV_GF at 50 mg mL^{-1}. After preliminary tests, these concentrations were established in order to carry out the investigations with a correct relationship between polymer and cells, thus guaranteeing correct cellular activity.

4.9.1.3 Yeast preparation

A positive control phagocytosis assay was carried out by using yeast *Saccharomyces cerevisiae* (Sigma), as a target (Parrinello et al. 2017). The yeast suspension (0.25%; w/v) was prepared in distilled water (1×10^7 cells mL^{-1}), autoclaved for 15 min, washed twice (2000×g, 5 min, 4 °C), and incubated with eosin Y (4-Bromo-fluorescein) for 1 h at 20 °C to a final concentration of 0.05%. The yeast cells were washed four times and resuspended to a final concentration of 0.125% (w/v) in PBS and stored at 20 °C.

4.9.1.4 Viability and cell morphology

After collection, the haemocytes were placed on glass slides and their morphology was observed under Nomarsky differential interference contrast microscopy (Diaplan, Leika, Wetzlar). The morphology and phagocytic activity were observed by comparison to the shape of the haemocytes kept in MS (Cell control). Cell morphology and viability were revealed by the Acridine Orange Hydrochloride (AO) (Fluka BioChemika, Buchs, Switzerland) staining.

4.9.1.5 Phagocytosis in vitro assay

Haemocytes were placed on microscope slides and incubated in a humid chamber for 15 minutes to allow cellular adhesion. After incubation, on the cells were layered the yeast and/or the bio-plastics suspension to stimulate cellular activity. After 2 h of incubation at dark and at 20°C the slides were observed by Nomarski differential interference contrast optics and fluorescent apparatus (450–490-nm filter) (Diaplan, Leika, Wetzlar, D). The data of phagocytosis are expressed as percentual of phagocyting cells on the total cells.

4.9.2 Mussels in vivo particles exposures

Mussels *M. galloprovincialis* (5–6 cm long) were kept in tanks (15 L) with water (dissolved oxygen (DO) 8 mg L^{-1}; salinity 28‰; temperature 20 ± 2 °C). Specimens were exposed for 72 h at different conditions and type of plastic particles. One tank control condition without plastic particles, and 4 experimental tanks each one with a different plastic (2 mg/L for each): High Density Polyethylene (HDPE) as conventional plastic based on petroleum, PHA, PHB, and PLA. Experiments were carried out in duplicate (two tanks for each condition).

4.9.2.1 Plastic count

Particles were observed on pictures took through light microscopy and counted by image processing scientific software Fiji ImageJ measuring the longest diameter of each particle (Schneider et al., 2012).

4.9.2.2 Haemolymph collection

The haemolymph was extracted (1000 µL for each animal) from the posterior adductor muscle with a 1 mL sterilized syringe containing Alsever solution anticoagulant (200 µl; $Na_3C_6H_5O_7$, 27 mM, d-glucose 115 mM, NaCl 336 mM, EDTA 9 mM) and placed in plastic tubes. For lysozyme analysis the haemolymph was centrifuged (1000×g; 10min; 4 °C) discharged the pellet and kept the supernatant.

4.9.2.3 Total cells count

The haemolymph, containing the haemocytes, after being drawn (1 mL) by syringe from the posterior adductor muscle with a 1 mL and placed in plastic tubes. An aliquot was placed in a counting chamber. Haemocyte count was carried out using the Burker chamber (Superior Marienfeld, Lauda-Königshofen, Germany). Counts was carried out counting the number of cells in 4 squares (0.0025 mm^2) and performed in duplicate for each sample.

4.9.2.4 Extract preparation and protein concentration

The digestive gland was removed from five mussels for each experimental groups and were subsequently transferred into polycarbonate tubes with 500 µL TBS-buffer (NaCl 150 mM, Tris-HCl 10 mM, pH 7.4) on ice, then the resultant tissue slurry was centrifuged (22,500 rpm for 20 min at 4°C). The supernatant was collected, and protein concentration

measurement was conducted according to the method found in Bradford (1976). The sample absorbance was read at 595 nm (RAYTO RT-2100C) with TBS as blank, and a calibration curve defined through Bovine Serum Albumin (BSA) was used to obtain protein concentration expressed in mg/mL. Extracts were adjusted at 0.5 mg/mL before performing enzymatic assays.

4.9.2.5 Phenoloxidase (PO) assay

Phenoloxidase activity was measured spectrophotometrically according to Winder and Harris (1991), by using L-Dopa (3,4 dihydroxy-L-phenylalanine; Sigma-Aldrich, USA) as substrate and 6 mM MBTH (3-methyl-2 benzothiazolinone hydrazone hydrochloride; Sigma-Aldrich, USA) as a specific reagent. 50 μL of coral sample with 50 μL of trypsin from bovine pancreas (1 mg/mL; Sigma-Aldrich, USA) or 50 μL of distilled water as control, were incubated for 20 min at 20°C in 50 μL reaction mixture (20 mM L-DOPA and MBTH in distilled water). The absorbance was read within 60 min at 5 min intervals by spectrophotometric measurement at 505 nm. Phenoloxidase activity was expressed as units (U) per min where $1\,U = 0.001\,\Delta A540\,min^{-1}\,mg^{-1}$ protein.

4.9.2.6 Glutathione peroxidase (GPx) assay

Enzymatic activity was measured according to Ross et al. (2000). In 96-well flat-bottomed plates, 50 μL of sample at standard concentration (0.5 mg/mL) was incubated with 100 μL TMB (3,3′ 5,5′-tetramethylbenzidine; Sigma-Aldrich, USA). The reaction was stopped after 30 min of dark incubation with sulphuric acid (H_2SO_4) 2 M. The absorbance was read spectrophotometrically at 450 nm in a microplate reader (RT-2100C) and the Glutathione peroxidase produced was expressed in U/mg of protein according to the equation: U/mg = Abs * Vf / CP (Vf, final volume of the well; CP, protein concentration of the sample).

4.9.2.7 Lysozyme (LYS) assay

Lysozyme activity was measured using a turbidimetric assay modified for microplate reader (Sutton et al. 2006). In a suspension (0.025% in phosphate buffer 0.06M, pH 6.2) was measured the reduction of *Micrococcus lysodeikticus* (Sigma–Aldrich, St. Louis, MO, USA) at 450 nm. Absorbance was measured before and after the incubation (20 min at 37°C). The results were expressed as $U\,mg^{-1}$. A unit of LYS was defined as the amount of sample causing a decrease in absorbance of 0.001/min ($U\,min^{-1}$), and U/mL was calculated in

accordance with the formula: U/mL = (Δ abs/min^{-1} * dilution factor * 1000) / enzyme volume buffer.

4.9.2.8 Alkaline phosphatase (ALP) assay

Samples were incubated in a 96-well flat-bottomed plate with an equal volume of 4 mM p-nitrophenyl phosphate substrate (Sigma-Aldrich, USA) liquid in 100 mM ammonium bicarbonate containing 1 mM MgCl$_2$ (pH 7.8). The enzymatic kinetic was evaluated according to Ross et al. (2000) at regular intervals of 5 min to 1 h at 405 nm with a microplate reader (RAYTO RT-2100C). One unit (U) of activity was defined as the amount of enzyme required to release 1 µmol of p-nitrophenol produced in 1 min.

4.9.2.9 Esterase (EST) assay

The Esterase activity was evaluated according to the method of Ross et al. (2000), the same volume of coral sample was incubated with 0.4 mM p-nitrophenyl myristate substrate (Sigma-Aldrich, USA) in 100 mM ammonium bicarbonate containing 0.5% of Triton X-100 (pH 7.8, 30°C; Sigma-Aldrich, USA). The increase of the optical density and the determination of the activity were evaluated as for alkaline phosphatase.

4.9.2.10 Histological analysis

Digestive gland of mussels was fixed in a solution of paraformaldehyde (PFA) 4% in phosphate buffered saline (PBS) 0.1 M, pH 7.4 at 4 °C, for 4 h. Thereafter, tissue was dehydrated in increasing concentrations of ethanol (50%, 70%, 80%, 95% and Ethanol absolute by Sigma Aldrich), cleared with xylene and embedded in Paraplast (Bio-Optica, Italy). Histological sections (7 µm thickness) were prepared using a rotary automatic microtome (Leica Microsystems, Wetzlar, Germany), rehydrated in decreasing grades of ethanol (Ethanol absolute by Sigma Aldrich, 95%, 80%, 70%, 50%, 35%) and stained using the haematoxylin–eosin (H&E) method to evaluate morphological features. Digestive glands sections were then mounted by Eukitt (Bio-Optica, Milano, Italy) and observed using the objective 25x of Nikon Digital Sight DS-SM optical Microscope (Nikon, Tokyo, Japan).

*4.9.2.11 Statistical analysis*

Statistical analyses were performed using the Graphpad Prism 8.0.2 software. An ANOVA test, followed by a Tukey's multiple comparisons test, were performed to assess differences in the various group.

# 5 – RESULTS AND DISCUSSIONS

5.1 Preliminary analysis on scaffolds

FT-IR analysis and SEM observations were carried out to evaluate the conditions of the biopolymer scaffolds made using the TIPS method. By analysing the FT-IR spectra obtained for the PDLLA/PLLA scaffolds and PLLA, together with their respective references, it can be stated that no shifts of the peaks, or variations in the ratios between them, are observed. In the spectrum of the scaffold constituted by the PHA/PHB mixture (spectrum in red, **Figure 15**), a trend of the peaks analogous in part to those of the reference PHA 0 (spectrum in blue, **Figure 15**) and in part to those of the spectrum of the reference PHB 0 (spectrum in violet, **Figure 15**) can be seen, confirming the co-presence of the two materials constituting the structure. In particular, in the spectrum of the scaffold made up of PHA/PHB compared with the spectrum of the reference polymer PHB 0, a slight broadening to the left of the carbonyl peak (1721 cm^{-1}, **Reference 1**, **Figure 15**) and a slight increase of the absorbance of the peak referable to the bending of -CH (1453 cm^{-1}, **Reference 2**, **Figure 15**) and of the peak referable to the stretching of the -CO ester (1183 cm^{-1}, **Reference 3**, **Figure 15**). Those trends are instead observable in the homologs at the same wavelength as the PHA 0 reference spectrum. This can possibly be linked to the presence of PHV both in the PHA/PHB scaffold and in the PHA 0 reference.
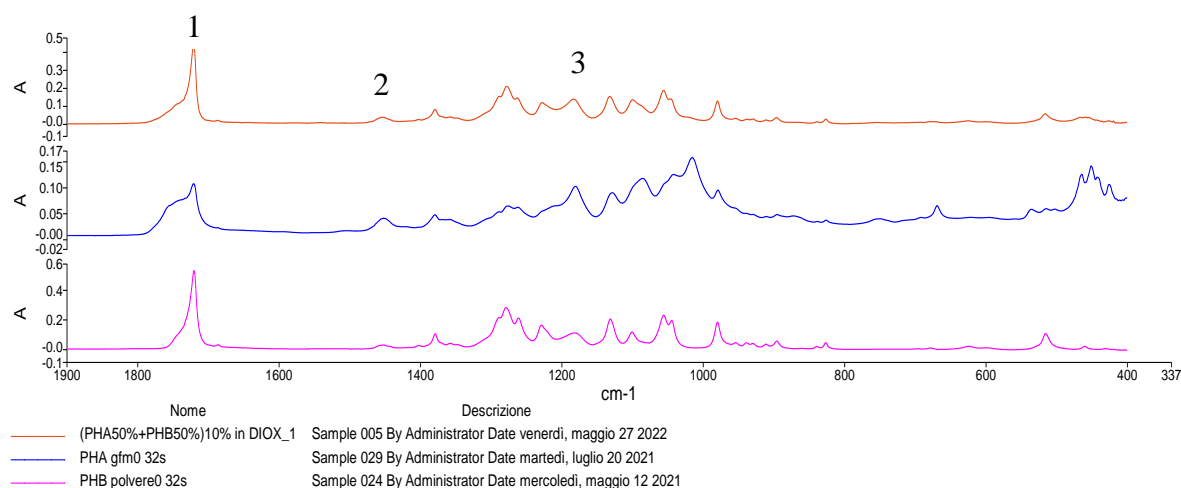
Figure 15 - Comparison of the FT-IR spectra obtained for the scaffold PHA/PHB 10% in dioxane (red spectrum), for the 0 PHA reference sample (blue spectrum), and the 0 PHB reference sample spectrum (spectrum in purple)

As a further preliminary analysis, we wanted to verify the actual porosity condition that we obtained for the scaffolds by means of SEM observations. Each scaffold analyzed showed a highly porous internal microstructure, lamellar type for scaffolds made in PDLLA/PLLA,

and honeycomb type for scaffolds made in PLLA and PHA. This structure is defined by the technical term "Ladder-like" (Sofokleous & Panagiotis, 2018; Goh & Ooi, 2008). Observing the section of the PDLLA/PLLA scaffolds, the lamellae appear of regular dimensions, with an amplitude of about 4 - 6 µm and a width of 40 µm (**Figure 16a**), with a constant orientation of about 45°, while the section of the scaffold in PLLA alone shows pores with a width between 7 - 13 µm (**Figure 16b**). In both samples, the surface of the individual lamellae is porous, confirming the presence of interconnections between the channels of the microstructure.
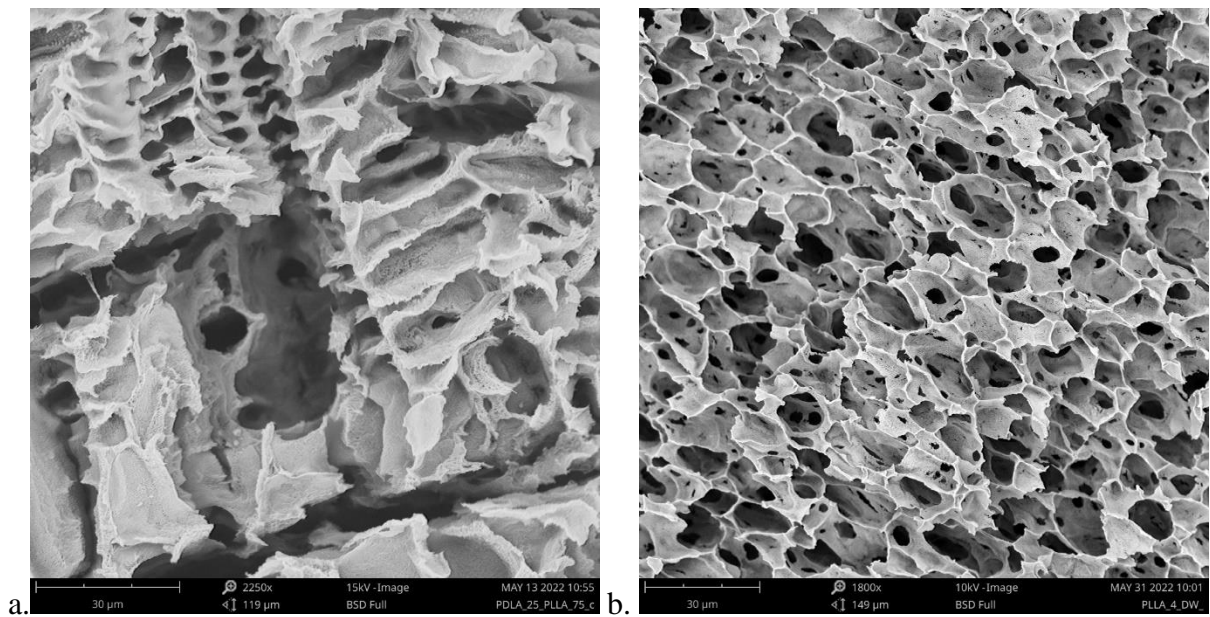
Figure 16 – SEM observation of the section of the PDLLA/PLLA scaffold (a. – 2250x; 15 kV) and of the PLLA scaffold (b. – 1800x; 10kV)

The SEM observation of the section of the scaffold made up of the PHA/PHB biopolymer mixture also showed a "Ladder-like" trend (Sofokleous & Panagiotis, 2018; Goh & Ooi, 2008), but with alveoli of the surfaces of the lamellae of greater width and with a greater number of interconnections of the channels compared to the PLA samples. Furthermore, granules of PHB powder not solubilized in dioxane are observed, integrated into the lamellar microstructure constituting the section of the scaffold (**Figure 17**).
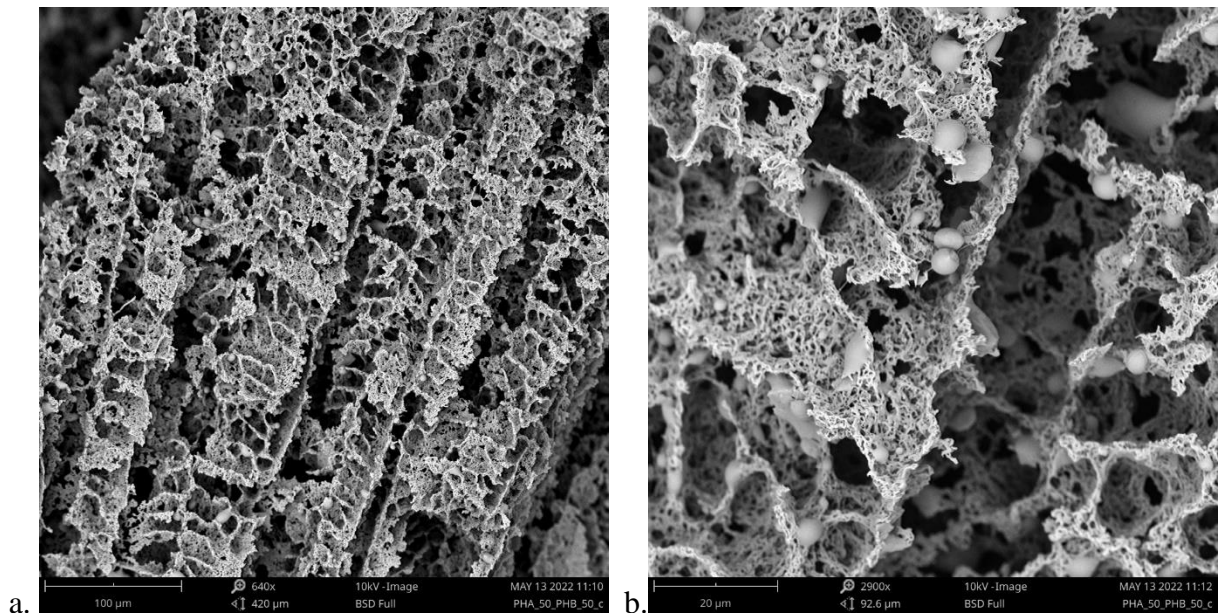
Figure 17 − SEM observation of the section of the PHA/PHB scaffold (a. – 640x; 10kV) (b. – 2900x; 10kV)

Scaffolds with a high degree of porosity were obtained, the large available surface area of which was found to be suitable for allowing the recruitment of biomass from the marine environment and for subsequent studies that were carried out with these scaffolds in the laboratory.

**5.2 Bacterial biomass recovered from the surface of biopolymers exposed in the sea**

Upon first sample recovery at the end of exposure time t_1 (60 days) (**Figure 18a**), total loss of all PHA/PHB scaffolds (including those expected to be recovered at time t_2 – 120 days) was observed. On the other hand, it was possible to recover both types of PLA scaffolds intact both at time t_1 and at time t_2 (120 days), which showed evident animal and plant colonization (**Figure 18a**, **Figure 18b**, **Figure 18c**). It was therefore possible to quantify the adhered biomass only for the PLLA/PDLLA and PLLA scaffolds.
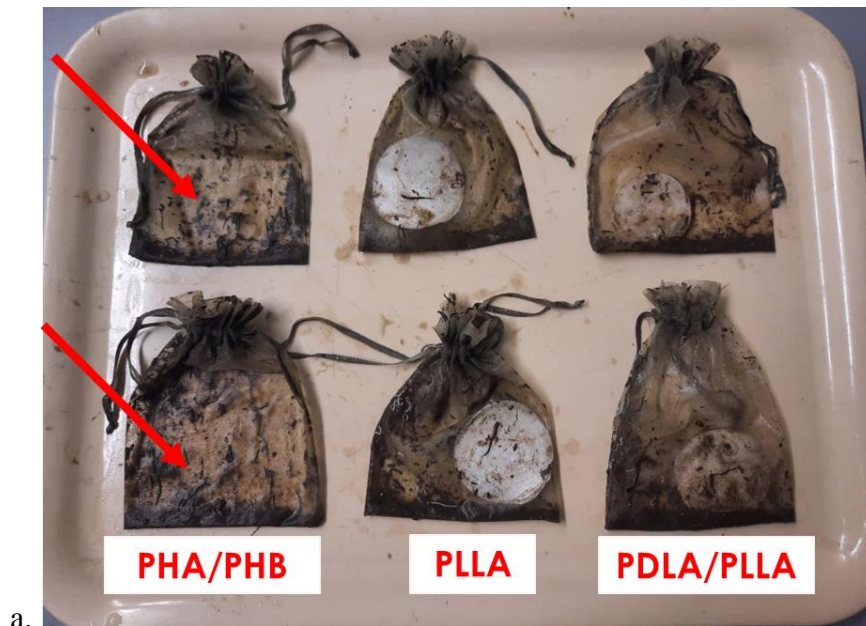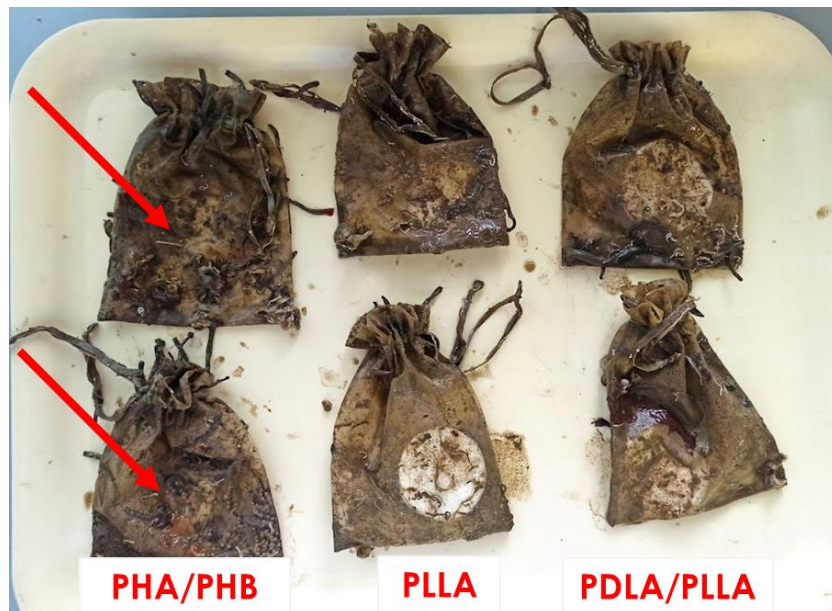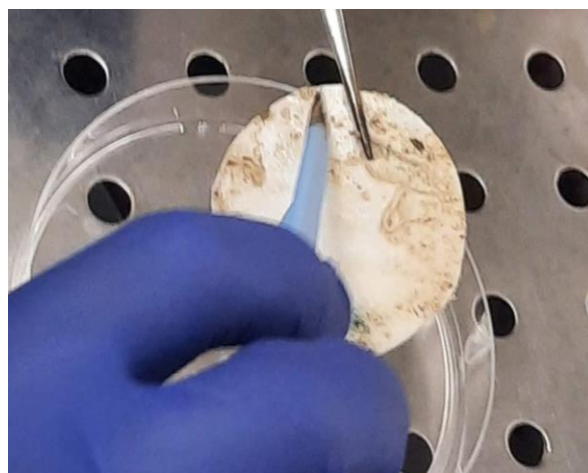
Figure 18 - (a) recovery of the biopolymer scaffolds after 60 days (t_1)

and (b) after 120 days (t_2) exposure in marine environment.

(c) conditions of a PLLA scaffold (sample B60) after recovery at time t_1 (60 days)

The biomass adhered to the surface of the PLLA and PDLLA/PLLA scaffolds was collected and quantified using the viable plate count method and using total soil dsDNA as a proxy The CFUs detected for the PDLLA/PLLA scaffolds at period t_1 and period t_2 (**Figure 19**) were 1.2×10^6 CFU/cm^2 and 1.3×10^5 CFU/cm^2, respectively. For scaffolds only in PLLA, on the other hand, the values respectively recorded were 6.5×10^5 CFU/cm^2 and 5.2×10^5 CFU/cm^2 respectively at period t_1 and period t_2. The biomass loss observed for both samples in the two sampling times was also confirmed by the results given by the quantification of the extracted metagenomic DNA, always related in terms of scaffold surface area (ng/cm^2).
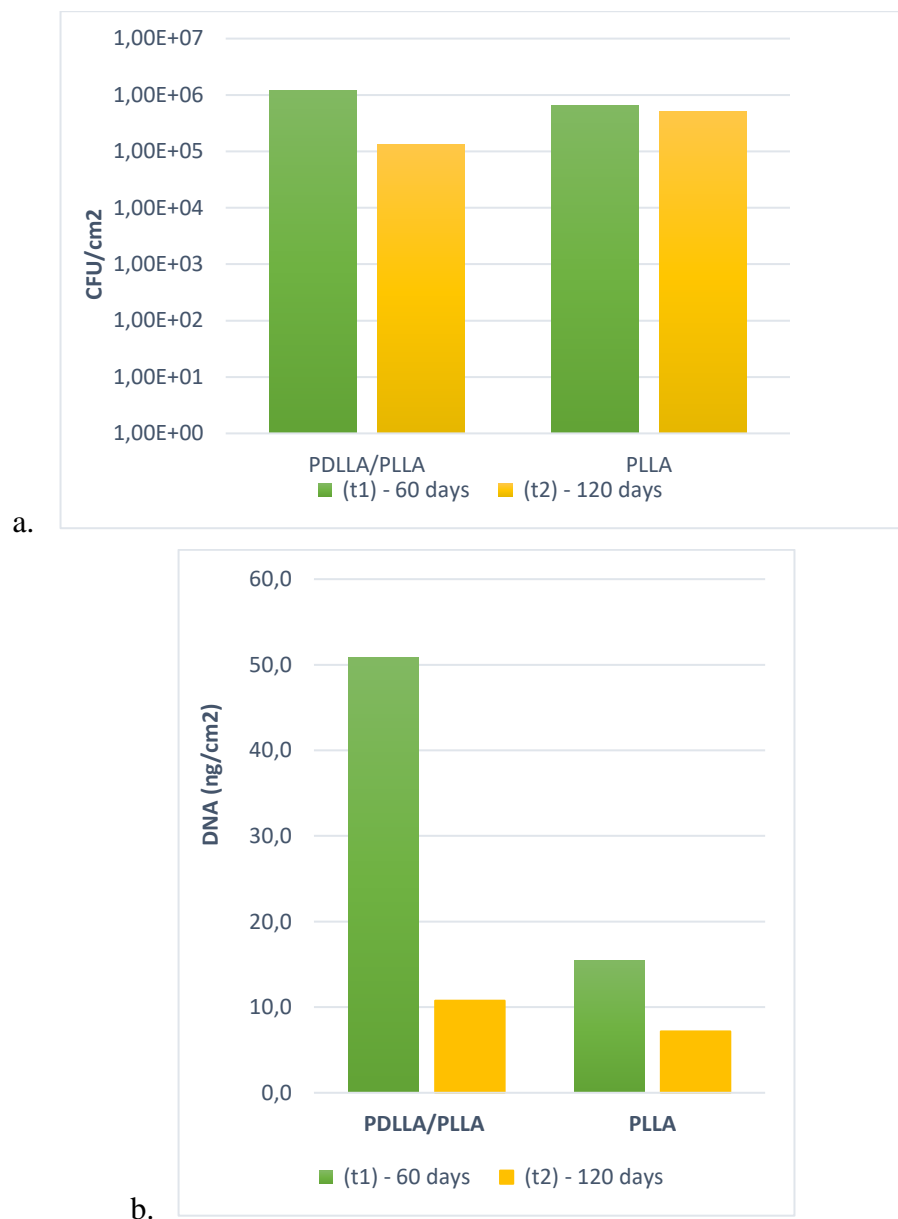
Figure 19 – Microbial biomass adhered to biopolymer scaffolds estimated as bacterial CFU/cm^2 (a) and as the quantity of metagenomic DNA (ng/cm^2) (b) after a period of 60 and 120 days of exposure at 9 m depth in the marine environment

The difference in the quantities of biomass detected at the end of the two exposure times could be due to seasonal fluctuations which strongly influence the structure of the biofilms, since the first exposure period took place in the period between July and August 2022, while the 120 days exposure lasted until October 2022 (Syranidou et al., 2017). A hypothesis that can be put forward to try to understand the differences detected not only at times t_1 and t_2, but also between the two polymers, could be that since the PDLLA/PLLA scaffolds contain a percentage of amorphous substance equal to 25% of the total polymeric content, this could have favored the adhesion of a greater microbial component capable of degrading it. Furthermore, it is assumed that at the end of the 120 days of exposure, the degradable component had been reduced by the action of some microorganisms present in the biofilm, with a consequent reduction in the attracted biological component (Rosli et al., 2021).

5.3 Bacterial biofilms adhered to PHAs and PLA bioplastics

The marine bacterial community forming a biofilm on PLLA and PDLLA/PLLA scaffolds after 60 and 120 days of exposition in the sea, and on PHA/PHB and PHB scaffolds after 60 days in microcosm with seawater non-sterilized, was characterized by Next Generation Sequencing (NGS). Since it was not possible to recover the samples in PHAs following field tests, the DNA was extracted from the biofilms developed following the microcosm tests with non-sterilized seawater. The number of reads and OTUs (Operational Taxonomic Unit) identified for each sample are shown below in **Table 2**:

Table 2 - The number of OTUs and Reads detected by NGS in the plastisphere of bioplastic samples at the end of the field and microcosms experiment

Scaffold typology	Sample name (BMR Genomics sample code)	Biomass recruitment	Exposition time (days)	Final Reads	OTUs
PDLLA/PLLA	A60	Field Experiment	60	57179	1230
PDLLA/PLLA	A120	Field Experiment	120	51037	942
PLLA	B60	Field Experiment	60	50877	815
PLLA	B120	Field Experiment	120	60099	1155
PHA/PHB	C60	Microcosm	60	54826	358
PHB	D60	Microcosm	60	41512	206

From an initial analysis of the results obtained, a variation in terms of composition and abundance of the microbial communities adhering to the biopolymer surfaces of the PLA samples was observed with the extension of the exposure time in the marine environment. In particular, the greatest diversity in terms of composition is observed for PDLLA/PLLA samples after 120 days of exposure. The biofilms recovered from the surfaces of the PHAs scaffolds following a 60 days exposure in the microcosm showed less biodiversity than the other types of bioplastics. In particular, the least diversity was observed in PHB scaffolds.

The results of the metagenomic analyses show the prevalence of the Bacteria domain (**Figure 20**): the percentages of the presence of this domain were between 97.7% and 99.5% for the samples exposed in the marine environment, while they were 100% for both PHAs samples exposed to the biomass present in microcosm. The *Archaea* domain (**Figure 20,**) was present only in the PLA samples exposed after 60 and 120 days, (0.5% - 2.4% respectively).
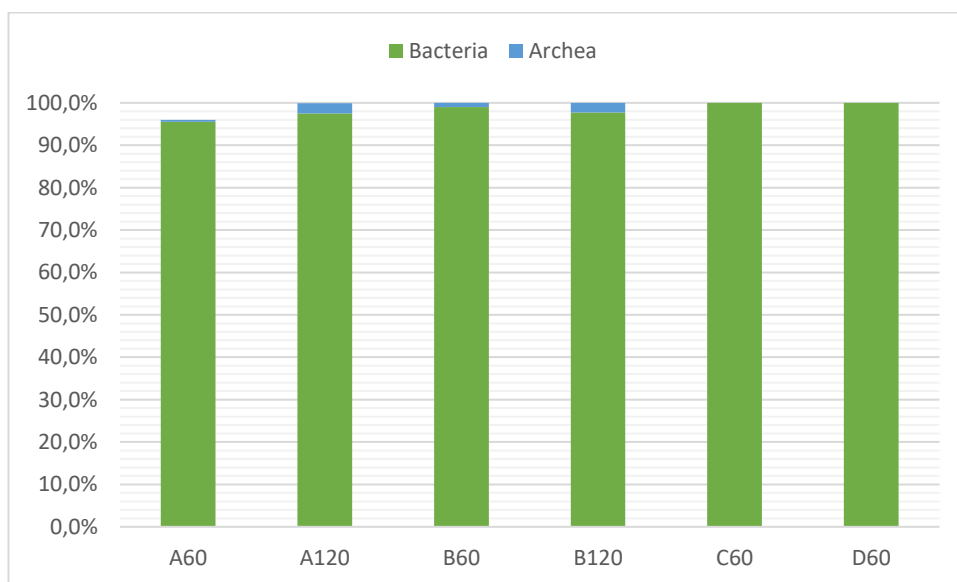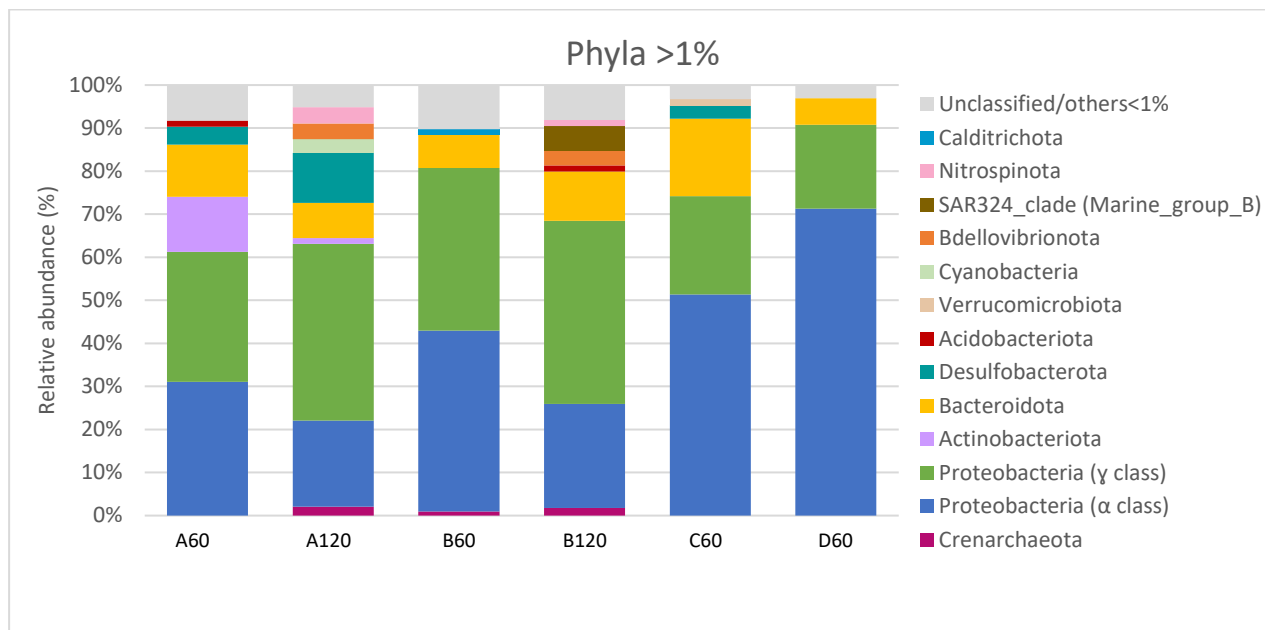

Figure 20 – Relative abundances (%) of domains from biofilms
of PDLLA/PLLA (A60 and A120), PLLA (B60 and B120), PHA/PHB (C60) and PHB (D60) scaffolds
after 60 and 120 days of exposure in a marine environment

The most abundant phylum for all samples was Proteobacteria (**Figure 21**), known to be the typical first surface colonizers in marine systems (Oberbeckmann et al., 2015). The presence of Proteobacteria belonging to alfa (α) and gamma (γ) classes was already observed after 60 days of exposure (both in the marine environment and in the microcosm) with a greater abundance in the PHB scaffold (equal to about 90% of the total community of the sample). This suggests a possible key role of α-Proteobacteria and γ-Proteobacteria in the biodegradation processes of PHB. For both samples from the scaffolds exposed in the sea, a

variation from the first sampling time (t_1) to the second sampling time (t_2) is observed. Indeed, after 60 days of exposure, a predominance of α-Proteobacteria was observed in all samples, suggesting a role in the initial stages of biodegradation. At the end of the 120 days of exposure in the sea, the number of α-Proteobacteria decreases and γ-Proteobacteria predominate, suggesting a role in the advanced stages. In addition to Proteobacteria, a high abundance of Actinobacteroidota and Bacteroidota was also observed in the biofilm from the PDLLA/PLLA scaffold, which decreases in terms of abundance with prolonged exposure. Furthermore, Bacteroidota is well represented also in the samples from microcosms. The predominance of the Proteobacteria, Actinobacteria, and Bacteroidota phyla is detected in other studies of plastisphere composition in marine environments (Huang et al., 2022; Sun et al., 2020). The Proteobacteria is the most abundant phylum associated with plastic waste worldwide (Roager & Sonnenschein, 2019) and members of these phyla are able to degrade organic compounds even of high molecular weight (Soleimani et al., 2021; Danso et al., 2018,). Recent studies have assigned gene sequences coding for PHA-depolymerase to the phyla Proteobacteria and Bacteroidota (Viljakainen & Hug, 2021), i.e., the enzyme that mediates the biodegradation of PHA. It is interesting to know that recent studies on the colonization sequences of the plastisphere have shown that in correspondence with the progressive increase of γ-Proteobacteria, a significant increase of Bacteroidota is observed (Wright, Langille & Walker, 2020).

In PDLLA/PLLA scaffolds Desulfobacterota phylum increased after 120 days of exposure to the sea compared to the sample of the same type of biopolymers analysed after 60 days of sea exposure. These are bacteria affiliated with the sulfate-reducing genera that have been identified in sulfate-rich sediments. (Vidal-Verdú et al., 2022). Instead, a particular trend is observed for the phylum Bdellovibrionota, which was detected only after 120 days of exposure both in the PDLLA/PLLA and PLLA scaffolds. This phylum was absent in the PHA/PHB and PHB scaffolds.
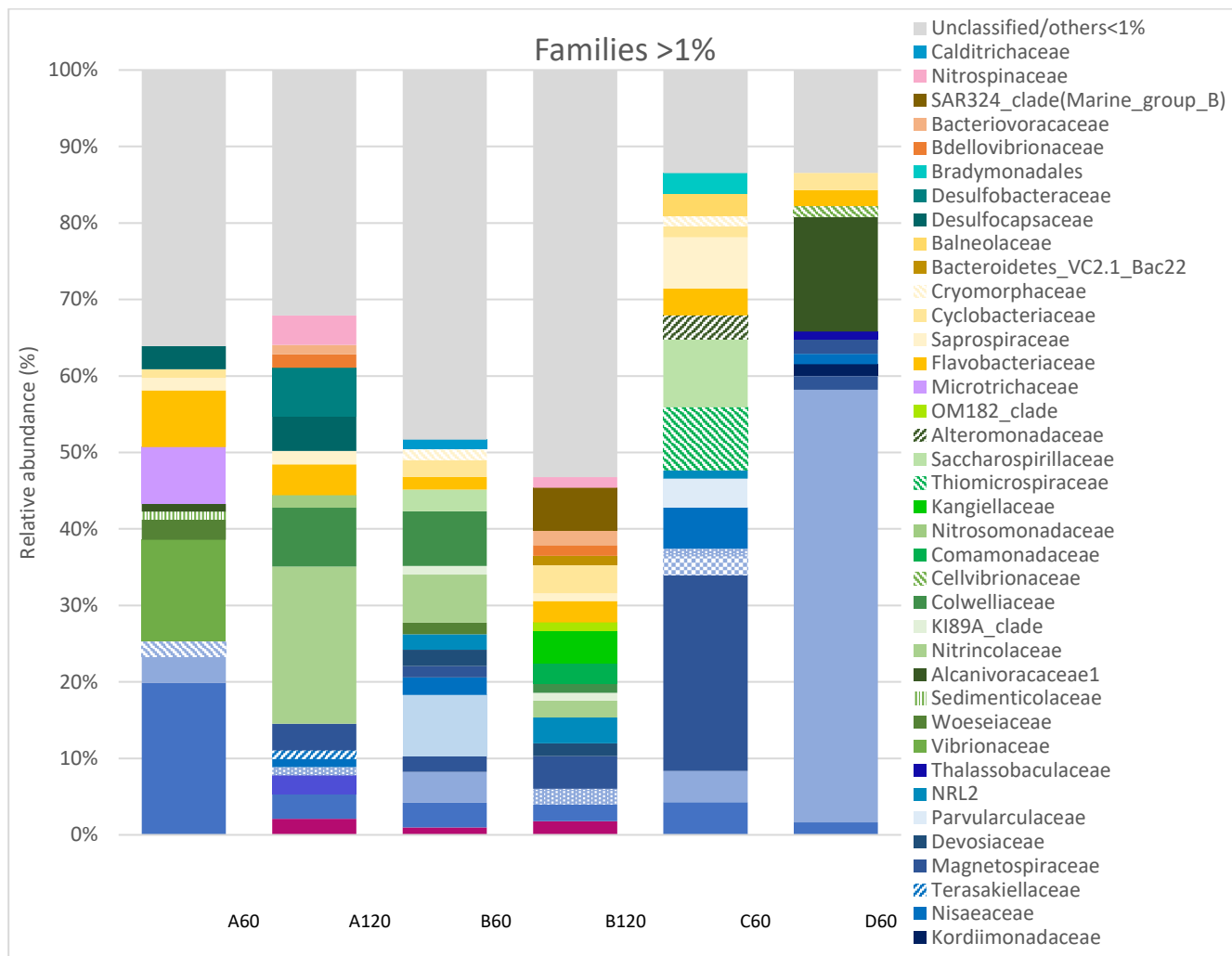
Figure 21 - Relative abundances (%) of phyla from biofilms of PDLLA/PLLA (A60 and A120), PLLA (B60 and B120), PHA/PHB (C60) and PHB (D60) scaffolds. For both the PDLLA/PLLA and PLLA samples, the abundances recorded after 60 (t_1) and 120 (t_2) days of exposure in the sea are reported, while for the PHA/PHB and PHB samples, the abundances recorded after 60 days of contact in microcosm with non-sterilized seawater (mt_1). Taxa $\geq$ 1% are shown. Unclassified/others includes unclassified taxa and identified taxa <1%.

At the family level, in the PDLLA/PLLA sample, a strong microbial succession is observed in terms of the abundance of families from the first to the second time (60 and 120 days) (**Figure 22**). It is evident how in the marine environment each plastisphere is different according to the type and composition of the biopolymers used to make the scaffolds, but also how as time increases the biofilm takes on a greater specificity depending on the substrate, and we observe mechanisms of microbial succession in the colonization processes of the microbial community. At the end of 60 days of exposure in the sea, a dominance of Rhodobacteraceae (19%) and Vibrionaceae (13%) was detected in PDLLA/PLLA sample. Rhodobacteraceae are associated with the plastisphere of HDPE (Girad et al., 2020), LDPE, and PET, and include members known to degrade complex carbon sources and hydrocarbon degraders bacteria (Delacuvellerie et al., 2019; Oberbeckmann et al., 2016). Furthermore, this family favors the formation of biofilms, plays an important role in several biogeochemical cycles, and being often a mutualist of eukaryotes, plays a crucial role in the succession of the microbial community on plastic surfaces (Bhagwat et al., 2021). The Vibrionaceae family is a ubiquitous family of potential animal and human pathogens, which do not contribute to the degradation of the substrate to which the biofilm adheres but take advantage of the adhesion to the plastic debris to increase their dispersion (Vidal-Verdú et al., 2022; Zettler et al., 2013). Their abundance could be since they have extremely rapid

growth (Delacuvellerie et al., 2019). At the end of the 120 days of exposure, the total disappearance of the Vibrionaceae and the drastic reduction of the Rhodobacteraceae (3%) was observed in the PDLLA/PLLA sample, while the dominant family became that of the Nitrincolaceae (20%) (**Figure 22**).

In PLLA scaffolds after 60 and 120 days of exposure, a high diversity of families with similar percentages of relative abundance was observed. The family of *Hyphomonodaceae* was detected with relative abundance of 25%; these are bacteria involved in the formation of marine biofilms and biofouling nucleators (Barreto Filho et al., 2021), as they produce long filaments called prosthecae and a polysaccharide matrix that allows them to adhere firmly to surfaces as primary colonizers (Abraham & Rohde, 2014). Furthermore, being strictly aerobic, the Hyphomonodaceae family prefers a position in the more superficial layers of the biofilms they have helped to form (Coons et al., 2021).

The least diversity of families is observed in the microcosms, in particular in the PHB sample, where a dominance of the Stappiaceae (56%) and Alcanivoracaceae (15%) was observed. Stappiaceae is a chemoorganotrophic family, which occupies various ecological niches and participates in important biogeochemical cycles and processes such, as example, oxidation and denitrification of CO_2 (Weber & King, 2007). Species belonging to this family have been isolated from crude oil and are known for the degradation of aromatic hydrocarbons such as O-xylene and phenanthrene (Prince et al., 2019), and their presence has also been associated with PET-specific OTUs (Delacuvellerie et al., 2019). Furthermore, in addition to having observed the growth of strains belonging to this family on β-hydroxybutyrate (Weber & King, 2007), recent studies focused on the production of PHAs by enrichment of microbial communities from estuarine sediments, have found that the genera dominant PHA-accumulators were mainly belonging to the Stappiaceae family (Bedade et al., 2021). The second most abundant family in the PHB scaffold is Alcanivoracaceae, although present in a much lower percentage than the previously described Stappiaceae. This family is generally predominant in marine environments affected by crude oil (Delacuvellerie et al., 2019). Alcanivoracaceae are a family with species involved in the degradation of aliphatic hydrocarbons of petroleum (Yakimov et al., 2022; Chernai et al., 2019; Catania et al., 2018; Catania et al., 2015; Yakimov et al., 1998), and has been associated with biofilms and degradation processes of plastic materials of petrochemical origin such as HDPE (Girard et al., 2020) and LDPE (Delacuvellerie et al., 2019).
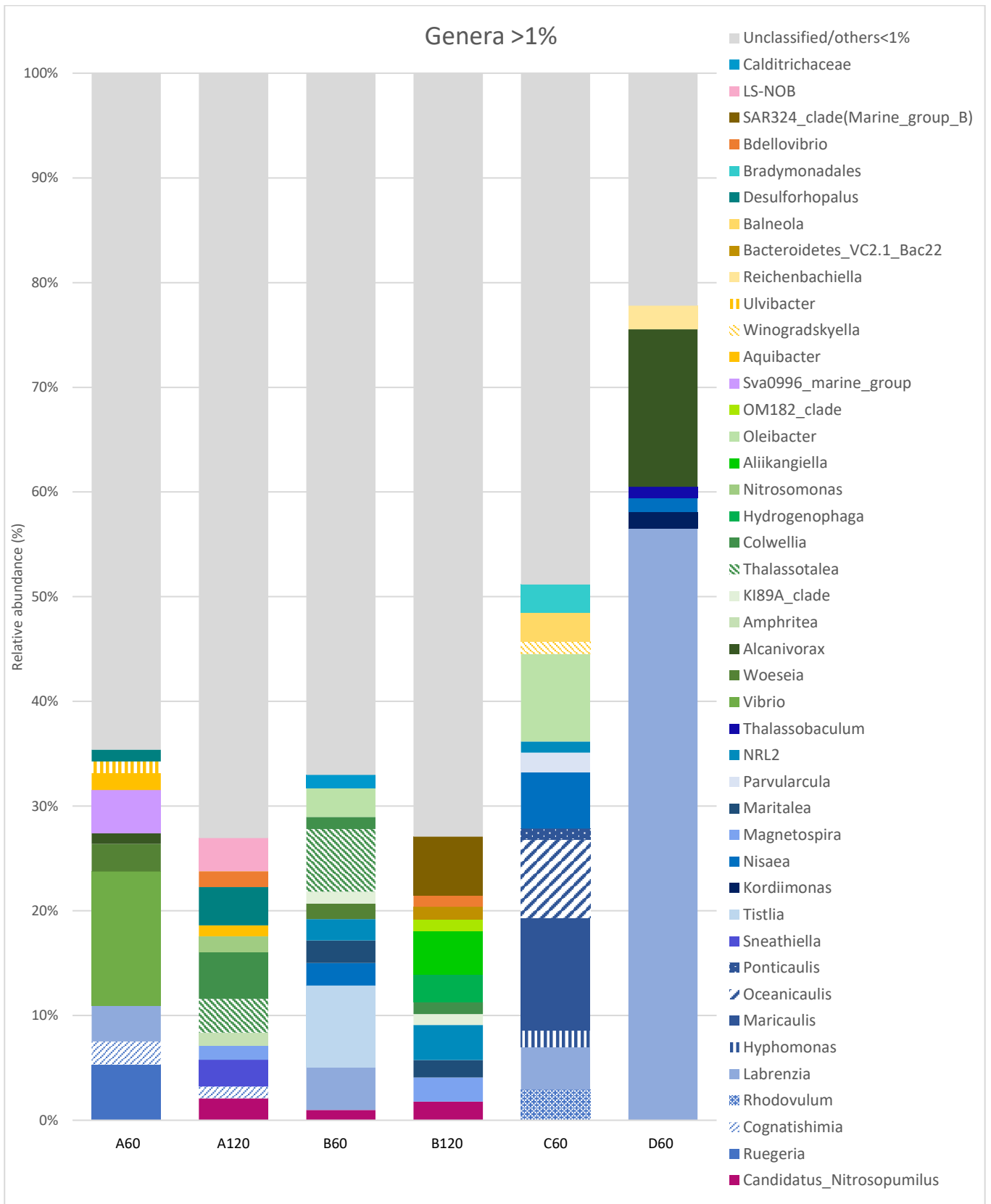
Figure 22 - Relative abundances (%) of families from biofilms of PDLLA/PLLA (A60 and A120), PLLA (B60 and B120), PHA/PHB (C60) and PHB (D60) scaffolds. For both the PDLLA/PLLA and PLLA samples, the abundances recorded after 60 (t_1) and 120 (t_2) days of exposure in the sea are reported, while for the PHA/PHB and PHB samples, the abundances recorded after 60 days of contact in microcosm with non-sterilized seawater (mt$_1$). Taxa $\geq$ 1% are shown. Unclassified/others includes unclassified taxa and identified taxa <1%

After the first 60 days of exposure in the marine environment, the PDLLA/PLLA scaffolds shows a predominance of the genera *Vibrio* (12%), *Ruegeria* (5%), and *Sva0996_marine_group* (4%). These same ones are no longer found at the next sampling time, while the genera *Colwellia* (4%), *Tahalassotalea* (3%), and *Desulforhopalus* (3%) become predominant (**Figure 23**). *Vibrio* is a generalist degrader, ubiquitous in the sea, which has also been found on polymeric surfaces dispersed in the sea, adopted by this genus as a substrate for their transport in the marine environment (Oberbeckmann et al., 2016). The genus *Vibrio* also includes pathogenic strains not only for humans but also for marine animals such as fish, shrimps, and crustaceans, thus representing a potential threat to animal health and ecological balance (Kirstein et al., 2016). Recent studies hypothesize the presence

of pathogenic *Vibrio* strains attached to plastic materials may contribute to the phenomenon of coral reef bleaching (Feng et al., 2020). Furthermore, *Vibrio* is a genus that several studies identify as one of the potential candidates for the recovery of environmental sites contaminated by hydrocarbons, as it is capable of leading to degradation rates higher than 70% (Adetitun et al., 2018; Imron & Titah, 2018). The genus *Ruegeria* is one of the organisms capable of degrading sulphonates to support organotrophic growth (Simon & Kroneck, 2013). This process is used in mechanisms that establish and maintain microbial associations between autotrophs and heterotrophs, such as the exchange of a sulphonate produced by a diatom and supplied to a bacterium of the genus *Ruegeria* in exchange for vitamin B12 (Berges et al., 2022). Furthermore, denitrification is a trait that is widely, but not universally, represented among species of the genus *Ruegeria* (Arahal et al., 2018). Species belonging to the genus *Sva0996_marine_group* perform important universally beneficial metabolic activities capable of ensuring stability in microbial communities even under abiotic and biotic perturbations in dynamic coastal waters, strengthening their ecological resilience (Chun et al., 2021). The genus *Sva0996_marine_group* has been detected as a component of the plastisphere adhered to plastic objects present on deep marine sediments at a water depth of 4150 m in the eastern equatorial Pacific Ocean (Krause et al., 2020). An abundant presence of the genus *Sva0996_marine_group* was also found in a recent study on the surface of a commercial non-biocidal antifouling-release, leading the authors to suggest that this genus constituted a key component in the community profile of fouling (Papadatou et al., 2021).

The genus *Colwellia* includes hydrocarbon-degrading bacteria (HCB). It is among the genera that have been found in the marine environment to be dominant on biofilms adhered to LDPE (Vaksmaa et al., 2021), but it has also been found in the early stages of biofilm formation on biopolymer material, such as poly(3-Hydroxybutyrate -co-3-Hydroxyhexanoate) (PHBH) (Morohoshi et al., 2022). Shifts of the microbial community at the genus level are also observed in the PLLA scaffolds between time t_1 and time t_2 (**Figure 23**). Both the genus *Tistilia*, the most abundant in the PLLA sample recovered at time t_1, and the genus *SAR 324*, the most abundant in the PLLA sample at time t_2, are both ubiquitous marine genera that inhabit the entire water column but are not yet been described in the literature as associated with biofilms of plastic materials. On the other hand, *Tistilia* a genus containing strains expressing genes for nitrogen fixation (Barreto Filho et al., 2021; Díaz-Cárdenas et al., 2010), and SAR324 a clade possessing metabolic pathways involved in nitrogen fixation carbon and sulphur metabolism (Boeuf et al., 2021), it can be assumed that the role played by these two genera is that of supporting the entire microbial community adhering to the surface of the plastic material, without any degradative capacity. The dominant genera observed in the biofilm of the PHA/PHB sample are *Maricaulis* (10%),

Oleibacter (8%), and *Oceanicaulis* (7%). *Oleibacter* is instead a genus associated with the degradation of petroleum. It has in fact been isolated in contaminated marine sites, both in seawater and in sediments(Catania et al., 2015; Teramoto et al., 2011). Finally, the predominant genera in the biofilm from the PHB sample are *Labrenzia* (56%) and *Alcanivorax* (15%) which are both known hydrocarbon degraders (Chernai et al., 2019). Furthermore, the genus *Labrenzia* was found to be among the producers of PHAs isolated from estuary sediments (Villanueva et al., 2010) and therefore could potentially also be able to degrade this type of bioplastic.

Figure 23 - Relative abundances (%) of genera from biofilms of PDLLA/PLLA (A60 and A120), PLLA (B60 and B120), PHA/PHB (C60) and PHB (D60) scaffolds. For both the PDLLA/PLLA and PLLA samples, the abundances recorded after 60 (t_1) and 120 (t_2) days of exposure in the sea are reported, while for the PHA/PHB and PHB samples, the abundances recorded after 60 days of contact in microcosm with non-sterilized seawater (mt_1). Taxa $\geq$ 1% are shown. Unclassified/others includes unclassified taxa and identified taxa <1%

5.4 Microcosms: preliminary observations, isolation, and identification of potentially degrading bacteria

To isolate and identify potential degrading bacteria capable of growing on PHAs and PLA bioplastics, microcosms containing inoculating bacterial biofilm adhered to the surface of the PDLLA/PLLA and PLLA scaffolds were prepared after 60 and 120 days of exposure in a marine environment. Since it was not possible to recover the PHA/PHB and PHB scaffolds, the microcosms were set up with non-sterilized sea water, to recreate the marine microenvironment on a laboratory scale and to be able to observe the progress of the degradation of these materials. All the flasks containing biomass after 24h of incubation presented moderate turbidity. The behavior of the polymeric materials was constant during the 60 days of testing in the microcosms, with the sole exception of the PHA/PHB scaffold fragments. These, in fact, unlike all other types of scaffolds, were deposited on the bottom of the microcosm flask already after the first 48 hours from start-up. The same event occurred about a week after starting for the control samples as well. Furthermore, starting from the fifth day, the sample fragments began to release a milky substance (**Figure 24**) and cracks and fractures appeared which gradually became more and more evident, until a fraction of the scaffold broke down into three distinguishable pieces.

Figure 24 – PHA/PHB microcosm after 5 days of incubation

Several fragments of much smaller size were observed at the bottom of the flasks of both the PHA/PHB microcosm and the PHB microcosm, while to a lesser extent, this was observed in the microcosms of the PLA samples. At the end of all tests in the microcosm, both with

the biomass recruited at time t_1 and at time t_2, and with non-sterilized sea water, all types of exposed scaffolds showed an easily flaky and slightly gelatinous consistency. Conversely, the fractions of the same polymeric materials placed in control vials with sterile seawater only maintained their consistency and integrity.

This result could represent evidence of the activity carried out by the microbial communities present within the microcosms, which would proceed in the degradation processes starting with a preliminary bio-fracturing of the material especially from the amorphous portion, which is more easily attacked (Syranidou et al., 2017) (Kumar et al., 2021). At the end of the tests in microcosms, the biofilm developed on the surface of the various scaffolds was collected and an aliquot was plated on a mineral medium containing the corresponding polymer as the only source of carbon to isolate potential bacteria degraders. The number of isolates from each sample is shown in **Table 3**.

Table 3 – Bacteria isolated by plastisphere able to use polymeric scaffold as unique carbon source

POLYMERIC SCAFFOLD	NUMBER OF PHENOTYPES	NUMBER OF ISOLATES
PHA/PHB	4	8
PHB	4	8
PDLLA/PLLA	5	14
PLLA	4	14

40 bacterial isolates with different phenotypes were obtained. Of these, 4 isolates produced an evident halo of degradation in the solid mineral medium (**Figure 25**), while the fifth phenotype, on the other hand, showed a consistent reduction of the polymeric material in the liquid mineral medium (**Figure 26**). Four bacterial strains were isolated from PHB sample, while one from PHA/PHB sample. None of the bacteria isolated from PDLLA/PLLA and PLLA scaffolds, showed visible signs of degradation, nor growth difference between the presence and absence of the polymer.
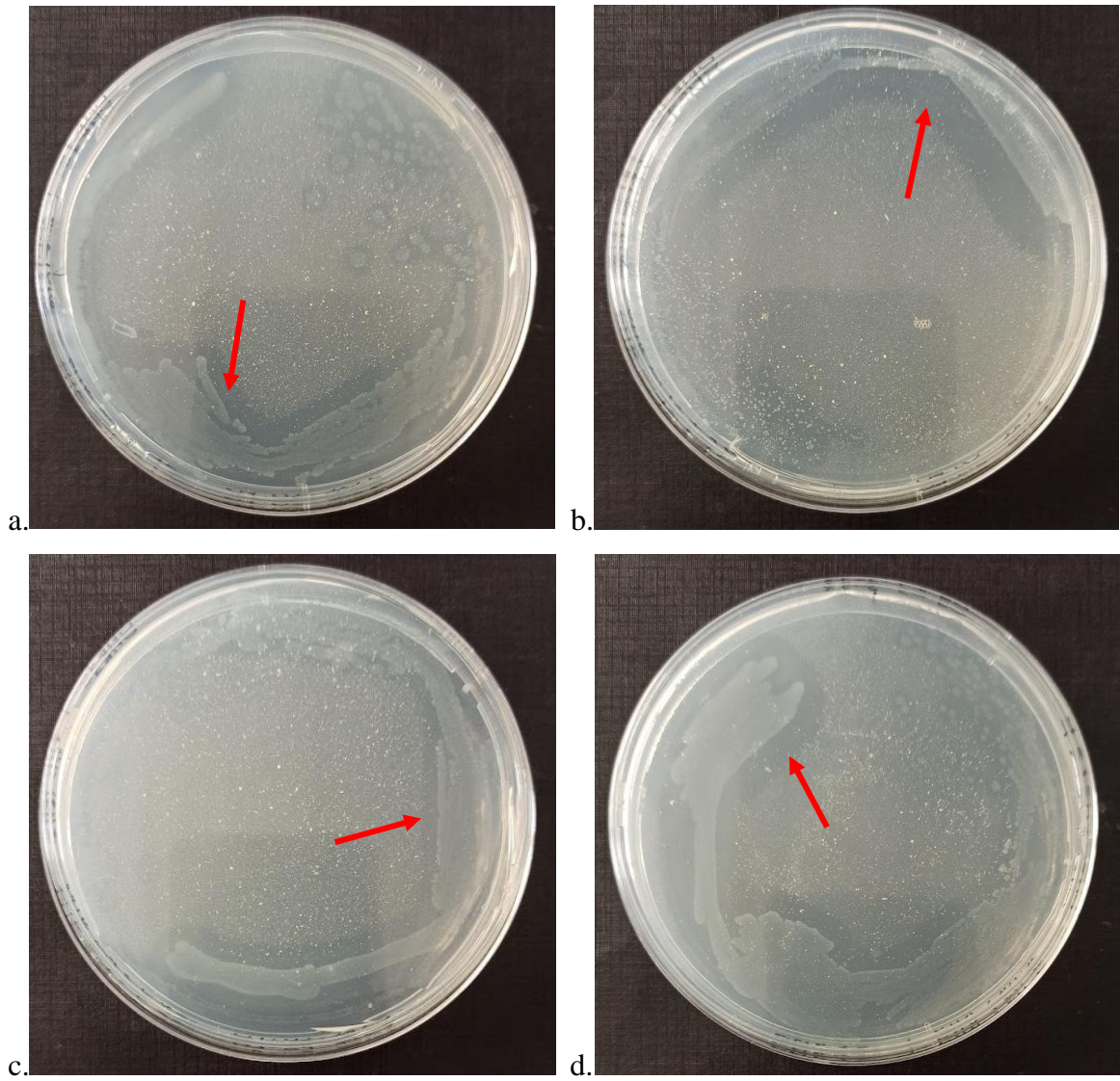
Figure 25 – Potential degrading bacteria isolated by PHB scaffold, after 60 days in microcosm with non-sterilized sea water for 60 days (Sample D60). The arrow indicate the halo degradation.
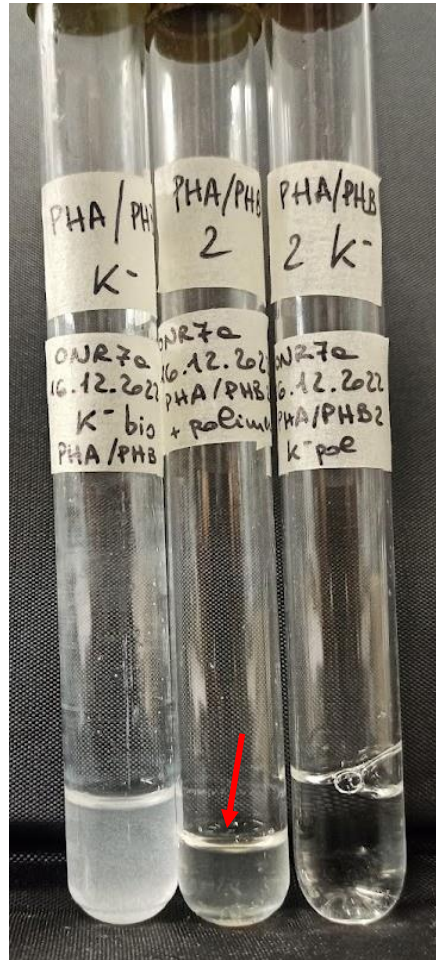
Figure 26 – Bacterial cultures of the strains isolated from PHA/PHB scaffold, exposed in a microcosm with non-sterilized seawater for 60 days (Sample C60). It can be observed how, compared to the control containing PHA and PHB powder (tube on the left), the turbidity given by the presence of biopolymers is considerably decreased, a sign of an evident degradation.

The bacterial strains isolated were identified by 16S rDNA sequencing (**Table 4**).

Table 4 - Bacterial sequences detected by 16S rDNA sequencing of 5 isolates able to grow on PHA/PHB and PHB as the sole carbon source.

Isolate code	16S rRNA database (Bacteria)					
	Phylum	Class	Family	Closest relative	similarity (%)	Accession number
C60	Alphaproteobacteria	Hyphomicrobiales	Stappiaceae	*Labrenzia sp.*	98	NR_153733.1
D60_1a, D60_1b, D60_2a, D60_2b	Gammaproteobacteria	Oceanospirillales	Alcanivoracaceae	*Alcanivorax sp.*	99	NR_133958.1
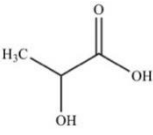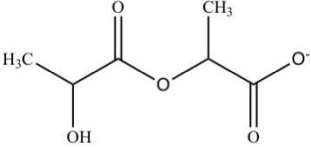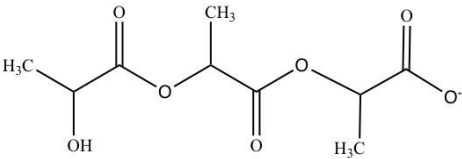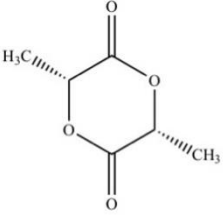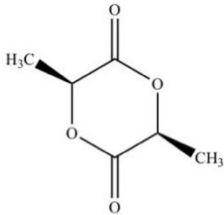
The bacterial strains isolated as a potential degrader from the PHA/PHB sample was affiliated to *Labrenzia* genus. *Labrenzia* is a strictly aerobic, Gram-negative, halophilic *α-Proteobacterium* of the *Stappiaceae* family, and is known to usually occur in marine environments, associated with ostriches, halophytes, and dinoflagellates. This genus can utilize a wide range of organic carbon sources for its growth, including fatty acids, intermediates of the tricarboxylic acid cycle, and sugars (Biebl et al., 2007). *Labrenzia* has also been found in contaminated marine environments, identified as a degrader of aromatic hydrocarbons. Furthermore, *Labrenzi*a is known to be capable of oxidizing β-hydroxybutyric acid, the precursor of polyester PHB (Camacho et al., 2016; Biebl et al., 2007). The strains isolated from the PHB samplewere affiliated to *Alcanivorax* genus. *Alcanivorax* is a *γ-Proteobacteria*, aerobic, Gram-negative, motile or sessile, chemo-organotrophic, capable of tolerating high salt concentrations (Rahul et al., 2014) and also in the marine carbon cycle (Dong et al., 2021). As already reported among the results of the metagenomic analyses, the genus *Alcanivorax* is one of the indigenous bacterial strains involved in the bioremediation of sites contaminated by hydrocarbons, such as sites where oil spills occurred, as they possess catabolic genes involved precisely in the degradation of aliphatic hydrocarbons both branched and linear alkanes (Chernai et al., 2019; Yakimov et al., 1998). Furthermore, it has been found in the natural marine environment associated with biofilms of HDPE (Girard et al., 2020), LDPE (Delacuvellerie et al., 2019), and PET (Oberbeckmann et al., 2014), and could play an important role in degradation processes of these materials. Bacteria belonging to the genus *Alcanivorax*, such as *Alcanivorax xenomutants* (Rahul et al., 2014) and *Alcanivorax borkumensis* (Zadjelovic et al., 2020) possess several genes for the degradation of alkanes, i.e. membrane enzymes involved in the oxidation of alkanes of different lengths (Yakimov et al., 2007; Van Beilen et al., 2004). Among the membrane enzymes involved in these degradative processes, the PHA depolymerase enzyme, ALC24_4107, is capable of hydrolysing aliphatic polyesters of both natural and synthetic origin, such as PHB, poly(hydroxybutyrate-covalerate) (PHBV), poly(ethylene succinate) (PES), polybutylene succinate (PBS) and polycaprolactone (PCL) (Cao et al., 2022; Crisafi et al., 2022; Zadjelovic et al., 2020). Another enzyme, ABO2449, encoded showed hydrolytic activity on PLA and other aliphatic polyesters, such as poly(hydroxybutylated-co-valerate) (PHBV), PCL, and poly(ethylene succinate) (PES) (Hajighasemi et al., 2016). In addition to the degradative process, studies confirm the ability of *Alcanivorax* to synthesize and accumulate PHAs using petroleum-derived hydrocarbons as a carbon source (Romo et al., 2014) and the presence of membrane proteins linked to directly involved or closely related metabolic

pathways to the metabolism of alkanes, in particular PhaC PHA synthetase, an enzyme capable of synthesizing polyhydroxyalkanoates (Sabirova et al., 2006).

5.5 Chemical compounds determined at the Orbitrap

The analysis carried out using the Orbitrap revealed the presence of degradation products only for the PLA samples, reported below in **Table 5**:

Table 5 - Chemical compounds determined at Orbitrap for the PLA samples

Compound name	Chemical structure
Lactic acid	
Dilactic acid	
Trilactid acid	
Lactide	

The products detected are therefore both monomeric units and oligomers with different molecular weights. Numerous studies conducted considering the degradation process of PLA biopolymer have demonstrated how the rate of degradability is drastically reduced in

seawater due to the high salinity that affects the diffusion of water in the polyester (Li et al., 2022; Wang et al., 2021; Haider et al., 2019; Deroiné et al., 2014; Tsuji et al., 2003).

It is possible that, unlike PHAs samples whose degradation occurs very quickly and at higher rates (Wang et al., 2021), it is precisely these very slow degradation rates of PLA samples that have made it possible to detect intermediate products as they have not yet been totally degraded by the action of the microorganisms present in the communities constituting the biofilm. Furthermore, the presence of monomers and oligomers as intermediate degradation products was detected in a study conducted on this same type of polymer degraded in phosphate-buffered saline; the study has, in fact, shown how the destruction of PLA proceeds through the hydrolysis of ester bonds followed by the formation of low molecular weight fragments, mainly lactic acid. Subsequently, there is the formation of oligomeric products through random chain scission processes and, subsequently, the depolymerization of the chain ends (Morozov et al., 2020). This is also confirmed by studies on the degradation process of PLA considering the role played by microbial communities. Microorganisms capable of degrading PLA first expel extracellular depolymerases with the production of oligomers, dimers, and monomers. Once low molecular weight products have been obtained, these can penetrate microbial membranes and allow the action of intercellular enzymes capable of further decomposing them into carbon dioxide, water, or methane.

From the comparison between the results obtained between the analyzes of the microbial communities adhering to the surfaces of the PLA samples and the literature, it emerged that the Actinobacteria, identified in the plastisphere of the A60 sample only, are considered the best degraders of this material (Teixeira et al., 2021; Butbunchu & Pathom-Aree, 2019; Qi et al., 2017). Second to Actinobacteria, the literature reports how Proteobacteria have been found in samples of PLA degraded in compost (Mayumi et al., 2008) and, furthermore, another study considers them capable of improving the efficiency of electron transfer in the anaerobic digestion of lactic acid (Guo et al., 2022). In the biofilms of the PLA samples recovered from the field tests (A60, A120, B60, and B120), percentages of between 61 and 90.7% of Proteobacteria were found in the entire community adhering to the surfaces of the biopolymeric materials. Actinobacteria and Proteobacteria were identified as the abundant phyla in plastispheres of PLA, PBAT, and PE polymers, suggesting that bacteria from these phyla can effectively colonize plastic surfaces and, consequently, can also biodegrade these plastics (Du et al., 2022; Mistry et al., 2022). In the same samples, Bacteroidetes bacteria were also found which facilitate the methanogenesis reaction by using lactic acid as a fermentation substrate to produce methane (Du et al., 2022; Guo et al., 2022).

5.6 Biological effects of bioplastics in mussels

5.6.1 Microplastic dimension

In **Table 6** are resumed the dimensions and the percentage of the particles of the different plastic. For HDPE, PHAs and PLA has been counted the diameter of single microparticles, whereas for PHB the dimensional range of the cluster formed in aqueous environment. We can observe that the prevalence of particles for each material belong to the range 1-50 μm.

Table 6 - Percentage of the dimensional range of the particles used for the in vitro and in vivo exposures of the different particle for HDPE, PHAs and PLA, and percentage of the dimensional range of the cluster formed in aqueous environment for PHB

	1-50 μm	51-150 μm	>150 μm
HDPE	69.3%	13.8%	16.9%
PHA	63.9%	23.2%	12.9%
PHB	88.8%	9.1%	2.0%
PLA	78.8%	17.9%	3.2%

5.6.2 In vitro phagocytic activity

The results of the *in vitro* assays are presented in **Figure 27**. In the figure are shown the images of the samples observed by microscope under optical light and UV fluorescent apparatus. In the different panels is observable the recognition from the haemocytes and the interaction with the microparticles which stimulate the cellular responses. In the control (**a-b**), are observable the vital haemocytes stained by acridine orange (AO) showing the regular motility and the ability to spread and adhere to the glass substrate. In (**b**) haemocytes AO stained are encircled in red and show the typical fluorescent pink colouration of the cytoplasm and brilliant green of the nucleus under the fluorescent light due to the presence of staining. Both in (**b**) and (**c**) red arrowheads indicate the cellular nuclei that in (**b**) appear, due to AO staining, as a typical green spot. Positive control of phagocytosis (**d**, **e**) was realized by placing the haemocytes in contact with yeast (**c**). Free yeast in (**c**) and (**d**) are encircled with a dotted blue line. In (**d**) and (**e**) encircled with continuous blue lines are evidenced the phagocytic haemocyte cell with visible engulfed yeasts. In (**d**) under the optical light, the engulfed yeast cells are visible inside the membrane cell. In (**e**) under the UV light is observable the typical green colour of the fluorescein-stained yeast cells that are strictly close when internalized by haemocytes (encircled in a continuous blue line). In (**f**) and (**g**) the green arrowheads show how PHB microparticles appear under an optical microscope. In (**g**) under the optical light and in (**h**) under UV light (encircled in green) the

haemocytes which phagocyted the microparticles are evidenced. In (**h**) the cells manifest the fluorescent pink colour due to the AO staining and the yellow arrowhead indicates the interference of the fluorescence due to the internalized microparticles. In (**i**) a PLA microparticle is detected under optical light. Under UV light (**i** inset), the PLA does not manifest fluorescence. In (**l**) the haemocytes encapsulate the microparticles coating the surface of the particles (orange circle). The orange arrowheads indicate the encapsulating haemocytes that coat the microparticle surface, whereas the orange dotted circles indicate the free haemocytes on the slide. In (**m**) the microparticles, differently from the case reported in **Figure 27.i**, show a green fluorescence attributable to the nuclei (AO stained) of the haemocytes that participate in the encapsulation. Encircled with dotted lines are the cells on the slide with clear green visible nuclei. Phagocytic cells, with engulfed micro particles of PLA are observable also in **Figure 27** panels (**n**) and (**o**) encircled in white.
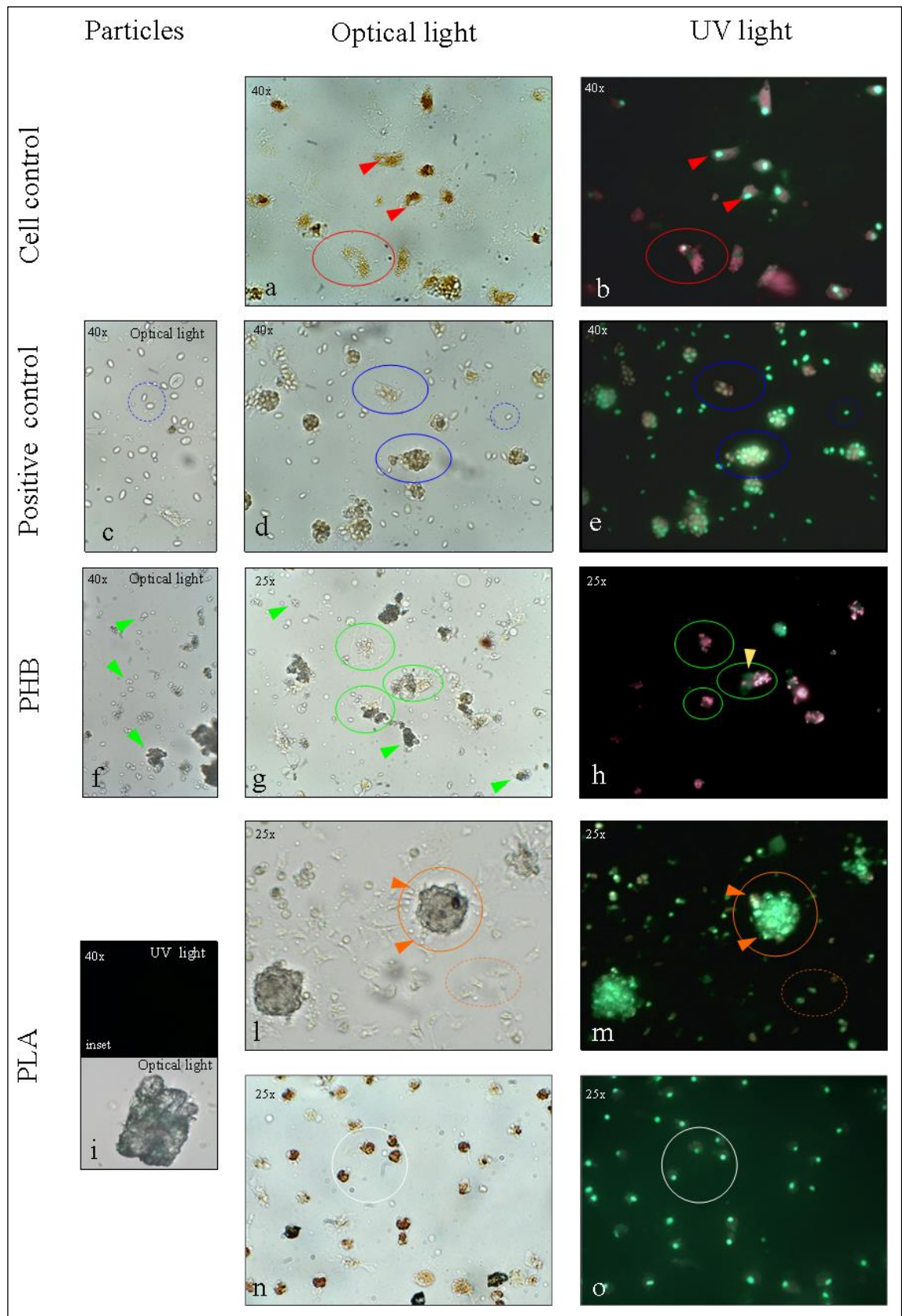
Figure 27 - Results of the *in vivo* assay. Samples observed under light microscope (a, c, d, f, g, l, i, n) and by UV apparatus (b, e, h, i inset, o). In (a) and (b) are observable the living cells stained by A/O. In (c, d, e) in observable the phagocytosis activities with yeast cells engulfed by haemocytes. In (f, g, h) haemocytes exposure to PHB. In (i, l, m, n, o) haemocytes exposure to PLA.

5.6.3 Number of haemocytes/mL of haemolymph

Figure 28 show the effect of the *in vivo* exposure to the different plastic particles on the number of haemocytes per mL of haemolymph. In particular in **Figure 28a** are shown the mean number of total cells count for the control conditions ($8.7*10^7 \pm 1.6*10^7$ cells/mL), HDPE exposures ($9.9*10^7 \pm 3.4*10^7$ cells/mL), PHA exposures ($10.8*10^7 \pm 2.2*10^7$ cells/mL), PHB exposures ($7.6*10^7 \pm 1.9*10^7$ cells/mL), PLA exposures ($14.2*10^7 \pm 5.0*10^7$ cells/mL).

5.6.4 Haemocytes phagocytic activity

In **Figure 28b** are shown the results about the haemocyte phagocytic activity after mussel in vivo exposure at different conditions indicate as percentage of phagocytic cells respect the total cells counted (CNT= 44% ± 6% cells, HDPE= 54% ± 9% cells, PHA= 60% ± 18% cells, PHB= 48% ± 13% cells, PLA= 20% ± 6% cells).
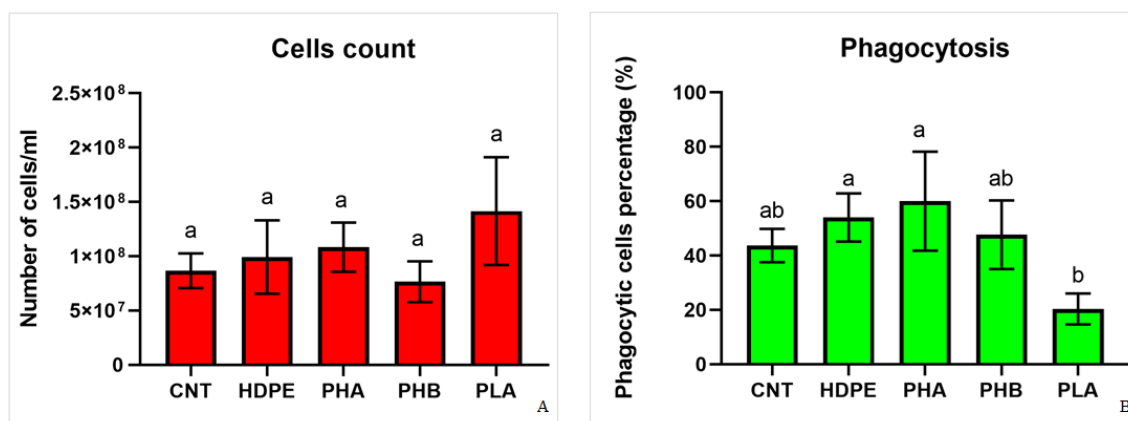
Figure 28 - Graphs indicating (A) the count of the cells in the haemolymph, (B) the phagocytosis activity of the haemocytes after in vivo microplastic exposures. Data are indicated as mean ± standard deviation. Different low-case letters above the bars indicate significance among the different treatment groups.

5.6.5 Enzymatic response

Enzymatic responses of mussel' digestive glands are shown in **Figure 29**. The one-way ANOVA test showed general difference among groups for PO activity (p value <0.0001). In detail, the values were significative higher in PHB and PLA groups respect the control mussels. GPx activity increased in all samples subjected to treatments with respect to control organisms. Multiple comparison analysis showed significant results for animals exposed to biopolymers compared to control group. However, there were no statistical differences between mussels exposed to different biopolymers. As regards LYS, the statistical analysis showed significant difference between experimental groups and control one. In detail, the

significative greatest amount of LYS was measured in samples exposed to PLA respect other groups. A similar trend was assessed for EST and ALP kinetic activity (one-way ANOVA p value <0.0001 and <0.05 respectively). The post-hoc Tukey test highlighted differences between group exposed to PHB and PLA polymers compared to the control group, with a significative increases of EST activity. Instead, for ALP the statistical analysis showed notably difference only in specimens exposed to PLA compared to other treatments.
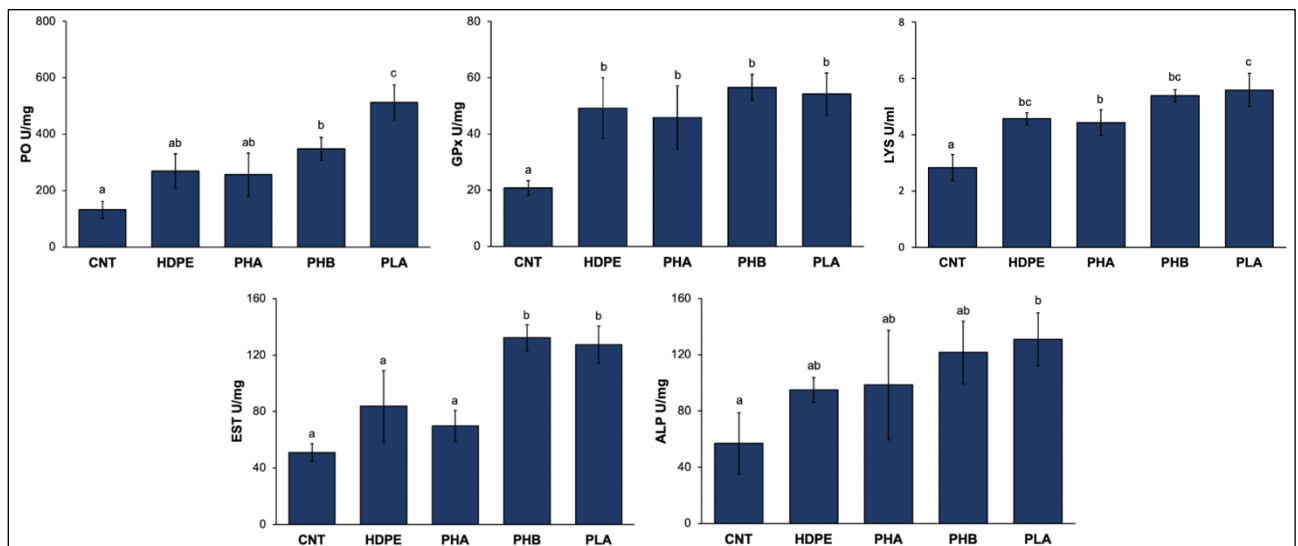
Figure 29 - Graphics show the enzymatic response of PO, GPx, LYS, EST and ALP in digestive gland of *M. galloprovincialis* after *in vivo* exposure. Data are indicated as mean ± standard deviation. The letters indicate statistically significant differences between treatments. Differences between means were considered significant for p < 0.05.

Enzymatic responses of mussel' haemolymph are shown in **Figure 30**. PO activity increased in all samples subjected to treatments with respect to control organisms. Multiple comparison analysis showed significant results for animals exposed to PHB and PLA biopolymers compared to other groups. The one-way ANOVA test showed general difference among groups for GPx activity. In detail, the values were significative higher in PHB and PLA groups respect the control mussels. The EST trend was similar to GPx activity for PHB and PLA groups compared to other, even if statistical analysis showed significative differences only for PLA-exposed mussels. Also in this case, the one-way ANOVA evidenced a p-value of <0.05 between treatments. A different behaviour was assessed for LYS and ALP kinetic activity (one-way ANOVA p value <0.05 and <0.0001 respectively). The post-hoc Tukey test highlighted differences between HDPE and PLA each other and compared to other groups. Instead, no differences were found among PHA and PHB groups and control samples.
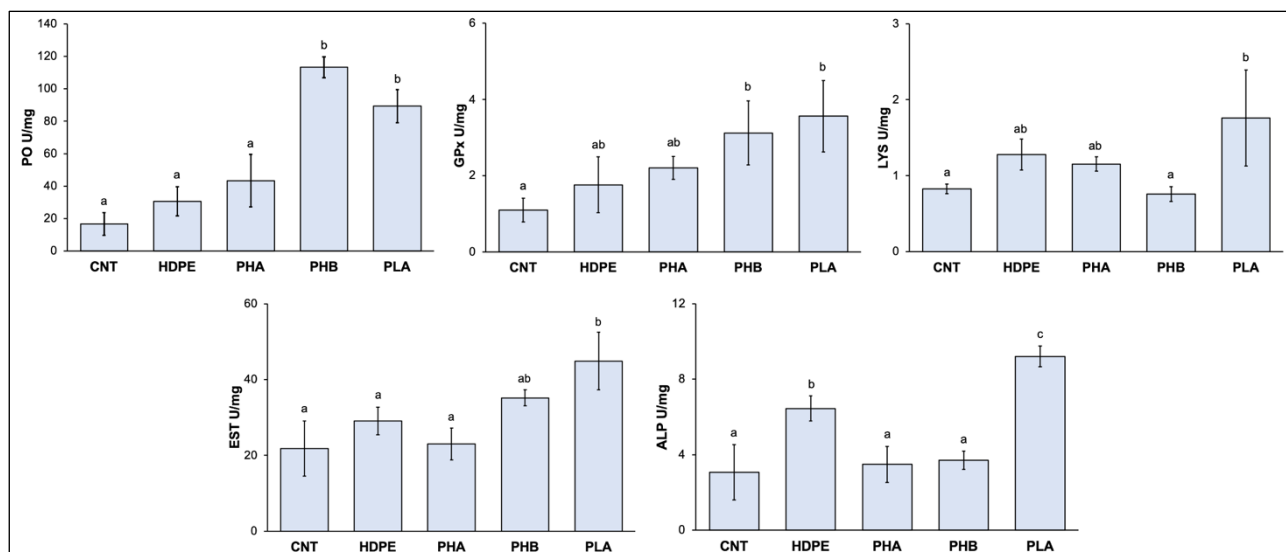
Figure 30 - Graphics show the enzymatic response of PO, GPx, LYS, EST and ALP in haemolymph of *M. galloprovincialis* after *in vivo* exposure. Data are indicated as mean ± standard deviation. The letters indicate statistically significant differences between treatments. Differences between means were considered significant for $p < 0.05$.

5.6.6 Histomorphology

Representative images of digestive gland' histomorphology is shown in **Figure 31**. The histological sections of the control group exhibited the typical organization of digestive tubules of marine bivalves. Instead, histological sections of the digestive gland showed an evident alteration in microtubular structure following HDPE exposure, causing tubular atrophy (characterized by large lumen and thin epithelium). Otherwise, exposure to bioplastics such as PHA and PHB did not cause evident histological alterations, keeping the tissue almost regular. PLA exposure showed a greater tubular atrophy respect to PHA and PHB exposure. In addition, a haemocytic infiltration was highlighted among the digestive tubules of digestive gland exposed to PHA, PHB and PLA, with a greater extent observed in those individuals expose to PHAs and PLA.
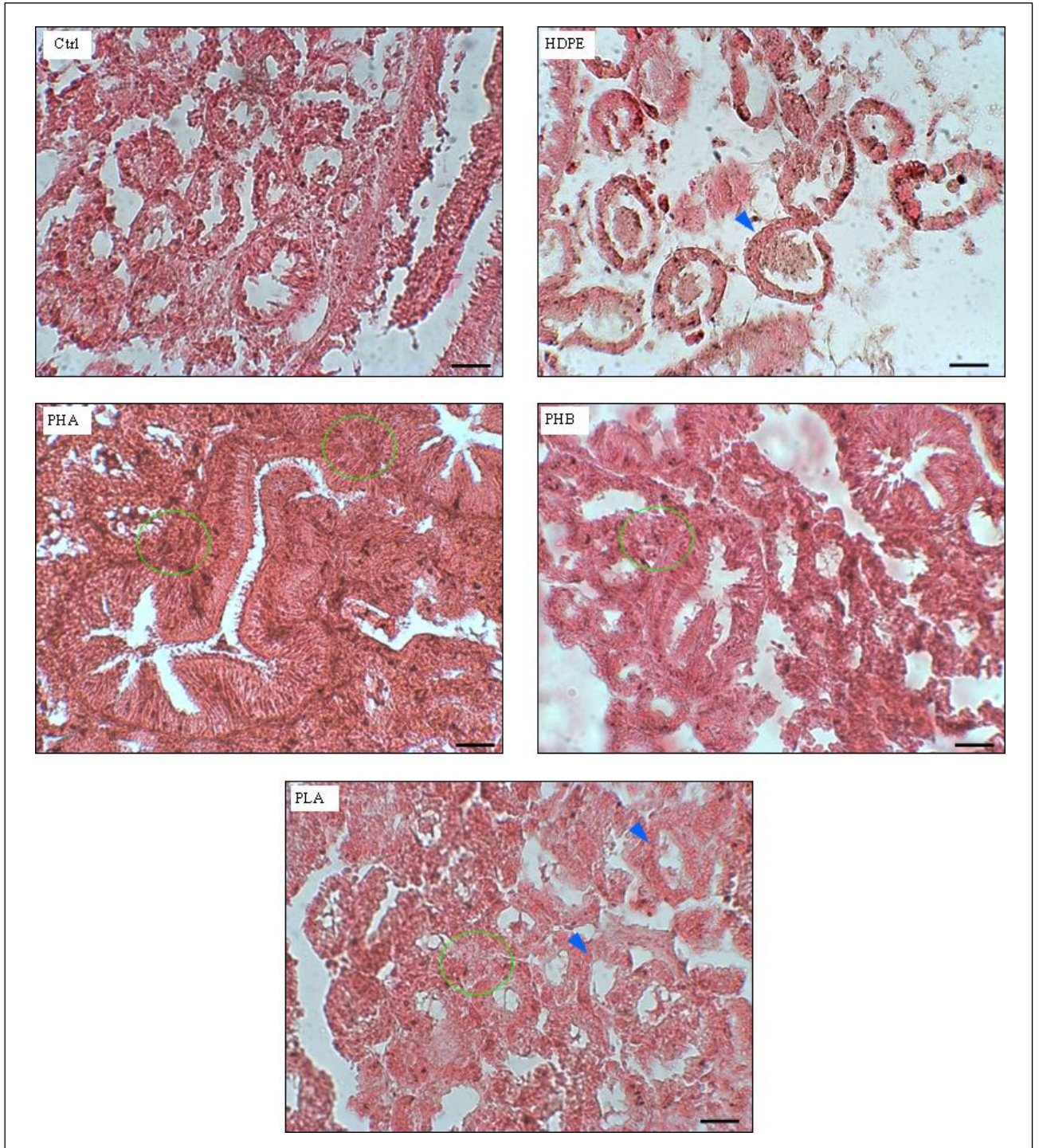
Figure 31 - Representative images of histological section of *M. galloprovincialis* digestive gland after microplastic exposure (H-E staining). Digestive tubule modifications are highlighted by blu headarrows, that indicating atrophic tubules. Green circles indicating intertubular haemocytes infiltration. Scale bar: 25 µm.

Our study on the biological effects of polyhydroxyalkanoates and poly-lactate exposure have demonstrated, once again, that bivalves such as *M. galloprovincialis* are of relevant interest because their sedentary lifestyle and their extensive filter-feeding activity that expose them to the particles present in their marine aquatic. Thanks to this habitus different biomarkers have been deeply investigated and to obtain information about the animal

response to environmental conditions and about the potential effect of new substances introduced for mankind's application. Here *in vitro* and *in vivo* we have shown the effect of exposures to bio microplastics of polyhydroxyalkanoates and poly-lactate through different biomarkers such us: cellular mediated activity (haemocyte phagocytosis or encapsulation), enzymatic activity, and histological modification.

The *in vitro* test of haemocytes exposures to microplastics triggered the cellular mechanism of recognition and destruction of the foreign particles through phagocytosis and encapsulation activity. In which the cells are activated to engulf or coat the larger the microparticles to eliminate them as a defence mechanism from non-self-agents. Haemocytes exposures to PHB and PLA microplastics triggered phagocytosis. It is indeed possible to observe the microparticles internalized in the cell's cytoplasm. In addition to phagocytosis, differently from PHB, the presence of larger particles of PLA stimulates the encapsulating activity. On the contrary, the PHA microparticles do not triggered any biological response either for phagocytosis and/or encapsulating activity.

The phagocytosis responses carried out from haemocytes is a highly protective process in all multicellular organisms, through which the host can protect itself against invading microorganisms and environmental particles and remove self-apoptotic cells/cell debris to maintain tissue homeostasis. The high sensitivity of this biological function to environmental factors and/or xenobiotics in several animal species has been demonstrated (Falleiros et al. 2003; Canesi et al. 2012; Sendra et al. 2020), emphasizing the usefulness of this approach in pollution monitoring programs. Another innate cellular response observed in our study is the encapsulation, like the well know pearl formation phenomenon, induced when labile haemocytes rupture upon encountering a foreign object of a large dimension. The released products may promote the formation of a coating of ameboid haemocytes around the object to restrict its growth or movement.

Our results are coherent with studies on different organisms (macroinvertebrates, fish, and mammals) demonstrating the reaction of phagocytic cells toward the microplastics (Merkley et al., 2021; Weber et al 2021; Scanes et al 2019; Gomiero et al., 2018).

The physiological responses in immune systems to plastic contamination can be dependent on multiple factors. Overall, the particle's size is a critical factor, in terms of their uptake into filter-feeding organisms along with the potential for contamination by co-absorbed chemicals. In addition, also the shape has an influence on the accumulation processes, migration in different tissues, immunity system activation, and toxicity of particles (Sendra 2020). With the aim to further investigate these interaction between the animals and the microplastics and the fate of these last ones, we performed i*n vivo* trials of

M.galloprovincialis exposed to the bio-microplastics. After the incubation period, the different biomarkers kept in consideration (number of haemocytes, phagocytic and enzymatic activity and histological alteration of the digestive gland) showed a certain impact on the living animals. The count of the number of cells *per* mL of haemolymph, even if without significant statistics, showed an increment of haemocytes in particular for PLA. For phagocytic activity, similar results of the cells count have been obtained for the control and after the exposure to HDPE, PHA, PHB. Differently, for PLA the haemocytes showed a reduced percentage of phagocytosis. It would seem that polylactic acid stimulate the production and recruitment in haemolymph of haemocytes, but at the same time it affects the capabilities of target recognition and engulfment. Analysis of enzymatic activities in haemolymph and in digestive glands permitted to observe a general increase in the activities respect the control, in particular caused by PHB and PLA microplastics. Histological analysis of the digestive gland revealed alterations of the microscopic structure of the microtubules following the exposure and haemocytes recruitment in the inter-microtubular spaces. Whereas the main haemocytes recruitment was induced by PHA, PHB and PLA, the main alteration was caused by HDPE and PLA microplastics, which caused microtubular alteration and in some case atrophy. We can suppose that the microplastics has been filtered by the mussel gills and transported in the digestive glands where they exerted this effect.

6 – CONCLUSIONS

In this doctoral project, a systematic study that took into account multiple aspects related to the presence and fate of bioplastics in the marine environment was conducted.

- A different structure and composition of microbial communities were observed between different types of plastic, suggesting that the type of polymer influences the plastisphere, probably favoring the abundance of bacteria capable of growing and degrading the biopolymer where they form the biofilm. Furthermore, time also affects the composition of the microbial community that adheres to the biopolymer. Indeed, a change in the composition of the plastisphere was observed for all samples as the exposure time at sea increased.
  The plastisphere-dominant bacteria identified in this study belong to genera known to degrade hydrocarbons and genera identified in other plastispheres of the same polymers. There are exceptions: the Nitrincolaceae family has not yet been detected in the PLA plastisphere, while the Stappiace family and the Hyphomonodaceae family have not yet been detected in the PHA plastisphere.

- The presence of degradation products originating exclusively from PLA samples can be linked to the slow degradation process of this material and can be attributed to non-cultivable degrading microorganisms since no potential degraders were isolated from plate tests for this type of polymer. In any case, the degradation into higher molecular weight monomers and oligomers was confirmed and it was possible to obtain the identification of potential PLA degraders presents in the composition of the biofilm collected from the surfaces of these polymers. It is believed that it is necessary to carry out further investigations that can clarify the degradation dynamics of polyhydroxyalkanoates and allow the effective isolation of potential polylactic acid degraders.

- We have demonstrated that the experiments conducted in the context of immunobiological investigations, here applied for the first time to the evaluation of the possible effects produced by bioplastics on marine organisms, constitute an effective systemic biomonitoring tool thanks to their high sensitivity and ability to respond effectively to presence of environmental pollutants. In fact, although the experimental data obtained *in vitro* and *in vivo* have a preliminary significance, they contribute to the idea that even PHAs and PLA bioplastics, considered green

alternatives to conventional plastic, can have different effects on invertebrates and vertebrates, due to direct or caused interaction from enlargement, in natural aquatic environments, where a negative effect is already found currently cited in the literature for other pollutants such as modification of nutrition, interruption of reproduction, offspring, production of pseudofeces, adhesion to the mantle and gills, histopathological damage and embryotoxicity. The approach adopted in the investigations conducted in this study through the evaluation of immunobiological biomarkers was therefore found to be valid for addressing the negative impacts of bioplastics on marine species and highlights interdisciplinary studies to decipher the results and better understand the risks faced by marine animals.

In conclusion, it's possible to state that there could be a potential risk of the environmental impact generated by the bioplastics evaluated here toward marine organisms and ecosystems. Therefore, the research conducted here aims to represent a starting point at which it is believed that further investigations are necessary aimed at evaluating the actual sustainability and environmental compatibility of biopolymeric materials, with the aim of preventing the displacement of the environmental problem generated by plastics of fossil origin to bioplastics.

The work described in this doctoral thesis lays the foundations of the methodological basis for an in-depth study of the problem of bioplastics.

REFERENCE

Abraham, W. R., & Rohde, M. (2014). The Family Hyphomonadaceae. The prokaryotes, 8, 283-299.

Adetitun, D., Akinmayowa, V., Atolani, O., & Olayemi, A. (2018). Biodegradation of jet fuel by three Gram negative Bacilli isolated from kerosene contaminated soil. Pollution, 4(2), 291-303.

Alday-Sanz, V., Roque, A., & Turnbull, J. F. (2002). Clearing mechanisms of Vibrio vulnificus biotype I in the black tiger shrimp Penaeus monodon. Diseases of aquatic organisms, 48(2), 91-99.

Arahal, D. R., Lucena, T., Rodrigo-Torres, L., & Pujalte, M. J. (2018). Ruegeria denitrificans sp. nov., a marine bacterium in the family Rhodobacteraceae with the potential ability for cyanophycin synthesis. International Journal of Systematic and Evolutionary Microbiology, 68(8), 2515-2522.

Aramvash, A., Gholami-Banadkuki, N., Moazzeni-Zavareh, F., & Hajizadeh-Turchi, S. (2015). An environmentally friendly and efficient method for extraction of PHB biopolymer with non-halogenated solvents. Journal of microbiology and biotechnology, 25(11), 1936-1943.

Arpia, A. A., Chen, W. H., Ubando, A. T., Naqvi, S. R., & Culaba, A. B. (2021). Microplastic degradation as a sustainable concurrent approach for producing biofuel and obliterating hazardous environmental effects: a state-of-the-art review. Journal of Hazardous Materials, 418, 126381.

Atiwesh, G., Mikhael, A., Parrish, C. C., Banoub, J., & Le, T. A. T. (2021). Environmental impact of bioplastic use: A review. *Heliyon*, *7*(9), e07918.

Auras, R. A., Lim, L. T., Selke, S. E., & Tsuji, H. (Eds.). (2011). Poly (lactic acid): synthesis, structures, properties, processing, and applications (Vol. 10). John Wiley & Sons.

Avio, C. G.; Gorbi, S.; Milan, M.; Benedetti, M.; Fattorini, D.; D'Errico, G.; Pauletto, M.; Bargelloni, L.; Regoli, F. Pollutants bioavailability and toxicological risk from microplastics to marine mussels. Environmental Pollution 198 (2015) 211e222 http://dx.doi.org/10.1016/j.envpol.2014.12.021

Bagheri, A. R., Laforsch, C., Greiner, A., & Agarwal, S. (2017). Fate of so-called biodegradable polymers in seawater and freshwater. Global Challenges, 1(4), 1700048.

Banaderakhshan, R., Kemp, P., Breul, L., Steinbichl, P., Hartmann, C., Fürhacker, M., 2022. Bisphenol A and its alternatives in Austrian thermal paper receipts, and the migration from reusable plastic drinking bottles into water and artificial saliva using UHPLC-MS/MS. Chemosphere 286, 131842. https://doi.org/10.1016/j.chemosphere.2021.131842

Barham, P. J., Keller, A., Otun, E. L., & Holmes, P. A. (1984). Crystallization and morphology of a bacterial thermoplastic: poly-3-hydroxybutyrate. Journal of Materials Science, 19, 2781-2794.

Barreto Filho, M. M., Walker, M., Ashworth, M. P., & Morris, J. J. (2021). Structure and long-term stability of the microbiome in diverse diatom cultures. Microbiology Spectrum, 9(1), e00269-21.

Basak, N., & Meena, S. S. (2022). Exploring the plastic degrading ability of microbial communities through metagenomic approach. Materials Today: Proceedings, 57, 1924-1932.

Bedade, D. K., Edson, C. B., & Gross, R. A. (2021). Emergent approaches to efficient and sustainable polyhydroxyalkanoate production. Molecules, 26(11), 3463

Berges, J. A., Young, E. B., Thamatrakoln, K., & Taylor, A. R. (2022). From genes to ecosystems: using molecular information from diatoms to understand ecological processes. In Advances in Phytoplankton Ecology (pp. 487-529). Elsevier.

Beyer, J.; Green, N.A.; Brooks, S.; Ian J. Allan, I.J.; Ruus, A.; Gomes, T.; Bråte, I.L.N.; Schøyen, M. Blue mussels (Mytilus edulis spp.) as sentinel organisms in coastal pollution monitoring: A review. Mar. Env. Res., 2017, 130, 338e365. http://dx.doi.org/10.1016/j.marenvres.2017.07.024

Bhagwat, G., Zhu, Q., O'Connor, W., Subashchandrabose, S., Grainge, I., Knight, R., & Palanisami, T. (2021). Exploring the composition and functions of plastic microbiome using whole-genome sequencing. Environmental Science & Technology, 55(8), 4899-4913.

Biebl, H., Pukall, R., Lünsdorf, H., Schulz, S., Allgaier, M., Tindall, B. J., & Wagner-Döbler, I. (2007). Description of Labrenzia alexandrii gen. nov., sp. nov., a novel alphaproteobacterium containing bacteriochlorophyll a, and a proposal for reclassification of Stappia aggregata as Labrenzia aggregata comb. nov., of Stappia marina as Labrenzia marina comb. nov. and of Stappia alba as Labrenzia alba comb. nov., and emended descriptions of the genera Pannonibacter, Stappia and Roseibium, and of the species

Roseibium denhamense and Roseibium hamelinense. International Journal of Systematic and Evolutionary Microbiology, 57(5), 1095-1107.

Boeuf, D., Eppley, J. M., Mende, D. R., Malmstrom, R. R., Woyke, T., & DeLong, E. F. (2021). Metapangenomics reveals depth-dependent shifts in metabolic potential for the ubiquitous marine bacterial SAR324 lineage. Microbiome, 9, 1-18.

Bolyen, E., Rideout, J. R., Dillon, M. R., Bokulich, N. A., Abnet, C. C., Al-Ghalith, G. A., ... & Caporaso, J. G. (2019). Reproducible, interactive, scalable and extensible microbiome data science using QIIME 2. *Nature biotechnology*, *37*(8), 852-857.

Bradford, N. J. A. B. (1976). A rapid and sensitive method for the quantitation microgram quantities of a protein isolated from red cell membranes. Anal. Biochem, 72(248), e254.

Butbunchu, N., & Pathom-Aree, W. (2019). Actinobacteria as promising candidate for polylactic acid type bioplastic degradation. Frontiers in microbiology, 10, 2834.

Camacho, M., Redondo-Gómez, S., Rodríguez-Llorente, I., Rohde, M., Spröer, C., Schumann, P., ... & Montero-Calasanz, M. D. C. (2016). Labrenzia salina sp. nov., isolated from the rhizosphere of the halophyte Arthrocnemum macrostachyum. International Journal of Systematic and Evolutionary Microbiology, 66(12), 5173-5180.

Canesi, L.; Ciacci, C.; Fabbri, R.; Marcomini, A.; Pojana, G.; Gallo, G. Bivalve molluscs as a unique target group for nanoparticle toxicity. Mar. Environ. Res. 2012, 76, 16 - 21. https://doi.org/10.1016/j.marenvres.2011.06.005

Cao, Y., Zhang, B., Cai, Q., Zhu, Z., Liu, B., Dong, G., ... & Chen, B. (2022). Responses of Alcanivorax species to marine alkanes and polyhydroxybutyrate plastic pollution: Importance of the ocean hydrocarbon cycles. Environmental Pollution, 313, 120177.

Cappello, T., De Marco, G., Conti, G. O., Giannetto, A., Ferrante, M., Mauceri, A., & Maisano, M. (2021). Time-dependent metabolic disorders induced by short-term exposure to polystyrene microplastics in the Mediterranean mussel Mytilus galloprovincialis. Ecotoxicology and Environmental Safety, 209, 111780.

Carfì Pavia, F., La Carrubba, V., & Brucato, V. (2013). Polymeric scaffolds based on blends of poly-l-lactic acid (PLLA) with poly-d-l-lactic acid (PLA) prepared via thermally induced phase separation (TIPS): Demixing conditions and morphology. Polymer bulletin, 70, 563-578.La

Caricato, R.; Giordano, M.E.; Schettino, T.; Maisano, M.; Mauceri, A.; Giannetto, A.; Cappello, T.; Parrino, V.; Ancora, S.; Caliani, I; Bianchi, N.; Leonzio, C.; Mancini, G.;

Cappello, S.; Fasulo, S.; Lionetto, M.G. Carbonic anhydrase integrated into a multimarker approach for the detection of the stress status induced by pollution exposure in Mytilus galloprovincialis: A field case study. Sci. Total. Environ. 2019, 690, 140 - 150. https://doi.org/10.1016/j.scitotenv.2019.06.446

Carrasco-Acosta, M., Santos-Garcia, M., & Garcia-Jimenez, P. (2022). Marine Bacteria Associated with Colonization and Alteration of Plastic Polymers. Applied Sciences, 12(21), 11093.

Catania, V., Cappello, S., Di Giorgi, V., Santisi, S., Di Maria, R., Mazzola, A., ... & Quatrini, P. (2018). Microbial communities of polluted sub-surface marine sediments. Marine Pollution Bulletin, 131, 396-406.

Catania, V., Santisi, S., Signa, G., Vizzini, S., Mazzola, A., Cappello, S., ... & Quatrini, P. (2015). Intrinsic bioremediation potential of a chronically polluted marine coastal area. Marine Pollution Bulletin, 99(1-2), 138-149.

Chan, C. M., Vandi, L. J., Pratt, S., Halley, P., Richardson, D., Werker, A., & Laycock, B. (2018). Composites of wood and biodegradable thermoplastics: A review. Polymer reviews, 58(3), 444-494.

Chernai, S., Djahnit, N., Catania, V., Hamdi, B., China, B., Cappello, S., & Quatrini, P. (2019). Isolation, characterization and determination of biotechnological potential of oil-degrading bacteria from Algerian centre coast. Journal of Applied Microbiology, 126(3), 780-795.

Chun, S. J., Cui, Y., Baek, S. H., Ahn, C. Y., & Oh, H. M. (2021). Seasonal succession of microbes in different size-fractions and their modular structures determined by both macro-and micro-environmental filtering in dynamic coastal waters. Science of the Total Environment, 784, 147046.

Coons, A. K., Busch, K., Lenz, M., Hentschel, U., & Borchert, E. (2021). Biogeography rather than substrate type determines bacterial colonization dynamics of marine plastics. PeerJ, 9, e12135

Coppola, G., Gaudio, M. T., Lopresto, C. G., Calabro, V., Curcio, S., & Chakraborty, S. (2021). Bioplastic from renewable biomass: a facile solution for a greener environment. Earth systems and environment, 5, 231-251.

Crisafi, F., Valentino, F., Micolucci, F., & Denaro, R. (2022). From Organic Wastes and Hydrocarbons Pollutants to Polyhydroxyalkanoates: Bioconversion by Terrestrial and Marine Bacteria. Sustainability, 14(14), 8241.

Curpan, A. S., Impellitteri, F., Plavan, G., Ciobica, A., & Faggio, C. (2022). Mytilus galloprovincialis: An essential, low-cost model organism for the impact of xenobiotics on oxidative stress and public health. Comparative Biochemistry and Physiology Part C: Toxicology & Pharmacology, 109302.

Dang, H., & Lovell, C. R. (2016). Microbial surface colonization and biofilm development in marine environments. Microbiology and molecular biology reviews, 80(1), 91-138.

Danso, D., Schmeisser, C., Chow, J., Zimmermann, W., Wei, R., Leggewie, C., ... & Streit, W. R. (2018). New insights into the function and global distribution of polyethylene terephthalate (PET)-degrading bacteria and enzymes in marine and terrestrial metagenomes. Applied and environmental microbiology, 84(8), e02773-17.

Delacuvellerie, A., Cyriaque, V., Gobert, S., Benali, S., & Wattiez, R. (2019). The plastisphere in marine ecosystem hosts potential specific microbial degraders including Alcanivorax borkumensis as a key player for the low-density polyethylene degradation. Journal of hazardous materials, 380, 120899

Deroiné, M., César, G., Le Duigou, A., Davies, P., & Bruzaud, S. (2015). Natural degradation and biodegradation of poly (3-hydroxybutyrate-co-3-hydroxyvalerate) in liquid and solid marine environments. Journal of Polymers and the Environment, 23, 493-505

Deroiné, M., Le Duigou, A., Corre, Y. M., Le Gac, P. Y., Davies, P., César, G., & Bruzaud, S. (2014). Accelerated ageing of polylactide in aqueous environments: Comparative study between distilled water and seawater. Polymer degradation and stability, 108, 319-329.

Détrée, C., & Gallardo-Escárate, C. (2017). Polyethylene microbeads induce transcriptional responses with tissue-dependent patterns in the mussel Mytilus galloprovincialis. Journal of Molluscan Studies, 83(2), 220-225.

Díaz-Cárdenas, C., Patel, B. K. C., & Baena, S. (2010). Tistlia consotensis gen. nov., sp. nov., an aerobic, chemoheterotrophic, free-living, nitrogen-fixing alphaproteobacterium, isolated from a Colombian saline spring. International journal of systematic and evolutionary microbiology, 60(6), 1437-1443.

Döhler, N., Wellenreuther, C., & Wolf, A. (2022). Market dynamics of biodegradable bio-based plastics: Projections and linkages to European policies. EFB Bioeconomy Journal, 2, 100028.

Dong, C., Lai, Q., Liu, X., Gu, L., Zhang, Y., Xie, Z., ... & Shao, Z. (2021). Alcanivorax profundimaris sp. nov., a novel marine hydrocarbonoclastic bacterium isolated from seawater and deep-sea sediment. Current Microbiology, 78, 1053-1060.

Du, Y., Liu, X., Dong, X., & Yin, Z. (2022). A review on marine plastisphere: biodiversity, formation, and role in degradation. Computational and Structural Biotechnology Journal, 20, 975-988.

Dyksterhouse, S. E., Gray, J. P., Herwig, R. P., Lara, J. C., & Staley, J. T. (1995). Cycloclasticus pugetii gen. nov., sp. nov., an aromatic hydrocarbon-degrading bacterium from marine sediments. *International Journal of Systematic and Evolutionary Microbiology, 45*(1), 116-123.

Eich, A., Mildenberger, T., Laforsch, C., & Weber, M. (2015). Biofilm and diatom succession on polyethylene (PE) and biodegradable plastic bags in two marine habitats: early signs of degradation in the pelagic and benthic zone?. PLoS One, 10(9), e0137201

Emadian, S. M., Onay, T. T., & Demirel, B. (2017). Biodegradation of bioplastics in natural environments. Waste management, 59, 526-536.

European   Bioplastics   –   Feedstock
https://www.european-bioplastics.org/bioplastics/feedstock/ (Accessed April, 2023)

European Commission, 2019. European Green Deal. Comun. Della Comm. Al Parlam. Eur. Al Consiglio, Al Com. Econ. E Soc. Eur. E Al Com. Delle Reg. 1–26.

European Union, 2018. Strategia europea per la plastica nell'economia circolare.

EzBioCloud Resources

Falleiros, Â.M.F.; Bombonato, M.T.S.; Gregório, E.A. Ultrastructural and quantitative studies of hemocytes in the sugarcane borer, Diatraea saccharalis (Lepidoptera: Pyralidae). Braz. Arch. Biol. Technol. 2003, 46, 287 -2 94.

Fan, P., Yu, H., Xi, B., & Tan, W. (2022). A review on the occurrence and influence of biodegradable microplastics in soil ecosystems: Are biodegradable plastics substitute or threat?. Environment International, 107244.

Feng, L., He, L., Jiang, S., Chen, J., Zhou, C., Qian, Z. J., ... & Li, C. (2020). Investigating the composition and distribution of microplastics surface biofilms in coral areas. Chemosphere, 126565.

Figueras, A., Moreira, R., Sendra, M., & Novoa, B. (2019). Genomics and immunity of the Mediterranean mussel Mytilus galloprovincialis in a changing environment. Fish & Shellfish Immunology, 90, 440-445.

Foley, C. J.; Feiner, Z. S.; Malinich, T. D.; Höök, T. O. A meta-analysis of the effects of exposure to microplastics on fish and aquatic invertebrates. Sci. Total Environ. 2018, 631, 550 - 559. https://doi.org/10.1016/j.scitotenv.2018.03.046

Frank, J. A.; Reich, C. I.; Sharma, S.; Weisbaum, J. S.; Wilson, B. A.; Olsen, G. J. (2008): Critical Evaluation of Two Primers Commonly Used for Amplification of Bacterial 16S rRNA Genes. In: *Applied and Environmental Microbiology* 74 (8), S. 2461–2470. DOI: 10.1128/AEM.02272-07.

Gagnaire B, Frouin H, Moreau K, Thomas-Guyon H, Renault T (2006) Effects of temperature and salinity on haemocyte activities of the Pacific oyster, Crassostrea gigas (Thunberg). Fish Shellfish Immunol 20:536–547

Galego, N.; Rozsa, C.; Sánchez, R.; Fung, J.; Vázquez, A.; Santo Tomás, J. Characterization and application of poly (β-hydroxyalkanoates) family as composite biomaterials. Polym. Test. 2000, 19, 485 - 492.

Gazzetta Ufficiale - Italy, 2021. Piano strategico 12 dicembre 2021 GU N. 72 del 24 marzo 2021. Gazz. Uff. Ser. Gen. 285, 2–5.

Gedik, K., & Eryaşar, A. R. (2020). Microplastic pollution profile of Mediterranean mussels (Mytilus galloprovincialis) collected along the Turkish coasts. Chemosphere, 260, 127570.

Girard, E. B., Kaliwoda, M., Schmahl, W. W., Wörheide, G., & Orsi, W. D. (2020). Textile waste and microplastic induce activity and development of unique hydrocarbon-degrading marine bacterial communities. bioRxiv, 2020-02.

Goh, Y. Q., & Ooi, C. P. (2008). Fabrication and characterization of porous poly (l-lactide) scaffolds using solid–liquid phase separation. Journal of Materials Science: Materials in Medicine, 19, 2445-2452.

Gomiero, A.; Strafella, P.; Pellini, G.; Salvalaggio, V.; Fabi, G. Comparative effects of ingested PVC microparticles with and without adsorbed benzo (a) pyrene vs. spiked

sediments on the cellular and sub cellular processes of the benthic organism Hediste diversicolor. Front. Mar. Sci. 2018, 5, 99. https://doi.org/10.3389/fmars.2018.00099

Gornati, R.; Maisano, M.; Pirrone, C.; Cappello, T.; Rossi, F.; Borgese, M.; Giannetto, A.; Cappello, S.; Mancini, G.; Bernardini, G.; Fasulo, S. Mesocosm System to Evaluate BF-MBR Efficacy in Mitigating Oily Wastewater Discharges: an Integrated Study on Mytilus galloprovincialis. Mar. Biotechn. 2019, 21, 773 – 790. https://doi.org/10.1007/s10126-019-09923-9

Guo, H., Hua, J., Cheng, J., Yue, L., & Zhou, J. (2022). Microbial electrochemistry enhanced electron transfer in lactic acid anaerobic digestion for methane production. Journal of Cleaner Production, 358, 131983.

Gupta, A. P., & Kumar, V. (2007). New emerging trends in synthetic biodegradable polymers–Polylactide: A critique. European polymer journal, 43(10), 4053-4074.

Hahn, S. K., Chang, Y. K., Kim, B. S., & Chang, H. N. (1994). Optimization of microbial poly (3-hydroxybutyrate) recover using dispersions of sodium hypochlorite solution and chloroform. Biotechnology and bioengineering, 44(2), 256-261.

Haider, T. P., Völker, C., Kramm, J., Landfester, K., & Wurm, F. R. (2019). Plastics of the future? The impact of biodegradable polymers on the environment and on society. Angewandte Chemie International Edition, 58(1), 50-62.

Hajighasemi, M., Nocek, B. P., Tchigvintsev, A., Brown, G., Flick, R., Xu, X., ... & Yakunin, A. F. (2016). Biochemical and structural insights into enzymatic depolymerization of polylactic acid and other polyesters by microbial carboxylesterases. Biomacromolecules, 17(6), 2027-2039.

Han, G. D., & Dong, Y. W. (2020). Rapid climate-driven evolution of the invasive species Mytilus galloprovincialis over the past century. Anthropocene Coasts, 3(1), 14-29.

Hellio, C., Bado-Nilles, A., Gagnaire, B., Renault, T., & Thomas-Guyon, H. (2007). Demonstration of a true phenoloxidase activity and activation of a ProPO cascade in Pacific oyster, Crassostrea gigas (Thunberg) in vitro. Fish & shellfish immunology, 22(4), 433-440.

Hoellein, T.; Rovegno, C.; Uhrin, A. V.; Johnson, E.; Herring, C. Microplastics in Invasive Freshwater Mussels (Dreissena sp.): Spatiotemporal Variation and Occurrence with Chemical Contaminants. Front. Mar. Sci. 2021, 8, 821. https://doi.org/10.3389/fmars.2021.690401

Hong, S. H., Park, J. H., Kim, O. Y., & Hwang, S. H. (2021). Preparation of chemically modified lignin-reinforced PLA biocomposites and their 3D printing performance. Polymers, 13(4), 667.

https://help.ezbiocloud.net/16s-rrna-and-16s-rrna-gene/ (Accessed May, 2023)

Huang, J. N., Wen, B., Miao, L., Liu, X., Li, Z. J., Ma, T. F., ... & Chen, Z. Z. (2022). Microplastics drive nitrification by enriching functional microorganisms in aquaculture pond waters. Chemosphere, 309, 136646.

Hubbe, M. A., Lavoine, N., Lucia, L. A., & Dou, C. (2021). Formulating Bioplastic Composites for Biodegradability, Recycling, and Performance: A Review. BioResources, 16(1).

Huffman Ringwood, A. (2021). Bivalves as biological sieves: Bioreactivity pathways of microplastics and nanoplastics. The Biological Bulletin, 241(2), 185-195.

Ilyas, R. A., Zuhri, M. Y. M., Aisyah, H. A., Asyraf, M. R. M., Hassan, S. A., Zainudin, E. S., ... & Sari, N. H. (2022). Natural fiber-reinforced polylactic acid, polylactic acid blends and their composites for advanced applications. Polymers, 14(1), 202.

Imron, M. F., & Titah, H. S. (2018). Optimization of diesel biodegradation by Vibrio alginolyticus using Box-Behnken design. Environmental Engineering Research, 23(4), 374-382.

Jacquel, N.; Lo, C. W.; Wu, H. S.; Wei, Y. H.; Wang, S. S. Solubility of polyhydroxyalkanoates by experiment and thermodynamic correlations. AIChE J. 2007, 53, 2704 - 2714. https://doi.org/10.1002/aic.11274

Johansen, M.R., Christensen, T.B., Ramos, T.M., Syberg, K., 2022. A review of the plastic value chain from a circular economy perspective. J. Environ. Manage. 302, 113975. https://doi.org/10.1016/j.jenvman.2021.113975

Kabasci, Stephan (2013). Bio-Based Plastics (Materials and Applications) || Poly(Lactic Acid). , 10.1002/9781118676646(), 171–239. doi:10.1002/9781118676646.ch8

Kirstein, I. V., Kirmizi, S., Wichels, A., Garin-Fernandez, A., Erler, R., Löder, M., & Gerdts, G. (2016). Dangerous hitchhikers? Evidence for potentially pathogenic Vibrio spp. on microplastic particles. Marine environmental research, 120, 1-8.

Kolahchi, A. R., & Kontopoulou, M. (2015). Chain extended poly (3-hydroxybutyrate) with improved rheological properties and thermal stability, through reactive modification in the melt state. Polymer degradation and stability, 121, 222-229.

Kourmentza, C., Plácido, J., Venetsaneas, N., Burniol-Figols, A., Varrone, C., Gavala, H. N., & Reis, M. A. (2017). Recent advances and challenges towards sustainable polyhydroxyalkanoate (PHA) production. Bioengineering, 4(2), 55.

Krause, S., Molari, M., Gorb, E. V., Gorb, S. N., Kossel, E., & Haeckel, M. (2020). Persistence of plastic debris and its colonization by bacterial communities after two decades on the abyssal seafloor. Scientific reports, 10(1), 9484.

Kumar, Rakesh, Verma, A., Shome, A., Sinha, R., Sinha, S., Jha, P.K., Kumar, Ritesh, Kumar, P., Shubham, Das, S., Sharma, P., Prasad, P.V.V., 2021. Impacts of plastic pollution on ecosystem services, sustainable development goals, and need to focus on circular economy and policy interventions. Sustain. 13, 1–40. https://doi.org/10.3390/su13179963

La Carrubba, V., Pavia, F. C., Brucato, V., & Piccarolo, S. (2008). PLLA/PLA scaffolds prepared via Thermally Induced Phase Separation (TIPS): tuning of properties and biodegradability. International Journal of Material Forming, 1, 619-622.

Li, G.; Zhao, M.; Xu, F.; Yang, B.; Li, X.; Meng, X.; Teng, L.; Sun, F.; Li, Y. Synthesis and Biological Application of Polylactic Acid. Molecules 2020, 25, 5023. https://doi.org/10.3390/molecules25215023

Li, H., Parisi, M. G., Toubiana, M., Cammarata, M., & Roch, P. (2008). Lysozyme gene expression and hemocyte behaviour in the Mediterranean mussel, Mytilus galloprovincialis, after injection of various bacteria or temperature stresses. Fish & shellfish immunology, 25(1-2), 143-152.

Li, Y. Z., Yao, L. H., Li, Y., Wang, Y. J., Wang, L. H., Jiang, Z. Q., ... & Weng, Y. X. (2022). Degradation kinetics and performances of poly (lactic acid) films in artificial seawater. Chemical Papers, 76(9), 5929-5941.

Liu, Y., Blain, S., Crispi, O., Rembauville, M., & Obernosterer, I. (2020). Seasonal dynamics of prokaryotes and their associations with diatoms in the Southern Ocean as revealed by an autonomous sampler. Environmental Microbiology, 22(9), 3968-3984.

Lobelle, D., & Cunliffe, M. (2011). Early microbial biofilm formation on marine plastic debris. Marine pollution bulletin, 62(1), 197-200.

Lopresti, F., Liga, A., Capuana, E., Gulfi, D., Zanca, C., Inguanta, R., Brucato, V., La Carrubba, V., Carfì Pavia, F., 2022. Effect of Polyhydroxyalkanoate (PHA) Concentration on Polymeric Scaffolds Based on Blends of Poly-L-Lactic Acid (PLLA) and PHA Prepared via Thermally Induced Phase Separation (TIPS). Polymers (Basel). 14. https://doi.org/10.3390/polym14122494

Luchtel, D. L., Martin, A. W., Deyrup-Olsen, I. N. G. R. I. T. H., & Boer, H. H. (1997). Gastropoda: pulmonata. Microscopic anatomy of invertebrates, 6, 459-718.

Machałowski, T., & Jesionowski, T. (2021). Hemolymph of molluscan origin: From biochemistry to modern biomaterials science. Applied Physics A, 127, 1-22.

Manfra, L., Marengo, V., Libralato, G., Costantini, M., De Falco, F., & Cocca, M. (2021). Biodegradable polymers: A real opportunity to solve marine plastic pollution?. Journal of Hazardous Materials, 416, 125763.

Manzoor, S., Naqash, N., Rashid, G., & Singh, R. (2022). Plastic material degradation and formation of microplastic in the environment: A review. Materials Today: Proceedings, 56, 3254-3260.

Mardis, E.R., (2008). Next-Generation DNA Sequencing Methods. The Annual Review of genomics and Human genetics, 9: 387-402.

Mayumi, D., Akutsu-Shigeno, Y., Uchiyama, H., Nomura, N., & Nakajima-Kambe, T. (2008). Identification and characterization of novel poly (DL-lactic acid) depolymerases from metagenome. Applied microbiology and biotechnology, 79, 743-750.

Merkley, S. D.; Moss, H. C.; Goodfellow, S. M.; Ling, C. L.; Meyer-Hagen, J. L.; Weaver, J.; Campen, M. J.; Castillo, E. F. Polystyrene microplastics induce an immunometabolic active state in macrophages. Cell. Bio. Toxicol. 2021, 38, 1 - 11. https://doi.org/10.1007/s10565-021-09616-x

Miller, M. E., Hamann, M., & Kroon, F. J. (2020). Bioaccumulation and biomagnification of microplastics in marine organisms: A review and meta-analysis of current data. PLoS One, 15(10), e0240792.

Minguez-Alarcon, L., Hauser, R., Gaskins, A.J., 2016. Effects of bisphenol A on male and couple reproductive health: a review. Fertil. Steril. 106, 864–870. https://doi.org/10.1016/j.fertnstert.2016.07.1118

Mistry, A. N., Kachenchart, B., Wongthanaroj, A., Somwangthanaroj, A., & Luepromchai, E. (2022). Rapid biodegradation of high molecular weight semi-crystalline

polylactic acid at ambient temperature via enzymatic and alkaline hydrolysis by a defined bacterial consortium. Polymer Degradation and Stability, 202, 110051.

Morohoshi, T., Taniguchi, A., Sugawara, A., Suzuki, T., & Sato, S. (2022). Effects of Marine Sand on the Microbial Degradation of Biodegradable Plastics in Seawater and Biofilm Communities that Formed on Plastic Surfaces. Microbes and environments, 37(4), ME22047.

Morozov, A. G., Razborov, D. A., Egiazaryan, T. A., Baten'kin, M. A., Aleynik, D. Y., Egorikhina, M. N., ... & Fedushkin, I. L. (2020). In vitro study of degradation behavior, cytotoxicity, and cell adhesion of the atactic polylactic acid for biomedical purposes. Journal of Polymers and the Environment, 28, 2652-2660.

Mülhaupt, R. (2013). Green polymer chemistry and bio-based plastics: dreams and reality. Macromolecular Chemistry and Physics, 214(2), 159-174. Mülhaupt, R. (2013). Green polymer chemistry and bio-based plastics: dreams and reality. Macromolecular Chemistry and Physics, 214(2), 159-174.

Nandy, S., Fortunato, E., & Martins, R. (2022). Green economy and waste management: An inevitable plan for materials science. Progress in Natural Science: Materials International.

Naser, A.Z.; Deiab, I.; Darras, B.M. Poly(lactic acid) (PLA) and polyhydroxyalkanoates (PHAs), green alternatives to petroleum-based plastics: a review. RSC Adv. 2021, 11, 17151-17196. https://doi.org/10.1039/D1RA02390J

Nofar, M., Sacligil, D., Carreau, P. J., Kamal, M. R., & Heuzey, M. C. (2019). Poly (lactic acid) blends: Processing, properties and applications. International journal of biological macromolecules, 125, 307-360.

Oberbeckmann, S., Löder, M. G., & Labrenz, M. (2015). Marine microplastic-associated biofilms–a review. Environmental chemistry, 12(5), 551-562.

Oberbeckmann, S., Osborn, A. M., &Duhaime, M. B. (2016). Microbes on a bottle: substrate, season and geography influence community composition of microbes colonizing marine plastic debris. *PLoS One*, *11*(8), e0159289.

Otero, P., Saha, S.K., Moane, S., Barron, J., Clancy, G., Murray, P., 2015. Improved method for rapid detection of phthalates in bottled water by gas chromatography-mass spectrometry. J. Chromatogr. B Anal. Technol. Biomed. Life Sci. 997, 229–235. https://doi.org/10.1016/j.jchromb.2015.05.036

Ottoni, B. L., Deus, R. M., Gobbo Junior, J. A., Carvalho, Â. M. G. D., & Battistelle, R. A. G. (2018). Communication and biodegradable packaging relationship: a paradigm for final disposal. Journal of Applied Packaging Research, 10(1), 2.

Paillard, C., Allam, B., & Oubella, R. (2004). Effect of temperature on defense parameters in Manila clam Ruditapes philippinarum challenged with Vibrio tapetis. Diseases of aquatic organisms, 59(3), 249-262.

Panaitescu, D. M.; Nicolae, C. A.; Frone, A. N.; Chiulan, I.; Stanescu, P. O.; Draghici, C., Iorga, M; Mihailescu, M. Plasticized poly (3-hydroxybutyrate) with improved melt processing and balanced properties. J. Appl. Polym. Sci. 2017, 134, 19. https://doi.org/10.1002/app.44810

Papadatou, M., Robson, S. C., Dobretsov, S., Watts, J. E., Longyear, J., & Salta, M. (2021). Marine biofilms on different fouling control coating types reveal differences in microbial community composition and abundance. MicrobiologyOpen, 10(4), e1231.

Parisi, M. G., Mauro, M., Sarà, G., & Cammarata, M. (2017). Temperature increases, hypoxia, and changes in food availability affect immunological biomarkers in the marine mussel Mytilus galloprovincialis. Journal of Comparative Physiology B, 187, 1117-1126.

Parisi, M. G., Mauro, M., Sarà, G., & Cammarata, M. (2017). Temperature increases, hypoxia, and changes in food availability affect immunological biomarkers in the marine mussel Mytilus galloprovincialis. Journal of Comparative Physiology B, 187, 1117-1126.

Parisi, M. G., Pirrera, J., La Corte, C., Dara, M., Parrinello, D., & Cammarata, M. (2021). Effects of organic mercury on Mytilus galloprovincialis hemocyte function and morphology. Journal of Comparative Physiology B, 191, 143-158.

Parisi, M.G.; Trapani, M.R.; Cammarata, M. Granulocytes of sea anemone Actinia equina (Linnaeus, 1758) body fluid contains and releases cytolysins forming plaques of lysis. Invertebr. Surviv. J. 2014, 11, 1, 39-46.

Parliament, E., 2022. Economia circolare: definizione, importanza e vantaggi. Europarl.Europa.Eu 1–4.

Parrinello, D.; Bellante, A.; Parisi, M.G.; Sanfratello, M.A.; Indelicato, S.; Piazzese, D.; Cammarata, M. The ascidian Styela plicata hemocytes as a potential biomarker of marine pollution: In vitro effects of seawater and organic mercury. Ecotoxicology and Environmental Safety, 2017, 136, 126 - 134 https://doi.org/10.1016/j.ecoenv.2016.11.001

Paul-Pont, I., Lacroix, C., Fernández, C. G., Hégaret, H., Lambert, C., Le Goïc, N., ... & Soudant, P. (2016). Exposure of marine mussels Mytilus spp. to polystyrene microplastics: toxicity and influence on fluoranthene bioaccumulation. Environmental pollution, 216, 724-737.

Pellis, A., Malinconico, M., Guarneri, A., & Gardossi, L. (2021). Renewable polymers and plastics: Performance beyond the green. New Biotechnology, 60, 146-158.

Pillai, A. B., Kumar, A. J., Thulasi, K., & Kumarapillai, H. (2017). Evaluation of short-chain-length polyhydroxyalkanoate accumulation in Bacillus aryabhattai. Brazilian journal of microbiology, 48, 451-460.

Pittura, L.; Avio, C. G. Giuliani, M. E.; D'Errico, G.; Keiter, S. H.; Cormier, B.; Gorbi, S Regoli, F. Microplastics as vehicles of environmental PAHs to marine organisms: combined chemical and physical hazards to the Mediterranean mussels, Mytilus galloprovincialis. Front. Mar. Sci. 2018, 5, 103. https://doi.org/10.3389/fmars.2018.00103

Plastics Europe, 2022. Plastics – the Facts 2022 81.

PlasticsEurope, 2018. The facts 2018. https://doi.org/10.1016/j.marpolbul.2013.01.015

Prince, R. C., Amande, T. J., & McGenity, T. J. (2019). Prokaryotic hydrocarbon degraders. Taxonomy, genomics and ecophysiology of hydrocarbon-degrading microbes, 1-39.

Qi, X., Ren, Y., & Wang, X. (2017). New advances in the biodegradation of Poly (lactic) acid. International Biodeterioration & Biodegradation, 117, 215-223.

Rahul, K., Sasikala, C., Tushar, L., Debadrita, R., & Ramana, C. V. (2014). Alcanivorax xenomutans sp. nov., a hydrocarbonoclastic bacterium isolated from a shrimp cultivation pond. International journal of systematic and evolutionary microbiology, 64(Pt_10), 3553-3558.

Raza, Z.A., Abid, S., Banat, I.M., 2018. Polyhydroxyalkanoates : Characteristics , production , recent developments and applications. Int. Biodeterior. Biodegradation 126, 45–56. https://doi.org/10.1016/j.ibiod.2017.10.001

Rehm, B. H., & Steinbüchel, A. (1999). Biochemical and genetic analysis of PHA synthases and other proteins required for PHA synthesis. International journal of biological macromolecules, 25(1-3), 3-19.

Ribeiro, F., Garcia, A. R., Pereira, B. P., Fonseca, M., Mestre, N. C., Fonseca, T. G., ... & Bebianno, M. J. (2017). Microplastics effects in Scrobicularia plana. Marine pollution bulletin, 122(1-2), 379-391.

Roager, L., & Sonnenschein, E. C. (2019). Bacterial candidates for colonization and degradation of marine plastic debris. Environmental science & technology, 53(20), 11636-11643.

Rochman, C. M.; Tahir, A.; Williams, S. L.; Baxa, D. V.; Lam, R.; Miller, J. T.; The, F.-C.; Werorilangi, S.; Teh, S. J. Anthropogenic debris in seafood: Plastic debris and fibers from textiles in fish and bivalves sold for human consumption. Sci. Rep. 2015, 5, 1 - 10. https://doi.org/10.1038/srep14340

Rodríguez, T., Represas, D., & Carral, E. V. (2023). Ecotoxicity of Single-Use Plastics to Earthworms. Environments, 10(3), 41.

Romo, D. M. R., Obando, M. C., Perdomo, M. I. G., & Izquierdo, P. F. (2014). PHA synthase genes in oil-degrading marine bacteria from the Colombian Pacific Coast. International Journal of Advanced Biotechnology and Research, 5(3), 404-414.

Rosli, N. A., Karamanlioglu, M., Kargarzadeh, H., & Ahmad, I. (2021). Comprehensive exploration of natural degradation of poly (lactic acid) blends in various degradation media: A review. International journal of biological macromolecules, 187, 732-741.

Ross, N. W., Firth, K. J., Wang, A., Burka, J. F., & Johnson, S. C. (2000). Changes in hydrolytic enzyme activities of naive Atlantic salmon Salmo salar skin mucus due to infection with the salmon louse Lepeophtheirus salmonis and cortisol implantation. Diseases of aquatic organisms, 41(1), 43-51.

Sabirova, J. S., Ferrer, M., Regenhardt, D., Timmis, K. N., & Golyshin, P. N. (2006). Proteomic insights into metabolic adaptations in Alcanivorax borkumensis induced by alkane utilization. Journal of bacteriology, 188(11), 3763-3773.

Saravanan, K., Umesh, M., & Kathirvel, P. (2022). Microbial Polyhydroxyalkanoates (PHAs): A Review on Biosynthesis, Properties, Fermentation Strategies and Its Prospective Applications for Sustainable Future. Journal of Polymers and the Environment, 30(12), 4903-4935.

Scanes, E.; Wood, H.; Ross, P. Microplastics detected in haemolymph of the Sydney rock oyster Saccostrea glomerata. Mar. Pollut. Bull. 2019, 149, 110537. https://doi.org/10.1016/j.marpolbul.2019.110537

Schneider, C. A., Rasband, W. S., & Eliceiri, K. W. (2012). NIH Image to ImageJ: 25 years of image analysis. Nature methods, 9(7), 671-675.

Sendra, M., Saco, A., Yeste, M. P., Romero, A., Novoa, B., & Figueras, A. (2020). Nanoplastics: From tissue accumulation to cell translocation into Mytilus galloprovincialis hemocytes. resilience of immune cells exposed to nanoplastics and nanoplastics plus Vibrio splendidus combination. Journal of hazardous materials, 388, 121788.

Sendra, M.; Carrasco-Braganza, M.I.; Yeste, P.M.; Vila, M. & Blasco, J.. Immunotoxicity of polystyrene nano plastics in different hemocyte subpopolation of Mytilus galloprovincialis. Scientific Reports, 2020, 10, 8637, https://doi.org/10.38/s41598-020-65596-8

Shen, M., Song, B., Zeng, G., Zhang, Y., Huang, W., Wen, X., & Tang, W. (2020). Are biodegradable plastics a promising solution to solve the global plastic pollution?. Environmental Pollution, 263, 114469.

Shokralla, S., Spall, J.L., Gibson, J.F., Hajibabaei, M., (2012). Next-generation sequencing technologies for environmental DNA research. Molecular ecology, 21 (8): 1794-1805

Shruti, V. C., & Kutralam-Muniasamy, G. (2019). Bioplastics: Missing link in the era of Microplastics. Science of The Total Environment, 697, 134139

Simon, C., Daniel, R., (2010). Metagenomic Analyses: Past and Future Trends. American society for microbiology. Applied and environmental microbiology, 77 (4): 1153-1161.

Simon, J., & Kroneck, P. M. (2013). Microbial sulfite respiration. In Advances in microbial physiology (Vol. 62, pp. 45-117). Academic Press.

Singh, A. K., Srivastava, J. K., Chandel, A. K., Sharma, L., Mallick, N., & Singh, S. P. (2019). Biomedical applications of microbially engineered polyhydroxyalkanoates: An insight into recent advances, bottlenecks, and solutions. Applied microbiology and biotechnology, 103, 2007-2032.

Smith, V. J. (2010). Immunology of invertebrates: cellular. eLS, 1-13.

Sofokleous, Panagiotis (2018). Functional 3D Tissue Engineering Scaffolds || Phase-separation technologies for 3D scaffold engineering., (), 101–126. doi:10.1016/B978-0-08-100979-6.00005-7

Soleimani, Z., Gharavi, S., Soudi, M., & Moosavi-Nejad, Z. (2021). A survey of intact low-density polyethylene film biodegradation by terrestrial Actinobacterial species. International Microbiology, 24, 65-73.

Sudesh, K., Abe, H., Doi, Y., 2000. Synthesis, structure and properties of polyhydroxyalkanoates: Biological polyesters. Prog. Polym. Sci. 25, 1503–1555. https://doi.org/10.1016/S0079-6700(00)00035-6

Sun, X., Chen, B., Xia, B., Li, Q., Zhu, L., Zhao, X., ... & Qu, K. (2020). Impact of mariculture-derived microplastics on bacterial biofilm formation and their potential threat to mariculture: A case in situ study on the Sungo Bay, China. Environmental Pollution, 262, 114336.

Sutton, J., Balfry, S., Higgs, D., Huang, C. H., & Skura, B. (2006). Impact of iron-catalyzed dietary lipid peroxidation on growth performance, general health and flesh proximate and fatty acid composition of Atlantic salmon (Salmo salar L.) reared in seawater. Aquaculture, 257(1-4), 534-557.

Syranidou, E., Karkanorachaki, K., Amorotti, F., Franchini, M., Repouskou, E., Kaliva, M., ... & Kalogerakis, N. (2017). Biodegradation of weathered polystyrene films in seawater microcosms. Scientific reports, 7(1), 17991.

Takahashi, S., Tomita, J., Nishioka, K., Hisada, T., & Nishijima, M. (2014). Development of a prokaryotic universal primer for simultaneous analysis of Bacteria and Archaea using next-generation sequencing. *PloS one*, *9*(8), e105592.

Tan, G. Y. A., Chen, C. L., Li, L., Ge, L., Wang, L., Razaad, I. M. N., ... & Wang, J. Y. (2014). Start a research on biopolymer polyhydroxyalkanoate (PHA): a review. Polymers, 6(3), 706-754.

Tavares da Silva, R., de Souza Grilo, M. M., Magnani, M., & de Souza Pedrosa, G. T. (2021). Double-Layer Plaque Assay Technique for Enumeration of Virus Surrogates. *Detection and Enumeration of Bacteria, Yeast, Viruses, and Protozoan in Foods and Freshwater*, 157–162 https://doi.org/10.1007/978-1-0716-1932-2_14

Teixeira, S., Eblagon, K. M., Miranda, F., R. Pereira, M. F., & Figueiredo, J. L. (2021). Towards controlled degradation of poly (lactic) acid in technical applications. C, 7(2), 42.

Teramoto, M., Ohuchi, M., Hatmanti, A., Darmayati, Y., Widyastuti, Y., Harayama, S., & Fukunaga, Y. (2011). Oleibacter marinus gen. nov., sp. nov., a bacterium that degrades petroleum aliphatic hydrocarbons in a tropical marine environment. International Journal of Systematic and EvolutionaryMicrobiology, 61(2), 375-380.

Tsuji, H., Daimon, H., & Fujie, K. (2003). A new strategy for recycling and preparation of poly (L-lactic acid): hydrolysis in the melt. Biomacromolecules, 4(3), 835-840.

UNEP – Marine Plastic Debris and Microplastics – Global Lessons and Research to Inspire Action and Guide Policy Change – United Nations Environment Programme, Nairobi (2016)

Vaksmaa, A., Knittel, K., Abdala Asbun, A., Goudriaan, M., Ellrott, A., Witte, H. J., ... & Niemann, H. (2021). Microbial communities on plastic polymers in the Mediterranean Sea. Frontiers in microbiology, 12, 673553.

Valappil, S. P., Misra, S. K., Boccaccini, A. R., Keshavarz, T., Bucke, C., & Roy, I. (2007). Large-scale production and efficient recovery of PHB with desirable material properties, from the newly characterised Bacillus cereus SPV. Journal of biotechnology, 132(3), 251-258.

Van Beilen, J. B., Marín, M. M., Smits, T. H., Röthlisberger, M., Franchini, A. G., Witholt, B., & Rojo, F. (2004). Characterization of two alkane hydroxylase genes from the marine hydrocarbonoclastic bacterium Alcanivorax borkumensis. Environmental microbiology, 6(3), 264-273.

Vanlautem, N. J.G., 1982. United States Patent, Patent number 4,705,604

Vidal-Verdú, À., Latorre-Pérez, A., Molina-Menor, E., Baixeras, J., Peretó, J., & Porcar, M. (2022). Living in a bottle: Bacteria from sediment-associated Mediterranean waste and potential growth on polyethylene terephthalate. MicrobiologyOpen, 11(1), e1259.

Viljakainen, V. R., & Hug, L. A. (2021). New approaches for the characterization of plastic-associated microbial communities and the discovery of plastic-degrading microorganisms and enzymes. Computational and Structural Biotechnology Journal, 19, 6191-6200.

Viljakainen, V. R., & Hug, L. A. (2021). The phylogenetic and global distribution of bacterial polyhydroxyalkanoate bioplastic-degrading genes. Environmental Microbiology, 23(3), 1717-1731.

Villanueva, L., Del Campo, J., & Guerrero, R. (2010). Diversity and physiology of polyhydroxyalkanoate-producing and-degrading strains in microbial mats. FEMS microbiology ecology, 74(1), 42-54.

Voelkerding, K.V., Dames, S.A., Durtschi, J.D., (2009). Next- Generation Sequencing: from basic research to diagnostics. Clinical chemistry, 55 (4): 641-658

Von Moos, N., Burkhardt-Holm, P., & Köhler, A. (2012). Uptake and effects of microplastics on cells and tissue of the blue mussel Mytilus edulis L. after an experimental exposure. Environmental science & technology, 46(20), 11327-11335.

Wang, G. X., Huang, D., Ji, J. H., Völker, C., & Wurm, F. R. (2021). Seawater-degradable polymers—fighting the marine plastic pollution. Advanced Science, 8(1), 2001121.

Wang, Y., Yin, J., & Chen, G. Q. (2014). Polyhydroxyalkanoates, challenges and opportunities. Current Opinion in Biotechnology, 30, 59-65.

Ward, C. P., & Reddy, C. M. (2020). We need better data about the environmental persistence of plastic goods. Proceedings of the National Academy of Sciences, 117(26), 14618-14621

Weber, A.; von Randow, M.; Voigt, A. L.; von der Au, M.; Fischer, E.; Meermann, B.; Wagner, M. Ingestion and toxicity of microplastics in the freshwater gastropod Lymnaea stagnalis: No microplastic-induced effects alone or in combination with copper. Chemosphere, 2021, 263, 128040. https://doi.org/10.1016/j.chemosphere.2020.128040

Weber, C. F., & King, G. M. (2007). Physiological, ecological, and phylogenetic characterization of Stappia, a marine CO-oxidizing bacterial genus. Applied and environmental microbiology, 73(4), 1266-1276

Wei, L., & McDonald, A. G. (2015). Peroxide induced cross-linking by reactive melt processing of two biopolyesters: Poly (3-hydroxybutyrate) and poly (l-lactic acid) to improve their melting processability. Journal of Applied Polymer Science, 132(13).

Winder, A. J., & Harris, H. (1991). New assays for the tyrosine hydroxylase and dopa oxidase activities of tyrosinase. European Journal of Biochemistry, 198(2), 317-326.

Wright, R. J., Langille, M. G., & Walker, T. R. (2021). Food or just a free ride? A meta-analysis reveals the global diversity of the Plastisphere. The ISME Journal, 15(3), 789-806.

Yakimov, M. M., Bargiela, R., & Golyshin, P. N. (2022). Calm and Frenzy: marine obligate hydrocarbonoclastic bacteria sustain ocean wellness. Current Opinion in Biotechnology, 73, 337-345.

Yakimov, M. M., Golyshin, P. N., Lang, S., Moore, E. R., Abraham, W. R., Lünsdorf, H., & Timmis, K. N. (1998). Alcanivorax borkumensis gen. nov., sp. nov., a new, hydrocarbon-degrading and surfactant-producing marine bacterium. International Journal of Systematic and Evolutionary Microbiology, 48(2), 339-348.

Yakimov, M. M., Timmis, K. N., & Golyshin, P. N. (2007). Obligate oil-degrading marine bacteria. Current opinion in biotechnology, 18(3), 257-266.

Zadjelovic, V., Gibson, M. I., Dorador, C., & Christie-Oleza, J. A. (2020). Genome of Alcanivorax sp. 24: a hydrocarbon degrading bacterium isolated from marine plastic debris. Marine Genomics, 49, 100686.

Zettler, E. R., Mincer, T. J., & Amaral-Zettler, L. A. (2013). Life in the "plastisphere": microbial communities on plastic marine debris. Environmental science & technology, 47(13), 7137-7146.

Zhang, F.; Man, Y. B.; Mo, W. Y.; Man, K. Y.; Wong, M. H. (). Direct and indirect effects of microplastics on bivalves, with a focus on edible species: A mini-review. Crit. Rev. Environ. Sci. 2020, 50, 2109-2143. https://doi.org/10.1080/10643389.2019.1700752

1 - Fourier Transform Infrared Spectroscopy (FT-IR)

Figure 1, **Figure 2** and **Figure 3** respectively show the FT-IR spectra of PHB_GF, PHBV_GF and PDLLA. The characterization of the three polymers is reported respectively in **Table 1**, **Table 2** and in **Table 3** (Sathiyanarayanan et al., 2017; Gumel et al., 2012; Sindhu et al., 2011).
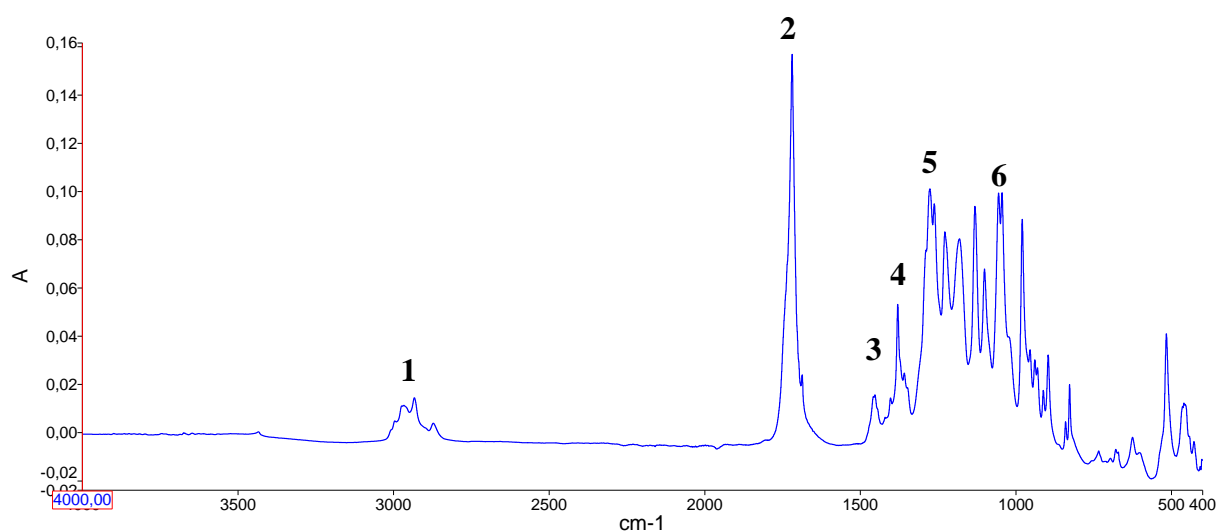
Figure 1 – FT-IR spectrum of PHB_GF (see **Table 1**)

Table 1 - Infra-Red characterisation values of PHB_GF

REFERENCE NUMBER	GROUP	WAVE NUMBER ν (CM^{-1})
1	ν CH	2988 - 2920
2	ν C=O	1721
3 - 4	δ CH	1452 - 1380
5	ν C-O (esters)	1300-1100
6	ν C-O (alcoholic)	1100-1000
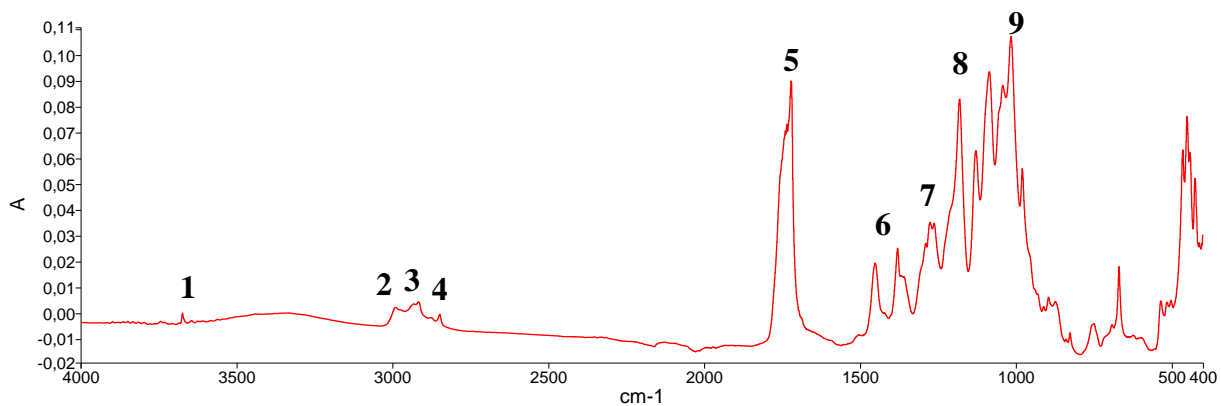
Figure 2 - FT-IR spectrum of PHBV_GF (see **Table 2**)

Table 2 - Infra-Red characterisation values of PHBV_GF

Reference number	GROUP	WAVE NUMBER ν (CM^{-1})
1	ν OH	3675
2 - 4	ν CH	2988-2920
5	ν C=O	1725
6 - 7	δ CH	1452-1380
8	ν C-O (esters)	1300-1150
9	ν C-O (alcoholic)	1150-1000

Figure 3 – FT-IR spectrum of PDLA (see **Table 3**)

Table 3 - Infra-Red characterisation values of PDLA

REFERENCE NUMBER	GROUP	WAVE NUMBER ν (CM^{-1})
1	ν OH	3297
2 - 4	ν CH	2988 - 2850
5	ν C=O	1750
6 – 7	δ CH	1453 - 1382
8	ν C-O (esters)	1300-1150
9	ν C-O (alcoholic)	1150-960

From the analysis of the FT-IR spectra reported above, it is possible to observe the typical characteristic bands of the biopolymers analysed and reported in the literature (Rebocho et al., 2020; Cuiffo et al., 2017; Singla et al., 2012). In fact, the bands at 2988 cm^{-1} and 2920 cm^{-1} (in PDLLA spectrum bands are at 2988 – 2850 cm^{-1}) are assigned to C-H stretching of -CH$_3$; the strong bands corresponding to the C=O bond extending from the carbonyl ester group of the polyhydroxyalkanoates to 1725 cm^{-1} for PHBV_GF, 1721 cm^{-1} for both PHB_GF and PHB and 1750 cm^{-1} for PLA are evident (Rebocho et al. 2020; Ciuffo et al., 2017; Singla et al., 2012), and corresponding bands to the asymmetric stretching of the C-O-C group by polyhydroxyalkanoates between 1100 and 1300 cm^{-1} (Abid et al. 2016). In the FTIR spectrum of PLA the characteristic absorption of ester C-O stretching is at 1187.45 cm^{-1} (Singla et al., 2012). Any variations in the bands as a result of chemical and/or biological exposures can allow to evaluate the possible degradation of the biopolymers. The spectra obtained from the FT-IR analyses carried out on the samples placed in contact with the synthetic sea water solution (SSW) (De Stefano et al., 2002) (**Figure 4**), did not show substantial differences with respect to the reference ones.
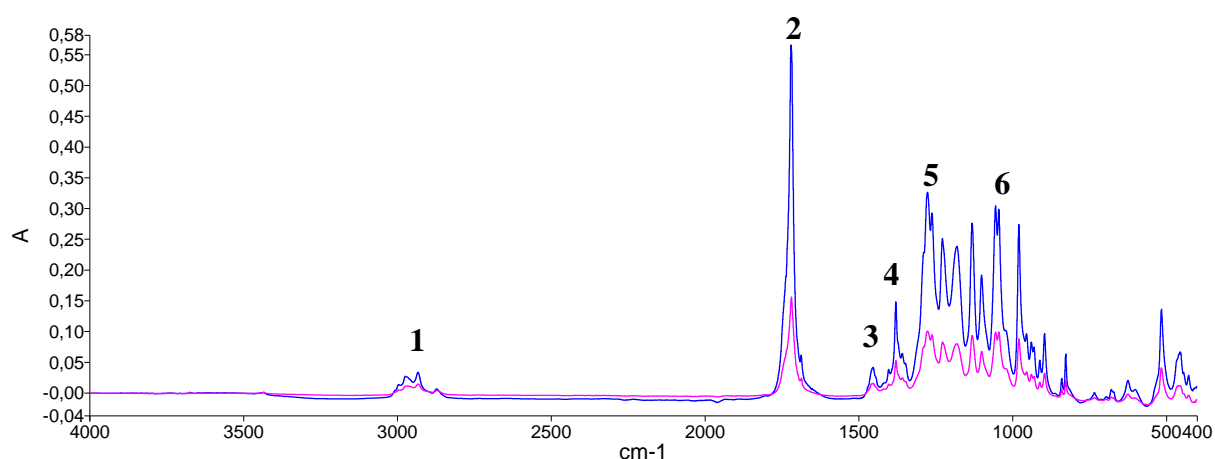
Figure 4 –FT-IR spectrum of PHB_GF in SSW (blue spectrum), compared with FT-IR spectrum of PHB_GF (pink spectrum) (see **Table 4**)

Table 4 - Infra-Red characterisation values of PHB_GF in SSW

REFERENCE NUMBER	GROUP	WAVE NUMBER ν (CM^{-1})
1	ν CH	2936
2	ν C=O	1721
3 - 4	δ CH	1450-1380
5	ν C-O (esters)	1300-1100
6	ν C-O (alcoholic)	1100-1000

With reference to the PHBV_GF sample in SSW, (**Figure 5**) however, a slight broadening of the hydroxyl peak is observed at the frequency of 3384 cm^{-1} (*Reference 1* in **Figure 5** and **Table 5**).
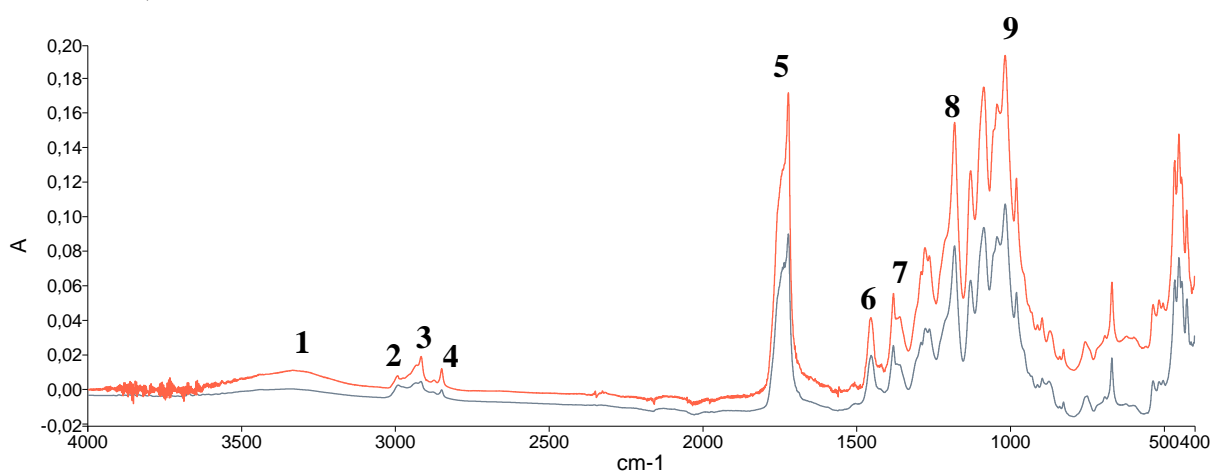
Figure 5 – FT-IR spectrum of PHBV_GF in SSW (red spectrum), compared with FT-IR spectrum of PHBV_GF (grey spectrum) (see **Table 5**)

Table 5 - Infra-Red characterisation values of PHBV_GF in SSW

REFERENCE NUMBER	GROUP	WAVE NUMBER ν (CM^{-1})
1	ν OH	3384
2 - 4	ν CH	2988 - 2920
5	ν C=O	1785-1700
6 - 7	δ CH	1452 - 1380
8	ν C-O (esters)	1300-1150
9	ν C-O (alcoholic)	1150-950

2 - Scanning Electron Microscopy (SEM)

The SEM observations of the PHB, PHB_GF and PHBV_GF samples were preliminarily carried out, without subjecting the samples to any test.

The first sample observed was the PHB (**Figure 6**): already from the overview it is clear that the sample consists of microparticles each with an average size of about 600 nm which, together with others of smaller size (about 300 nm), associate with each other giving rise to agglomerates having an average size of 8.0-9.0 µm (**Figure 6a**). Subjected to an irradiation of 15 kV, the sample showed an evident deterioration despite the preliminary metallization and, therefore, it was necessary to reduce the electron beam to 10 kV and to 5 kV - Low. By reducing the intensity of the electron beam, it was possible to appreciate the structure of the agglomerates more closely (**Figure 6b**).
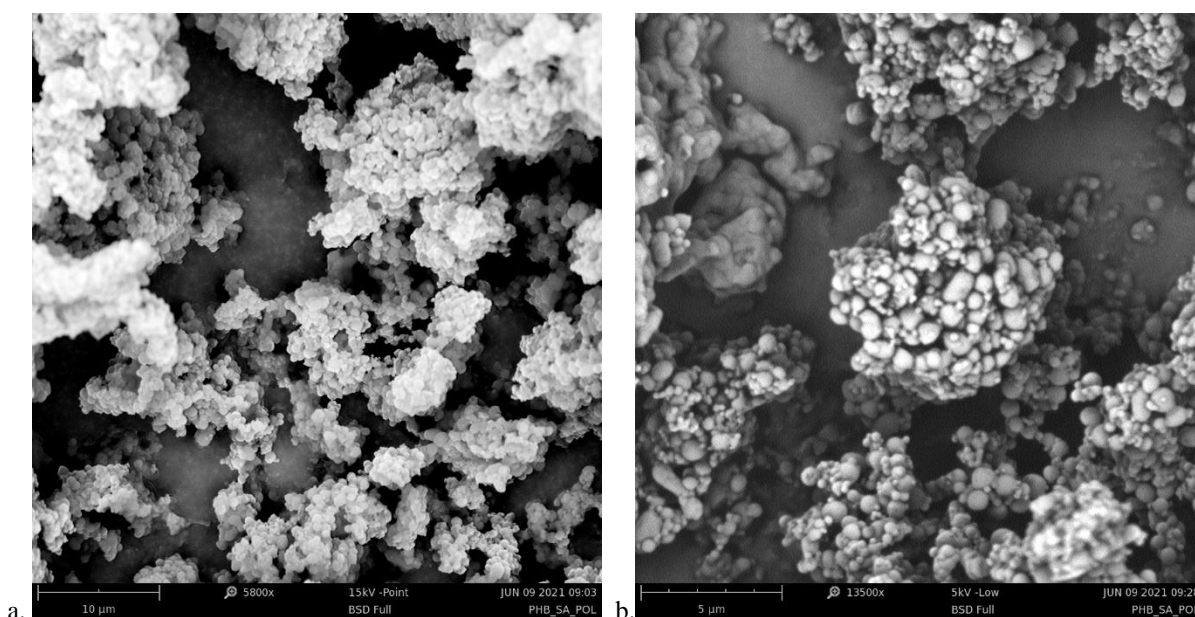
Figure 6 – SEM images of PHB (a. – 5800x; 15 kV) (b. – 13500x; 5 kV-Low)

The second sample observed was the PHBV_GF pellet in section, which showed a surface characterized by small and large fractures. These lesions are particularly marked on the edge, where scales and laminations of the surface were also found (Figure 7a): this could be due to the friction between the polymer and the walls of the extruder during the pelletisation phase. On the same surface (Figure 7b) the presence of some microparticle clusters was found, similar to those observed in the sample of PHB powder (Figure 6). These particles have not been altered by the radiation from the instrument, possibly thanks to the metallization process. The presence of microparticles could confirm the hypothesis that the pellet is produced from powder and may represent the first dispersed particles in the physical disintegration of polymers, contributing to the formation of micro or nanoparticles.
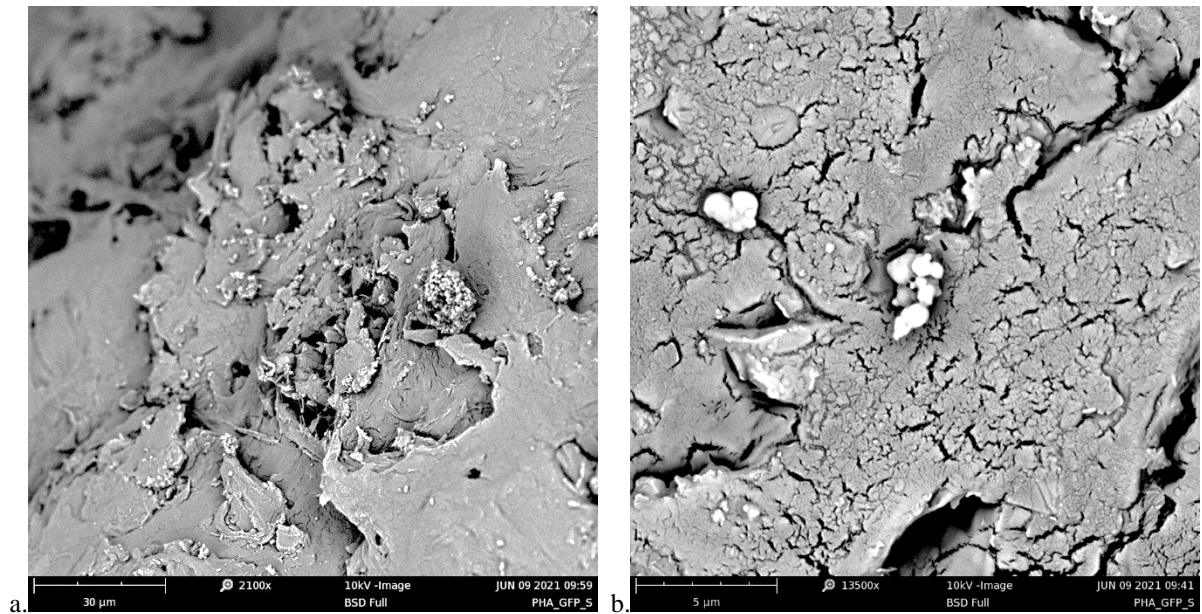
Figure 7 – SEM images of PHBV_GF – convex surface (a. – 2100x; 10 kV) (b. – 13500x; 10 kV)

On the other hand, observing the cutting surface of the PHBV_GF sample, the fractures appeared different, more ordered and oriented towards the same direction; this could be due to the action of the cut during pelletisation (Figure 8a). The surface of the sample appears smooth, with some lignin fibers, partially adhered to the structure of the biopolymer material. The micrograph in Figure 8b shows agglomerates of microparticles on the surface of lignin fibers.
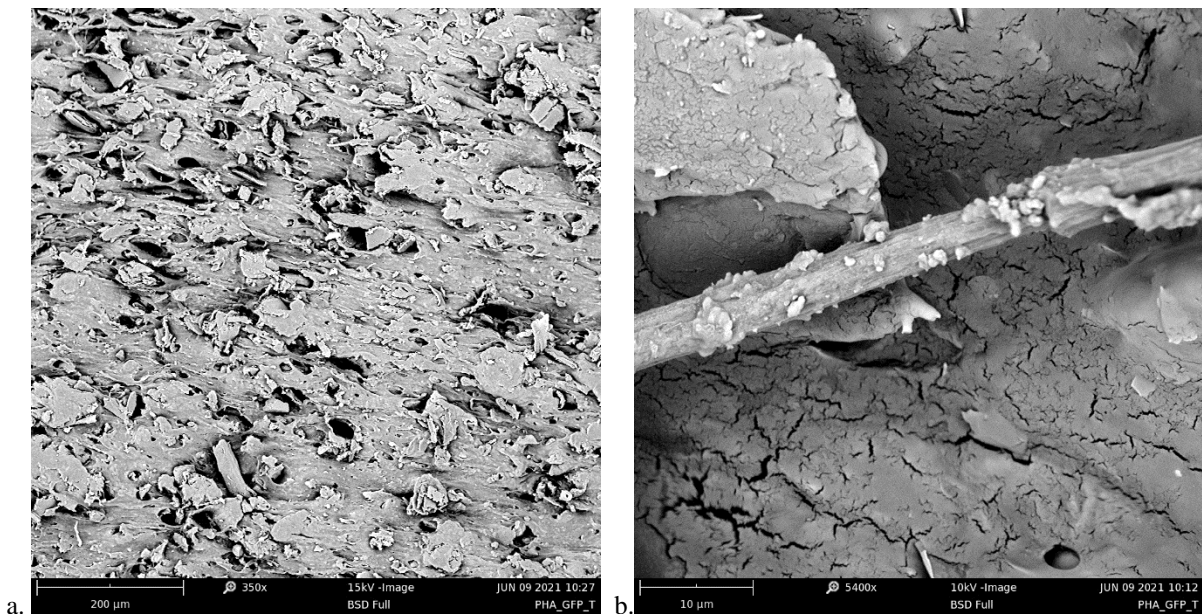
Figure 8 – SEM images of PHBV_GF – cutting surface (a. – 350x; 15 kV) (b. – 5400x; 10 kV)

Lastly, the pellet of the PHB_GF sample was observed. In the micrograph of the section of the pellet, the surface (**Figure 9a**) appeared very homogeneous, free of fractures, with deposits of impurities and accumulations of microparticles similar in shape and size to

those observed in the PHB powder sample (**Figure 6**). and in the PHBV_GF pellet sample (**Figure 7**). The presence of microparticles also in this sample could validate the hypothesis of the pelletisation process made starting from biopolymer powder. The sample appears to be very uniform: even close to the cut point, at low magnifications, it does not show the fractures and alterations observed in the same region of the PHBV_GF pellet sample. By observing in detail, the agglomerates of microparticles, these were found to be more compact than those observed in the other samples (**Figure 9b**).

a.   b.
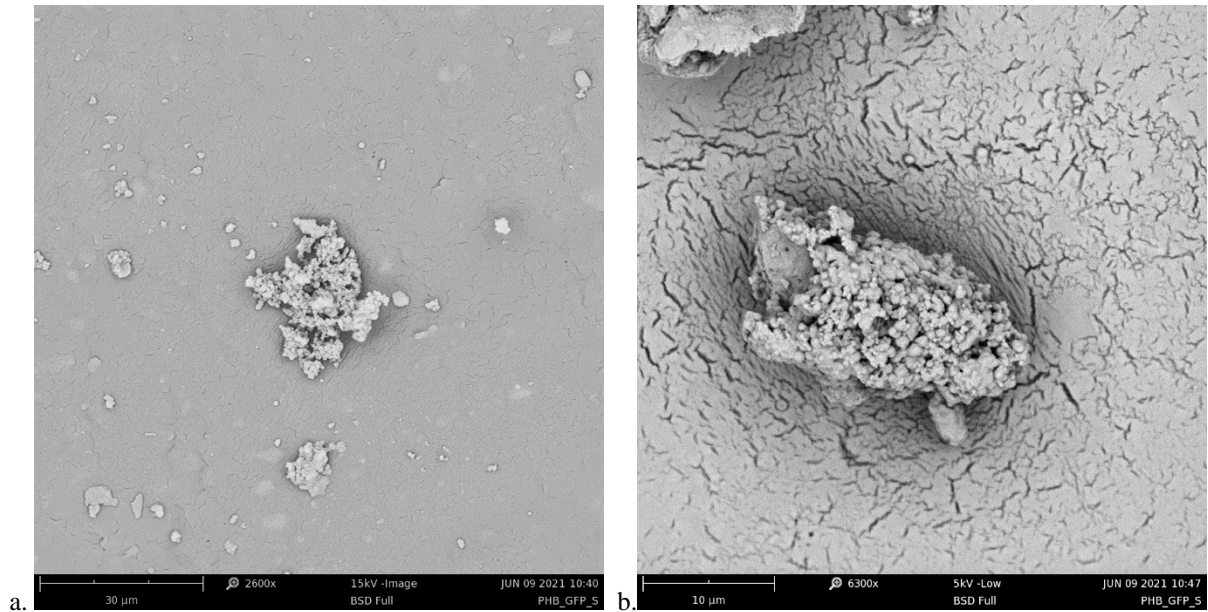
Figure 9 – SEM images of PHBV_GF – convex surface (a. – 2600x; 15 kV) (b. – 6300x; 5 kV-Low)

The observation of the cut of the pellet (**Figure 10**) of the same sample, PHB_GF, shows a different trend of the surface which has streaks oriented towards a single direction. This could probably be due to the shear effect during pelletisation (**Figure 10a**). Furthermore, there are accumulations of microparticles already visible even at low magnifications; some of which are large (**Figure 10b** shows an agglomeration of about 120 µm in length by 36 µm in maximum width) (**Figure 10b**).
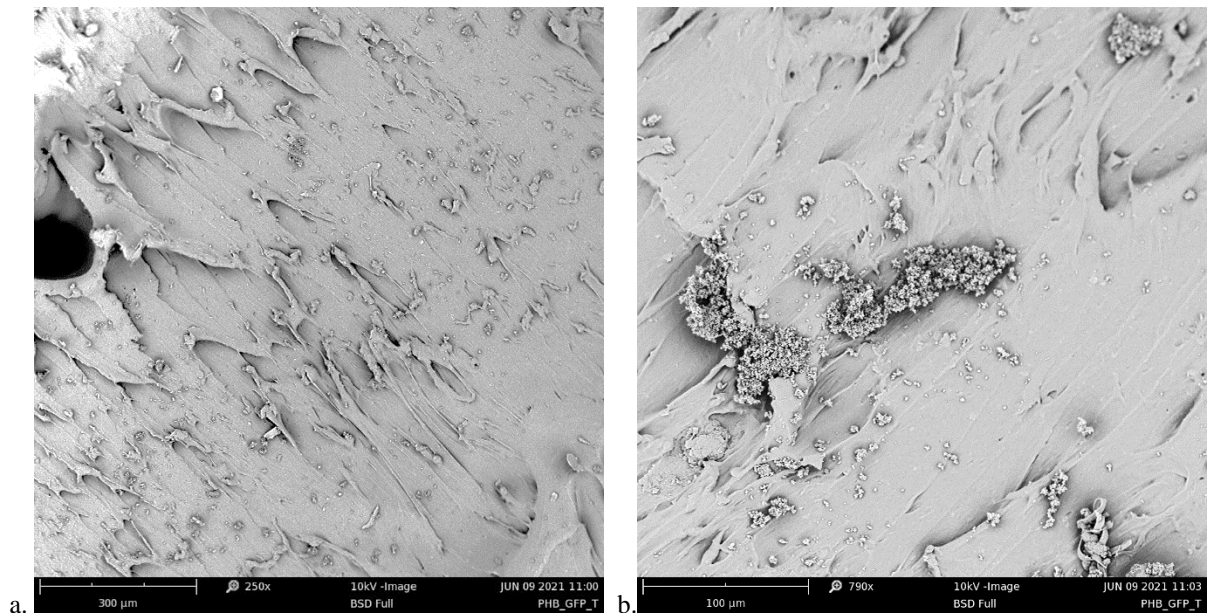
Figure 10 – SEM images of PHBV_GF – cutting surface (a. – 250x; 10 kV) (b. – 790x; 10 kV)

The SEM observation of the PHBV_GF sample placed in contact with distilled water showed an evident deposition of impurities (light in color compared to the pellet) larger in shear than in the section. The surface of the pellet was degraded compared to the surface observed in the PHBV_GF sample (**Figure 11a**), while the lignin fibers are numerous and clearly evident (the sample is a composite to which wood flour has been added as a conditioning agent) with a diameter of approximately 1 µm that do not appear to have suffered damage from the degradation process (**Figure 11b**).
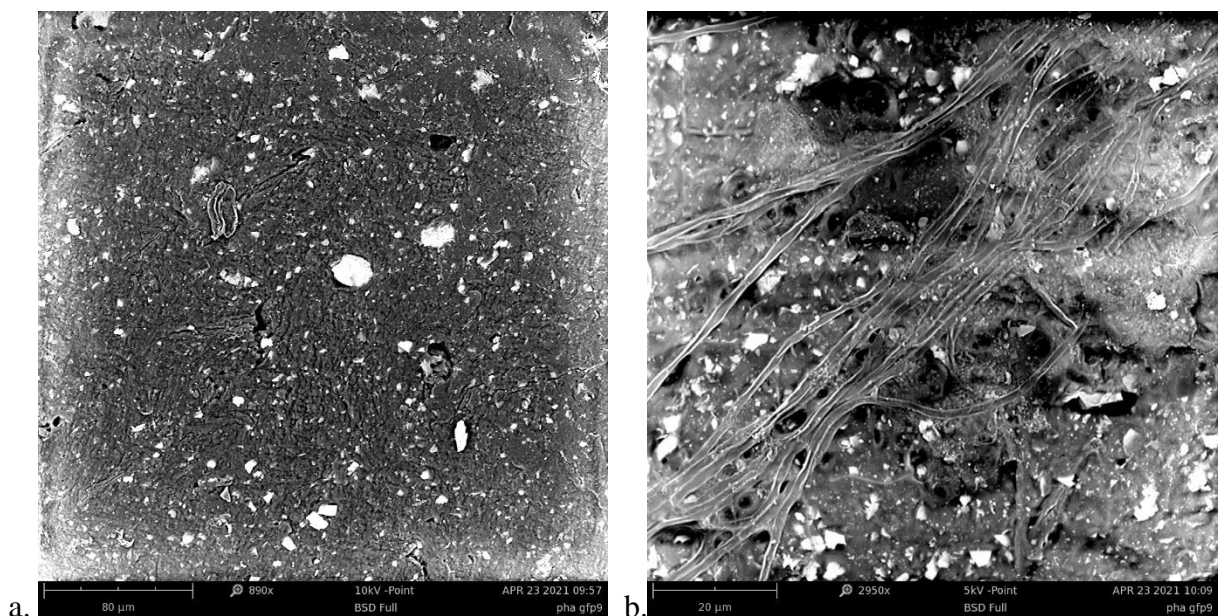


Figure 11 – SEM images of PHBV_GF after degradation test in distilled water – convex surface (a. – 890x; 10 kV) and cutting surface (b. – 2950x; 5 kV)

The PHBV_GF sample was placed in contact with the synthetic marine solution (SSW) (**Figure 12a**) it resulted in visibly more deterioration than the previous sample on the edges already at 230 magnifications. It also has more inclusions within the channels produced by

the degradation process on the surface of the pellet. Also in this sample, the lignin fibers are observed which maintain a diameter of about 1 μm, evident both in cut and in section. (**Figure 12b**).
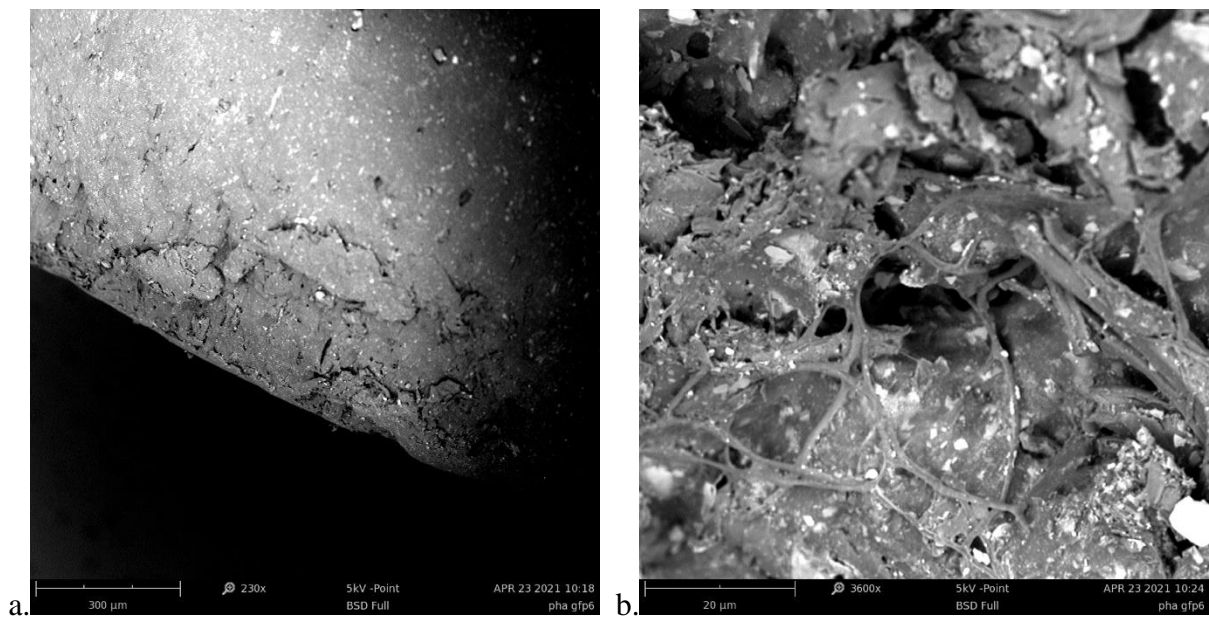
Figure 12 – SEM images of PHBV_GF after degradation test in distilled water – convex surface (a. – 230x; 5 kV) (b. – 3600x; 5 kV)

Observation of the section of the PHBV_GF sample placed in a pH 4.1 solution showed a smoother surface condition (**Figure 13a**) but with the presence of inclusions and deposits (**Figure 13b**). Furthermore, unlike the reference samples and the samples placed in distilled water and in SSW, the sample placed in an acidified solution resulted to be particularly sensitive to the irradiation of the instrument, with evident and rapid alterations already at 5 kV.
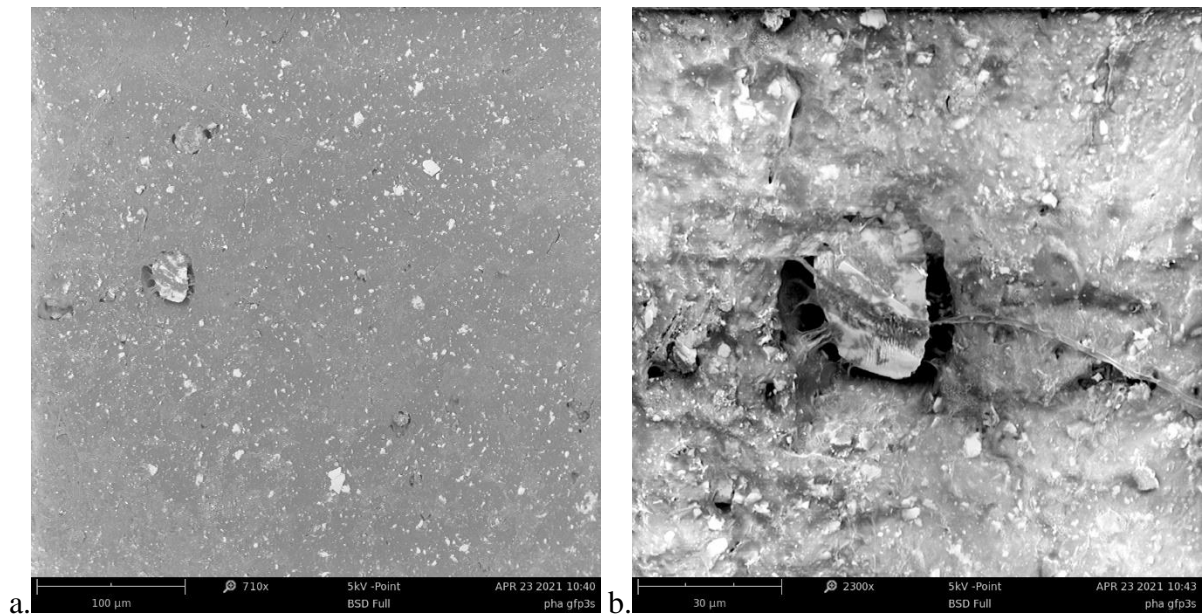
Figure 13 – SEM images of PHBV_GF after degradation test in in a pH 4.1 solution – convex surface (a. – 710x; 5 kV) (b. – 2300x; 5 kV)

Instead, observe the same sample on the cut surface. greater erosion can be seen with respect to the convex surface (**Figure 14a** and **Figure 14b**). The cut surface is also less sensitive to the working conditions than the previous observations of the sectional sample, not undergoing visible alterations as the magnification increases. Inclusions are less present, just as there is a lower presence of lignin fibers. The fibers present are evidently altered in shape, therefore it is possible that they have been attacked by the acid, with subsequent degradation (**Figure 14c**).
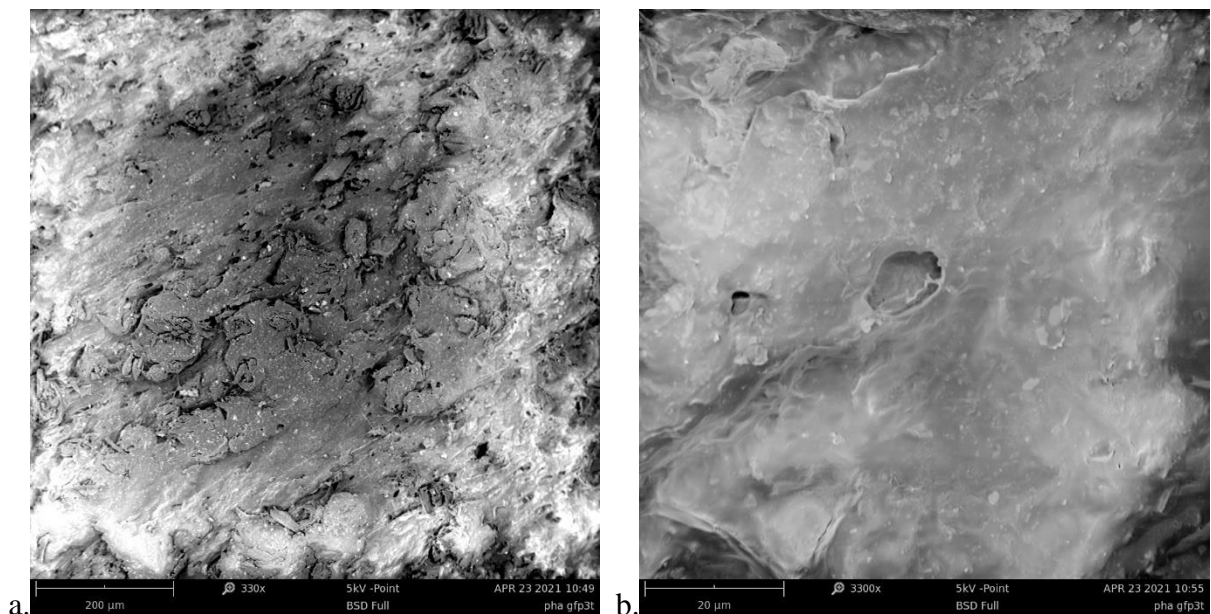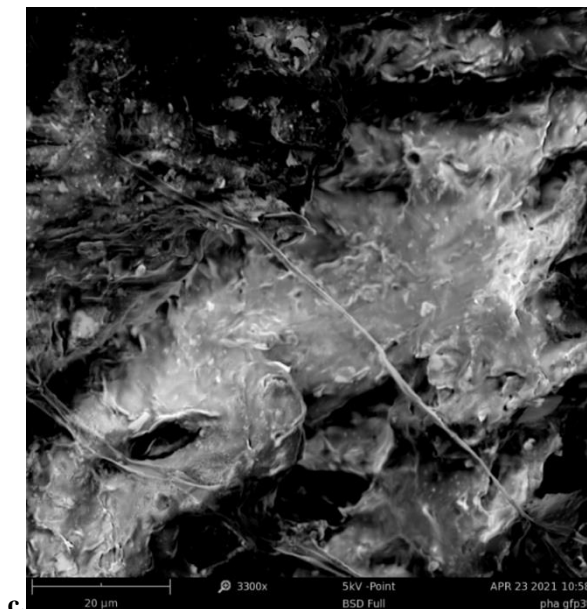
Figure 14 – SEM images of PHBV_GF after degradation test in in a pH 4.1 solution – cutting surface (a. – 330x; 5 kV) (b. – 3300x; 5 kV) (c. detail on the altered lignin fibres – 3300x; 5kV)

Observation of the PHBV_GF sample placed in a pH 10.65 solution (**Figure 15a**), shows less erosion than the other samples and the presence of inclusions (comparable to those observed in the sample placed in SSW) and deposits appears evident, near the cutting point. The sample, as observed for the sample placed in acidic conditions, is unstable and it can be observed that the effect of irradiation, even at low magnifications (260x), causes a greater penetration of the inclusions into the structure of the pellet. Furthermore, the lignin fibers are altered as observed in the case of the sample placed at pH 4.1. The micrograph of the cut sample reveals more evident lignin fibers compared to the sample placed in an acid solution, but in fewer numbers than the samples placed in distilled water and in SSW. Careful observation of the lignin fibers shows that they are altered and not well defined, as if a film had been deposited on them (**Figure 15b**). There are also both inclusions and deposits on the entire surface of the polymer.
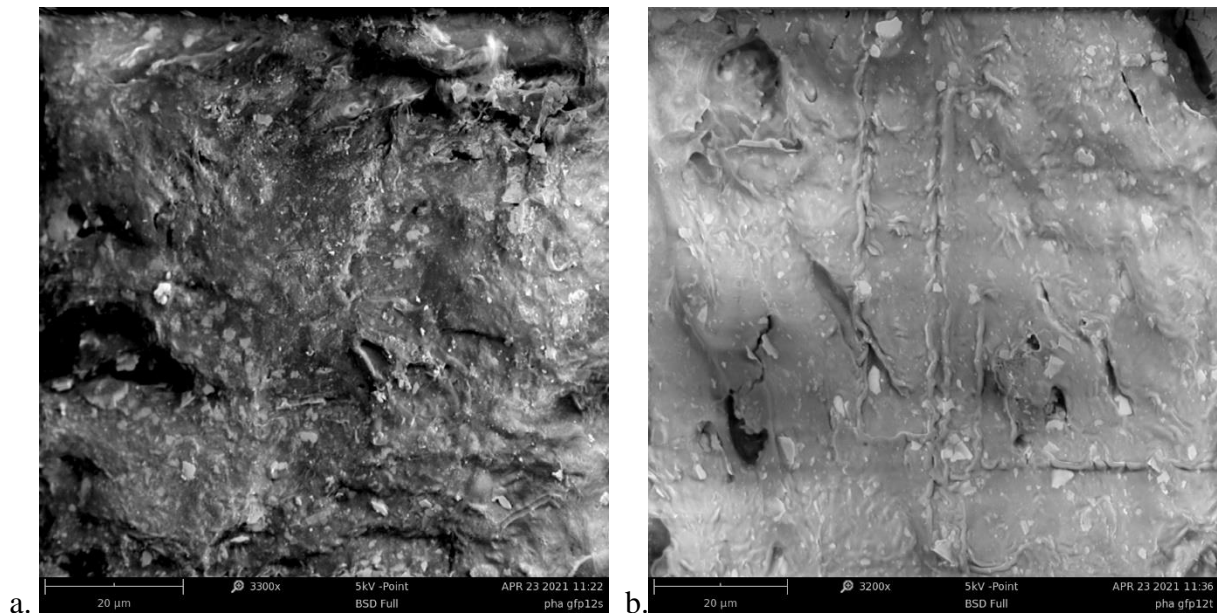
Figure 15 – SEM images of PHBV_GF after degradation test in in a pH 10.65 solution – convex surface
(a. – 3300x; 5 kV) and cutting surface (b. – 3200x; 5 kV)

3 - Thermal investigations

3.1 Differential Scanning Calorimetry (DSC)

From the analysis of the thermogram obtained from the DSC analysis of the PHB_GF ground sample, a melting temperature Tm was detected: 171.3° C (*Reference 2*, **Figure 16** and **Table 6**), preceded by a single endothermic peak corresponding to the glass transition (Tg: 55.14° C; *reference 1*, **Figure 16** and **Table 6**). The thermogram shows no exothermic peaks.
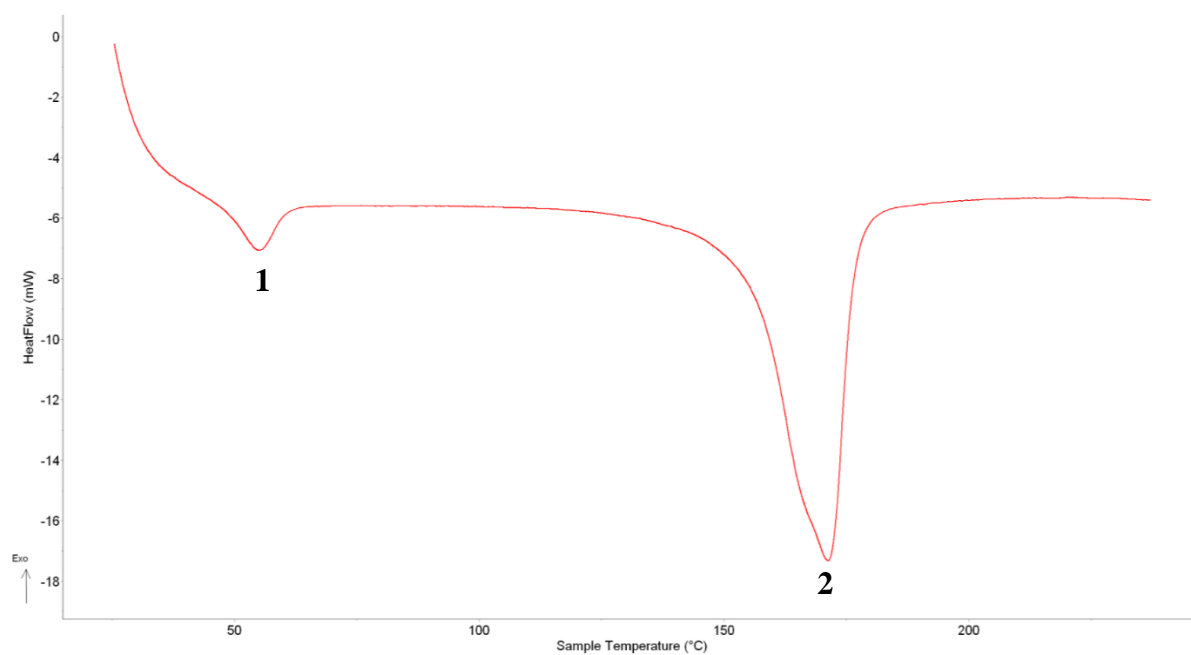


Figure 16 – DSC thermogram of ground PHB_GF (see **Table 6**)

Table 6 - DSC characterisation values of ground PHB_GF

REFERENCE NUMBER	PHASE TRANSITIONS	TEMPERATURE (°C)	HEAT FLOW (MW)
1	Glass transition	55.14	-7.055
2	Melting temperature	171.03	-17.302

The thermogram obtained from the DSC analysis of the PHB Sigma Aldrich powder sample shows, instead, a single endothermic peak corresponding to the melting temperature of the sample Tm: 178° C (*Reference 1*, **Figure 17** and **Table 7**) (Nishida et al., 2018). There are no other peaks, neither endothermic nor exothermic, beyond this one.
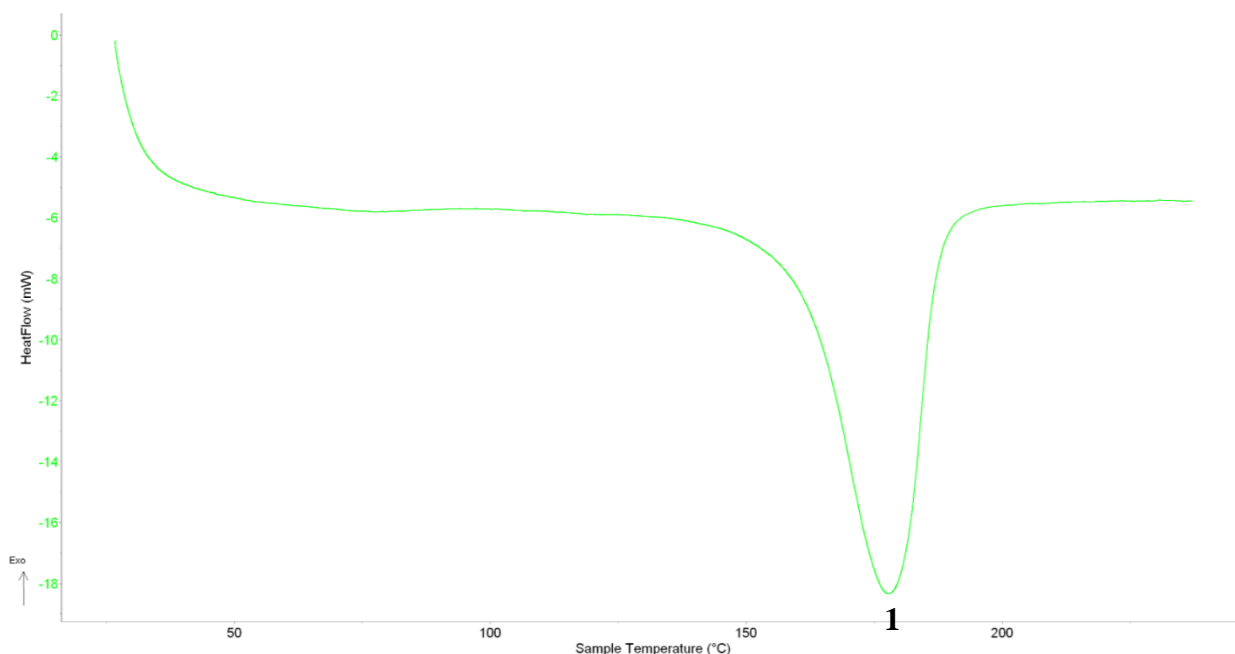
**Figure 17 –** DSC thermogram of PHB powder (see **Table 7**)

Table 7 - DSC characterisation values of PHB powder

REFERENCE NUMBER	PHASE TRANSITIONS	TEMPERATURE (°C)	HEAT FLOW (MW)
1	Melting temperature	177.75	-18.344

The comparison graph between the thermograms obtained from the DSC analyses of the ground PHB Good Fellow and PHB Sigma Aldrich powder samples is shown below (**Figure 18**, **Table 8**).
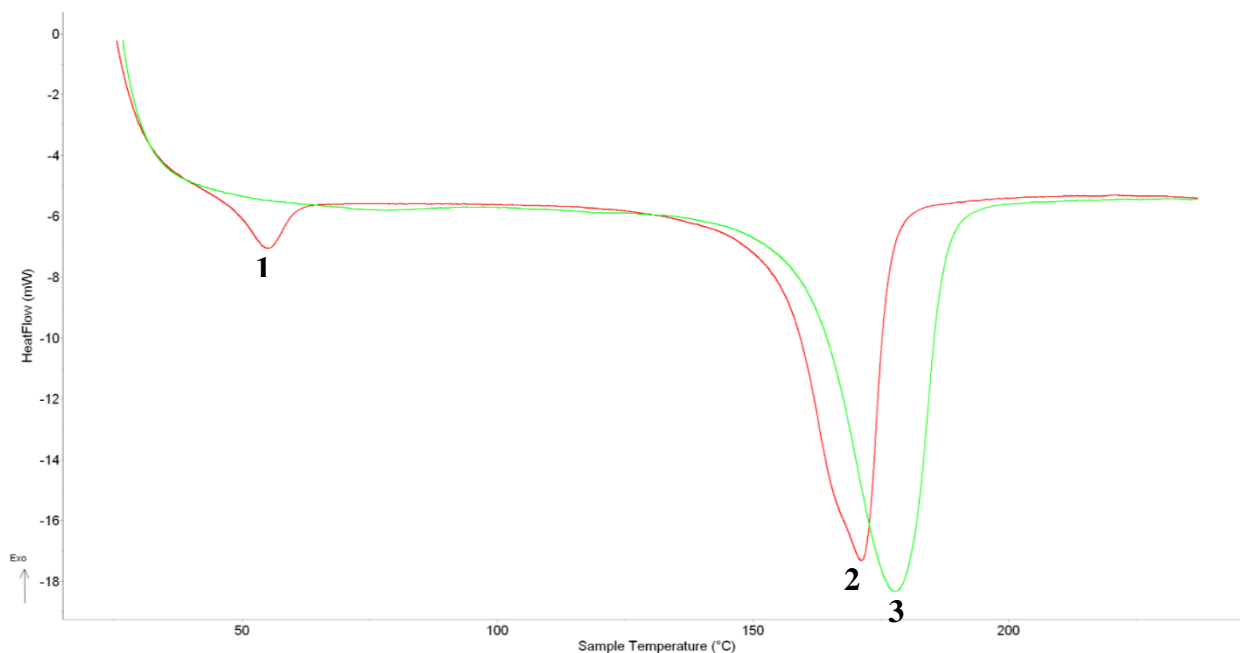
Figure 18 – Comparison between DSC thermogram of PHB powder and ground PHB_GF (see **Table 8**)

Table 8 - DSC characterisation values of PHB powder and ground PHB_GF

REFERENCE NUMBER	PHASE TRANSITIONS	TEMPERATURE (°C)	HEAT FLOW (MW)
1	Glass transition PHB_GF	55.14	-7.055
2	Melting temperature PHB_GF	171.03	-17.302
3	Melting temperature PHB	177.75	-18.344

From the DSC analysis of the ground PHBV_GF sample, a melting temperature Tm: 154.91° C was obtained (*Reference 3*, **Figure 19** and **Table 9**). In addition, the curve also shows an endothermic reaction corresponding to the glass transition (Tg: 61.26°C; *reference 1*, **Figure 19** and **Table 9**) and exothermic reactions such as crystallization (Tc: 100.59°C; *reference 2*, **Figure 19** and **Table 9**) and the oxidative degradation of the sample (*Reference 4*, **Figure 19** and **Table 9**).
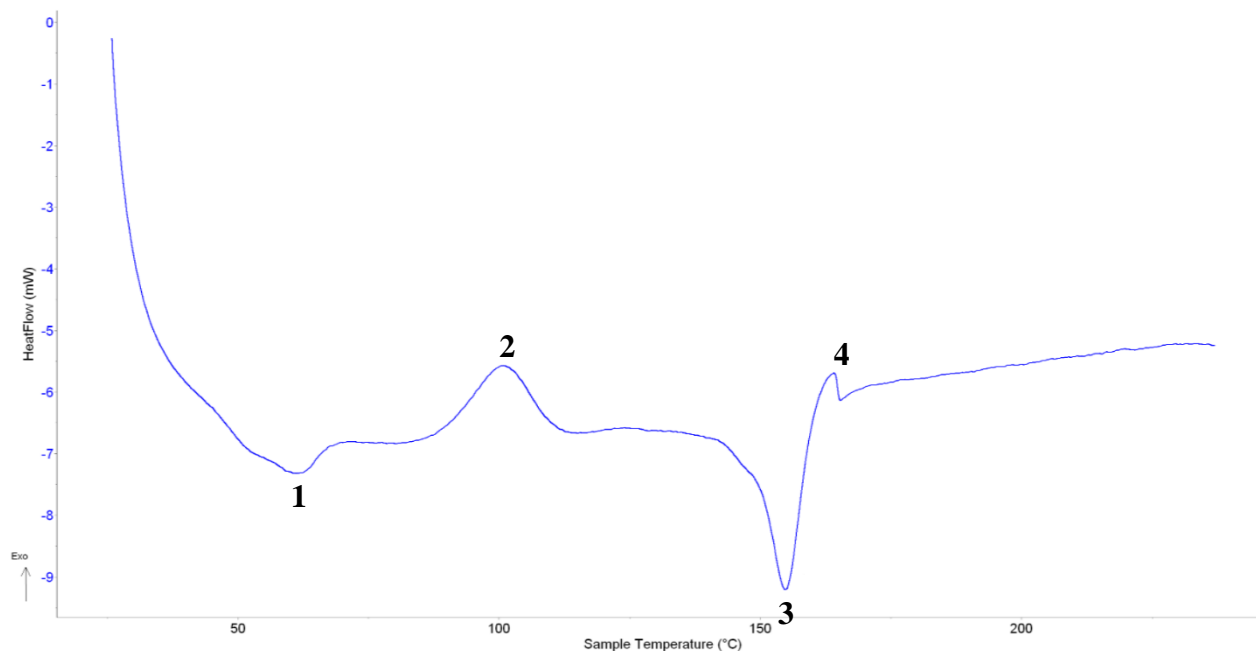
Figure 19 – DSC thermogram of ground PHBV_GF (see **Table 9**)

Table 9 – DSC characterisation values of ground PHBV_GF

REFERENCE NUMBER	PHASE TRANSITIONS	TEMPERATURE (°C)	HEAT FLOW (MW)
1	Glass transition	61.26	-7.318
2	Crystallization temperature	100.59	-5.576
3	Melting temperature	154.91	-9.209
4	Oxidative degradation	163.97	-5.698

The irregular trend of the DSC thermogram of the PHBV_GF sample is attributable to the presence of two polymers, PHB and PHV, with the further presence of wood flour (Mehrpouya et al, 2021). Considering the PHB powder and PHBV_GF samples, it can be observed that the presence of PHV influences the melting temperature of PHB (Jaquel et al., 2007; Reis et al., 2015; Nishida et al., 2018) bringing it from 177.75°C to 154.91°C. Furthermore, the presence of two distinct endothermic peaks in the thermograms of the PHBV_GF and PHB_GF samples may be due to the pelletising process which forms two zones with different crystallinity of the polymer. To support this thesis, the DSC thermogram of the PHB powder sample shows a single endothermic peak possibly due to the purity of the polymer.

3.2 Thermo-gravimetric analysis (TGA)

The thermogravimetric analysis of the ground PHB_GF sample (**Figure 20**) showed two peaks in which thermal degradation occurs: the first is between 247.29 and 351.81° C,

corresponding to the loss of 88% of the original mass of the sample; the second, however, is between 351.81 and 499.26° C, where a further 8.4% of the mass of the sample is lost, with an overall loss of mass of 96.4%.
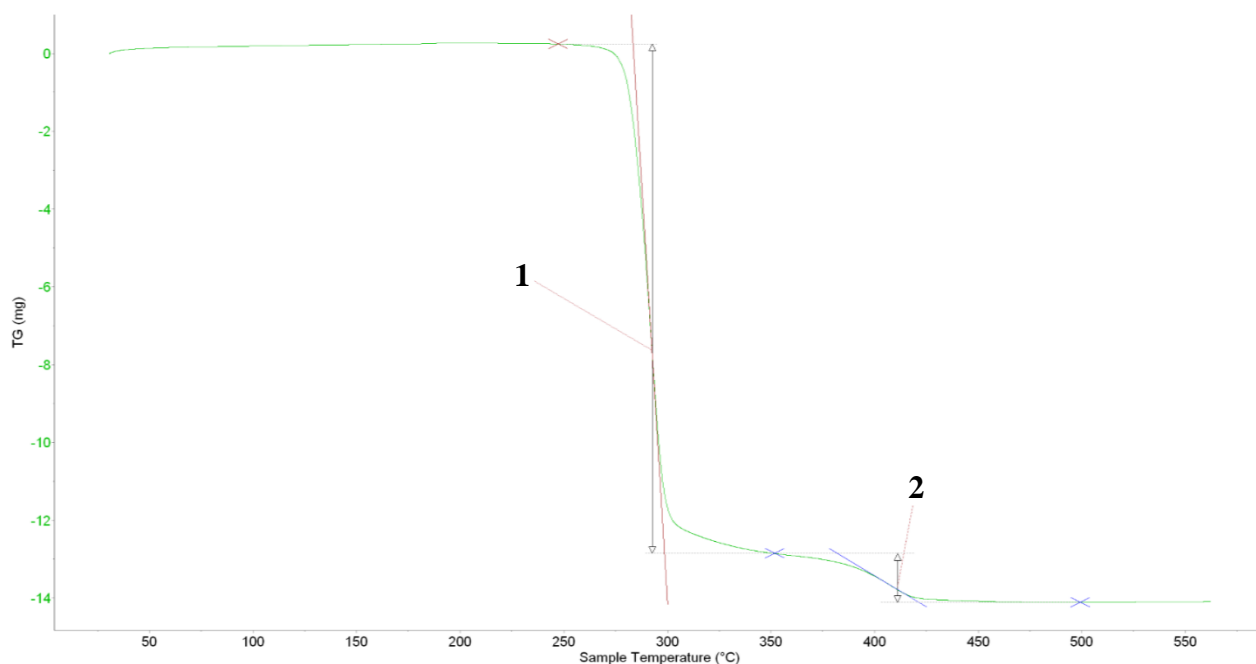
Figure 20– TGA thermogram of ground PHB_GF (see **Table 11**)

Table 10 - TGA characterisation values of ground PHB_GF

REFERENCE NUMBER	DEGRADATION TEMPERATURE RANGE (°C)	ΔM (MG)	ΔM (%)	RESIDUAL MASS (MG)
1	247.29 – 351.81	-13.102	- 87.93	1.798
2	351.81 – 499.26	- 1.256	- 8.43	0.542

The TGA thermogram of Sigma Aldrich PHB powder (**Figure 21**) showed a total thermal degradation of the sample (100%) in the temperature range between 234.17 and 330.82° C.
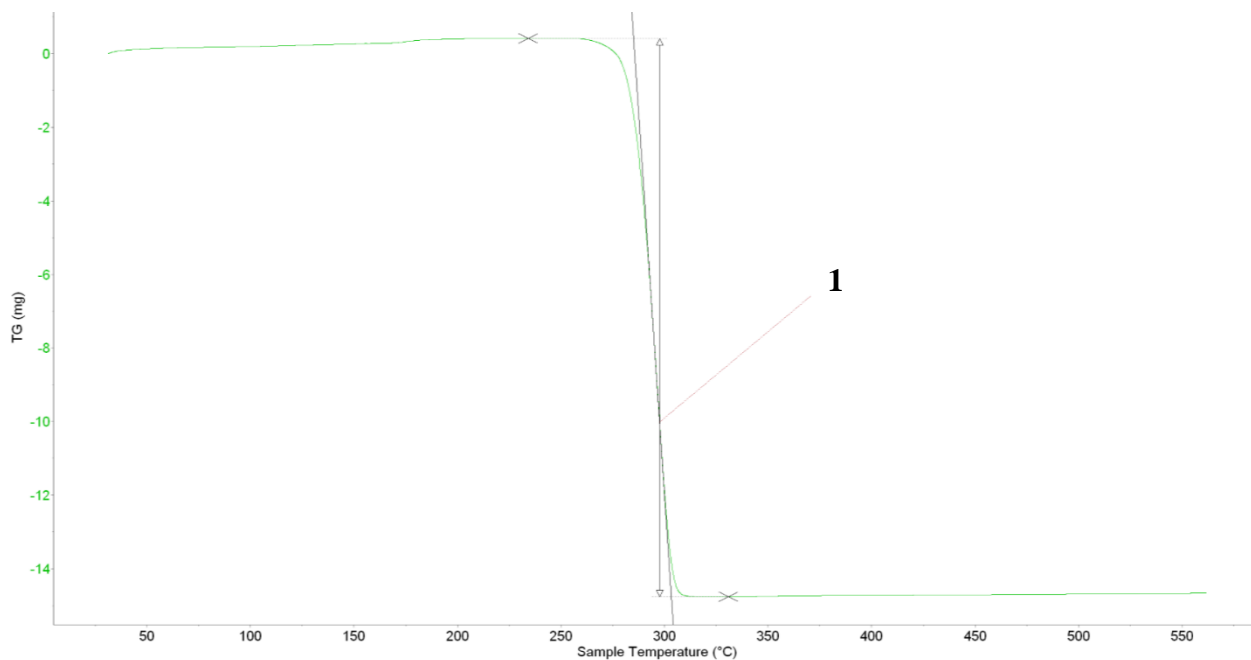
Figure 21 – TGA thermogram of PHB powder (see **Table 12**)

Table 11 - TGA characterisation values of PHB powder

REFERENCE NUMBER	DEGRADATION TEMPERATURE RANGE (°C)	ΔM	REFERENCE NUMBER	DEGRADATION TEMPERATURE RANGE (°C)
1	234.17 – 330.82	-15.176	-100.501	- 0.076

From **Figure 22**, which shows the thermogram of the Good Fellow's PHA biopolymer, it can be seen that thermal degradation of the polymer takes place in the temperature range between 243.18 and 486.44° C, with a loss of mass equal to 81%.
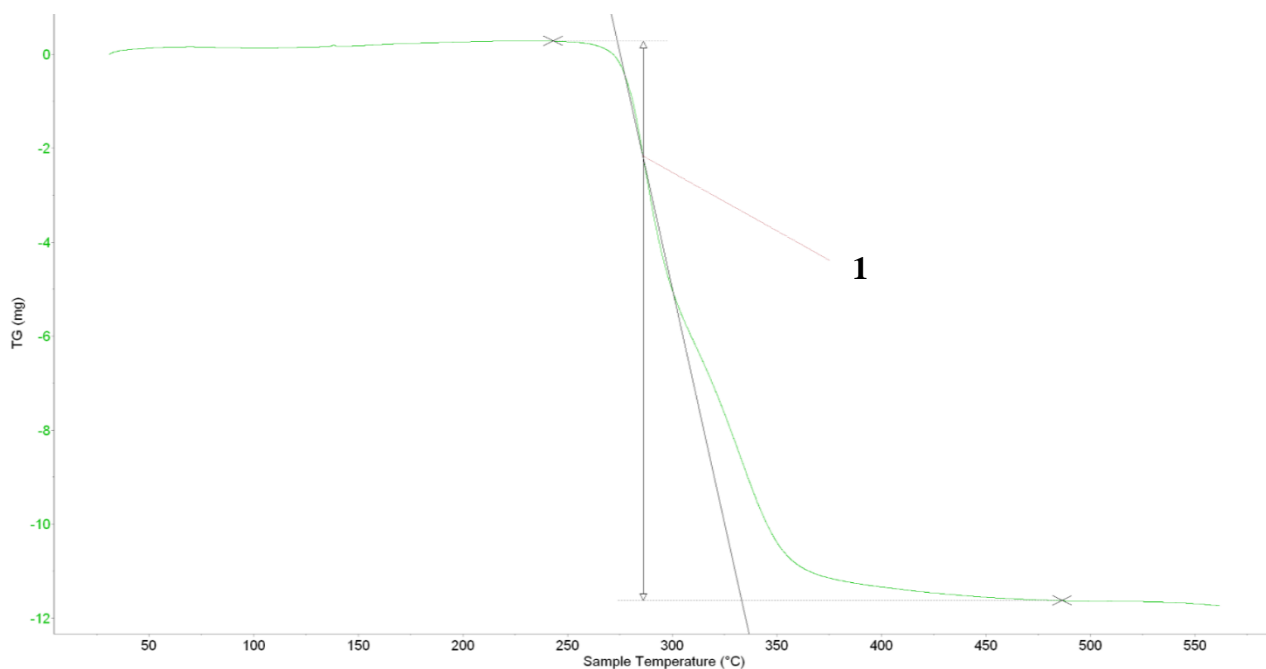
Figure 22 – TGA thermogram of ground PHBV_GF (see **Table 12**)

Table 12 – TGA characterisation values of ground PHBV_GF

REFERENCE NUMBER	DEGRADATION TEMPERATURE RANGE (°C)	ΔM (MG)	ΔM (%)	RESIDUAL MASS (MG)
1	243.18 – 486.44	-11.905	- 80.998	2.795

From the TGA analyses conducted it emerged that the PHBV_GF sample showed greater thermal stability. Under the same experimental conditions, in fact, the samples of PHB (ground Good Fellow and Sigma Aldrich powder) underwent overall degradation of 96.4% and 100% respectively; this is due to the β-elimination of the carboxyl ester group and the formation of crotonic acid (Bugnicourt et al. 2014). The thermal degradation curve deriving from the β-elimination of the carboxylic ester group of the two polymers constituting the PHBV_GF sample appears instead to take place in a pseudo-single-stage process which led to an overall weight loss of 81% in a range temperature range than the PHB samples. Furthermore, the lower degradation of the latter could be due to the fact that the sample was added to wood flour during the pelletisation phase. In fact, the organic residue can be degraded only at higher temperatures, above 600-650°C (Aoyagi et al. 2002), therefore we can assume that not all the organic fraction of this sample was degraded during the analysis and that the addition of wood flour, therefore, contributed to guaranteeing greater thermal stability of the PHBV_GF sample. Regarding the thermal degradation of the PHB powder and ground PHB_GF samples, we can see how the thermal degradation process of the powder started at a lower temperature and that it took place in a narrower temperature range.

120

On the contrary, the degradation of the PHB_GF sample took place in two distinct phases, attributable to the presence of materials added in the pelletisation phase which would require different degradation temperatures with respect to the degradation temperature of the polymer itself. As verified in the PHBV_GF sample, it can be stated that also in the case of the PHB_GF pelletised sample, compared to the pure powder form of the same polymer, the presence of added substances considerably contributed to the increase in the thermal stability of the sample.

4 - Cristallinity Index and Crystallinity Degree

The percentage of crystallinity of the polymer (Xc) was also calculated using the **Equation (1)**:

$$X_c = \frac{\Delta H_m}{\Delta H_{100}} \times 100 \qquad \textbf{(1)}$$

where ΔH_m is the melting enthalpy of the polymer, obtained from the value of the area under the melting curve of its DSC thermogram, while ΔH_{100} represents the theoretical enthalpy of 100% crystalline PHB, equal to 146.6 J g^{-1} (Kolahchi et al., 2015; Barham, 1984; Wei et al., 2015; Badawi et al., 2014). Crystallinity Index (CI) values calculated for each polymer are reported below (**Table 13**):

Table 13 – Crystallinity Index (CI) obtained from FTIR analysis

BIOPOLYMER	FTIR ANALYSIS		
	-CH band intensity (A.U.)	-C-O-C band intensity (A.U.)	Crystallinity Index (%)
PHBV_GF (GROUND)	0.05	0.1	50%
PHBV_GF	0.02	0.05	40%
PHB_GF	0.065	0.10	59%
PHB	0.1	0.11	91%

A decrease in crystallinity was observed from the pure PHB polymer in powder to the PHB-GF polymer pellet: this suggests that the pelletisation process, and any further transformation process, make the polymer more amorphous with a consequent increase in its solubility.

In confirmation of this, a further decrease in the value of the Crystallinity Index is observed for the PHBV_GF polymer, which is obtained from the copolymerization of PHB and PHV, is added to wood flour and has been subjected to a pelletisation process. Further confirmations can be obtained from the analysis of the Crystallinity Degree (X_c), calculated

for each polymer and shown in **Table 14**, in which it is observed a major value for PHB pure powder very low value for PHBV_GF, which also contains some percentage of valeric acid and wood flour (Galego et al., 2000).

Table 14 - Crystallinity Degree (X_c) obtained from DSC analysis

BIOPOLYMER	DSC ANALYSIS	
	ΔH_m (J/g)	Crystallinity Degree (X_c)
PHBV_GF (GROUND)	7.085	5%
PHB_GF (GROUND)	62.283	43%
PHB (PURE POWDER)	86.122	59%

5 - Nuclear magnetic resonance spectroscopy (NMR)

The PHBV_GF and PHB powder samples were studied by solid-state ^{1}H-NMR spectroscopy. **Figure 23** shows the ^{13}C-NMR spectrum of PHA, which reveals the presence of 6 signals attributable to butyric acid carbons (at 169.8, 68.5 42.8 and 21.2 ppm) and to valeric acid carbons (at 33.2 ppm and 16.9 ppm) (*References 4* and *6*, **Figure 23**, **Table 15**) (Sabarinathan et al., 2018; Badawi et al., 2014; Tan et al., 2014)

.
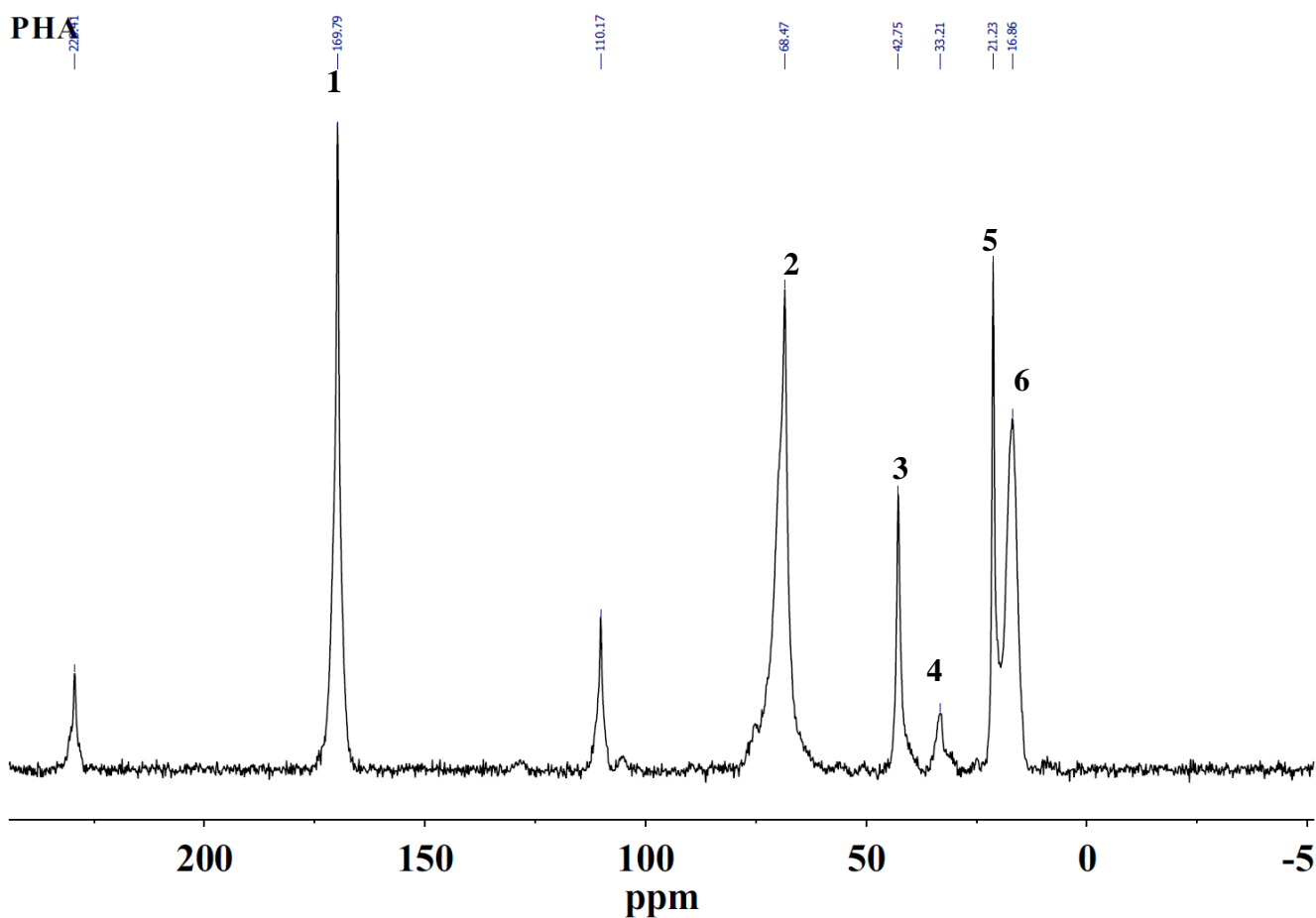
Figure 23 – ^{13}C-NMR solid-state spectra of ground PHBV_GF (see **Table 15**)

Table 15 – ^{13}C-NMR solid-state characterisation of ground PHBV_GF

REFERENCE NUMBER	GROUP	δ (PPM)
1	-C=O	169.79
2	-CH	68.47
3	-CH$_2$	42.75
4	-CH$_2$	33.21
5	-CH$_3$	21.23
6	-CH$_3$	16.86

The ^{13}C-NMR spectrum of the PHB Sigma Aldrich powder sample, on the other hand, showed only 4 signals (**Figure 24**, **Table 16**) (Nygaard et al., 2021), all attributable to butyric acid carbons (at 169.8, 68.5 42.8 and 21.2 ppm). No signals for valeric acid carbons were recorded for this sample.

PHB
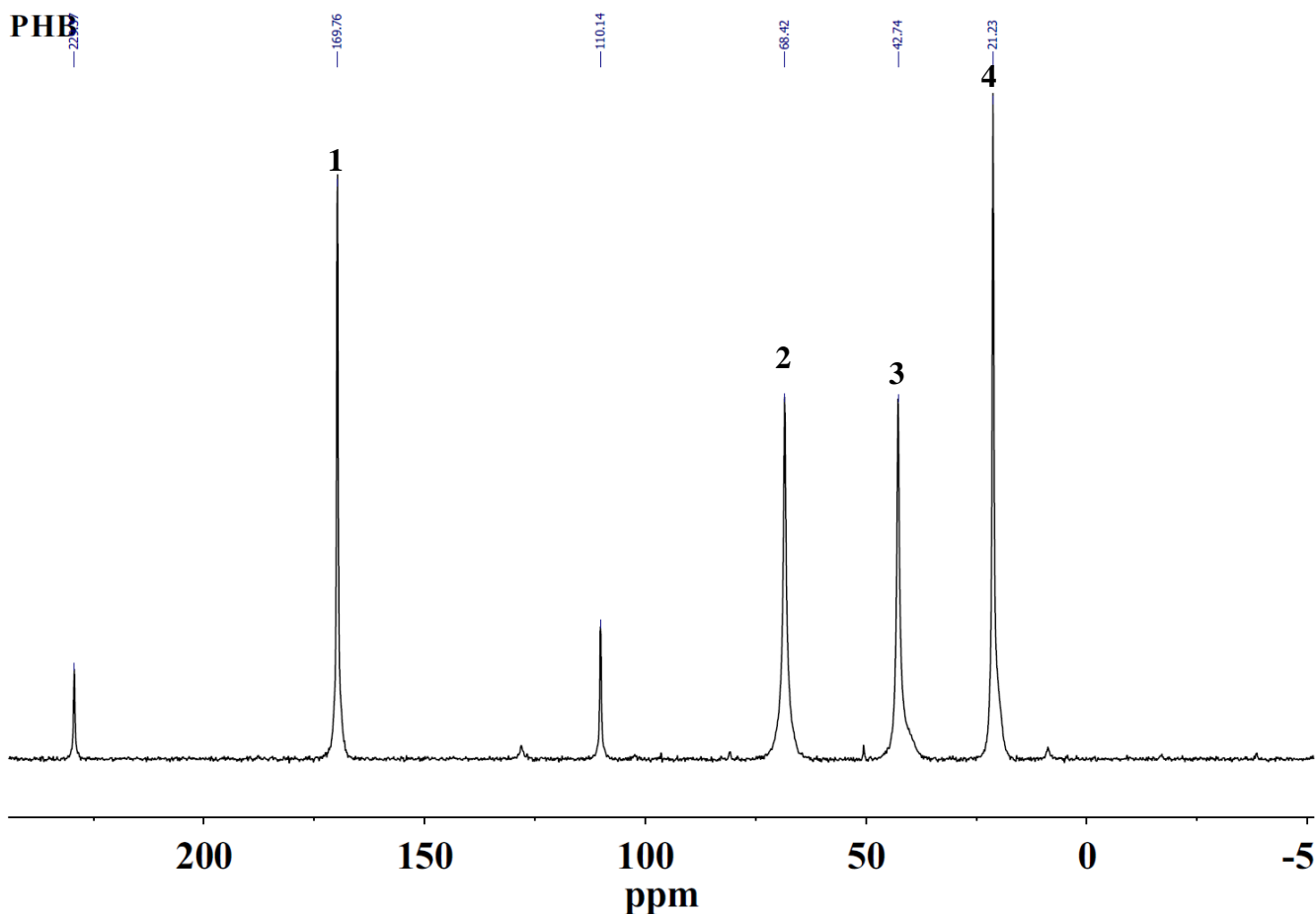
Figure 24 – ^{13}C-NMR solid-state spectra of PHB powder (see **Table 16**)

Table 16 – ^{13}C-NMR solid-state characterisation of PHB powder

REFERENCE NUMBER	GROUP	δ (PPM)
1	-C=O	169.76
2	-CH	68.42
3	-CH$_2$	42.74
4	-CH$_3$	21.23
	-	

The characterization of the polymers continued with the recording of spectra in the liquid phase, using deuterated chloroform (CDCl$_3$) as the solvent. ^{1}H and ^{13}C-NMR, one-dimensional and two-dimensional heteronuclear (^{1}H-^{13}C HSQC NMR) and homonuclear (^{1}H-^{1}H COZY NMR) spectra of ground PHA were recorded. The analysis of the ^{1}H-NMR spectrum in CDCl$_3$ (Abd-El-Haleem, 2009; Salgaonkar et al., 2013), highlighted the co-presence of polyhydroxybutyrate and polyhydroxyvalerate, as evidenced by the presence of 6 peaks, whose attributions are explained in **Figure 25** and **Figure 26** and in **Table 17**.
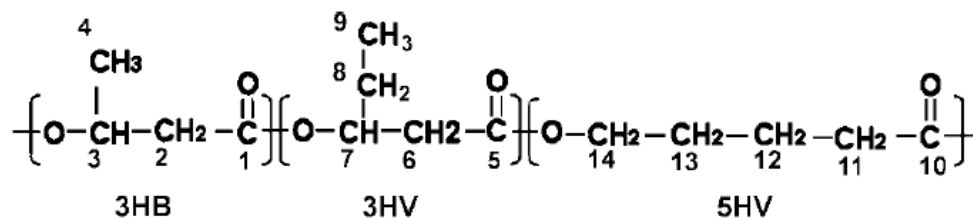
Figure 25 – PHA poli(3HB-co-3HV-co-5HV) molecule structure
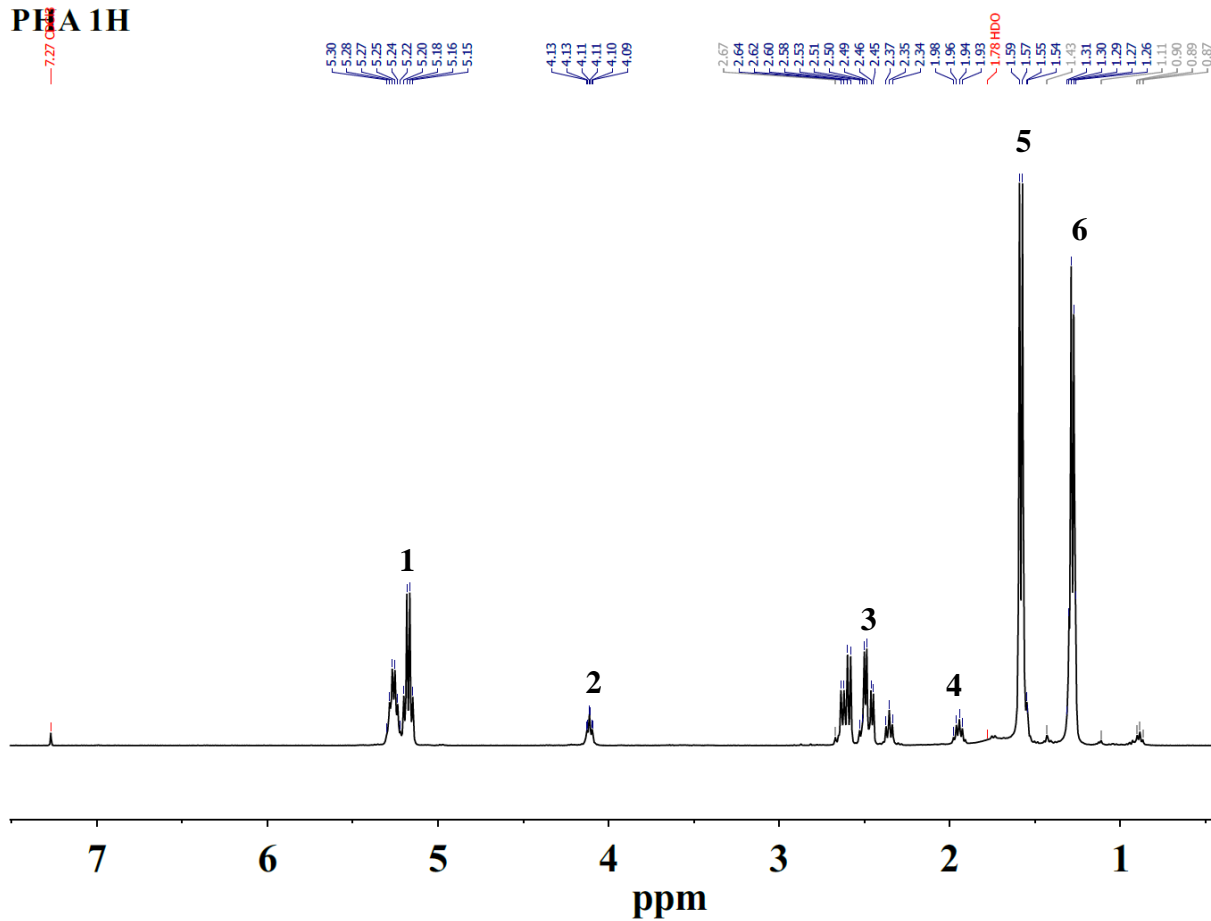
Figure 26 – ^{1}H-NMR spectra in liquid phase (CDCl$_3$) of ground PHBV_GF (see **Table 17**)

Table 17 – ^{1}H-NMR in liquid phase (CDCl$_3$) characterisation of ground PHBV_GF

REFERENCE SPECTRA NUMBER (FIGURE)	REFERENCE NUMBER IN MOLECULE STRUCTURE (FIGURE)	GROUP	δ (PPM)
1	3 - 7	-CH	5.15 – 5.30
2	14	-CH$_2$	4.09 – 4.13
3	2	-CH$_2$	2.34 – 2.67
4	12	-CH$_2$	1.93 – 1.98
5	8	-CH$_2$	1.54 – 1.59
6	4 e 9	-CH$_3$	1.26 – 1.31

The study of the ^{13}C-NMR spectrum of the same sample produced a spectrum with 6 peaks, as further confirmation of what has already been seen in the proton spectrum (**Figure 27**, **Table 18**), corresponding to the carbonyl -C=O (*References 1* and *5*, **Figure 25**; *reference 1*, **Figure 27** and **Table 18**), to the methine group -CH (*References 3* and *7*, **Figure 25**; *reference 2*, **Figure 27** and **Table 18**), to the -CH$_2$ groups (*Reference 2*, **Figure 26**, **Table 17**; *reference 3*, **Figure 27** and **Table 18**), to the methylene group (-CH$_2$) (*References 8* and *12*, **Figure 25**; *reference 4*, **Figure 27** and **Table 18**), to the methyl group (-CH$_3$) of 3HB (*Reference 4*, **Figure 25**; *reference 5,* **Figure 27** and **Table 18**) and the 3HV (*Reference 9*, **Figure 25**; *reference 6*, **Figure 27** and **Table 18**).

PHA 13C
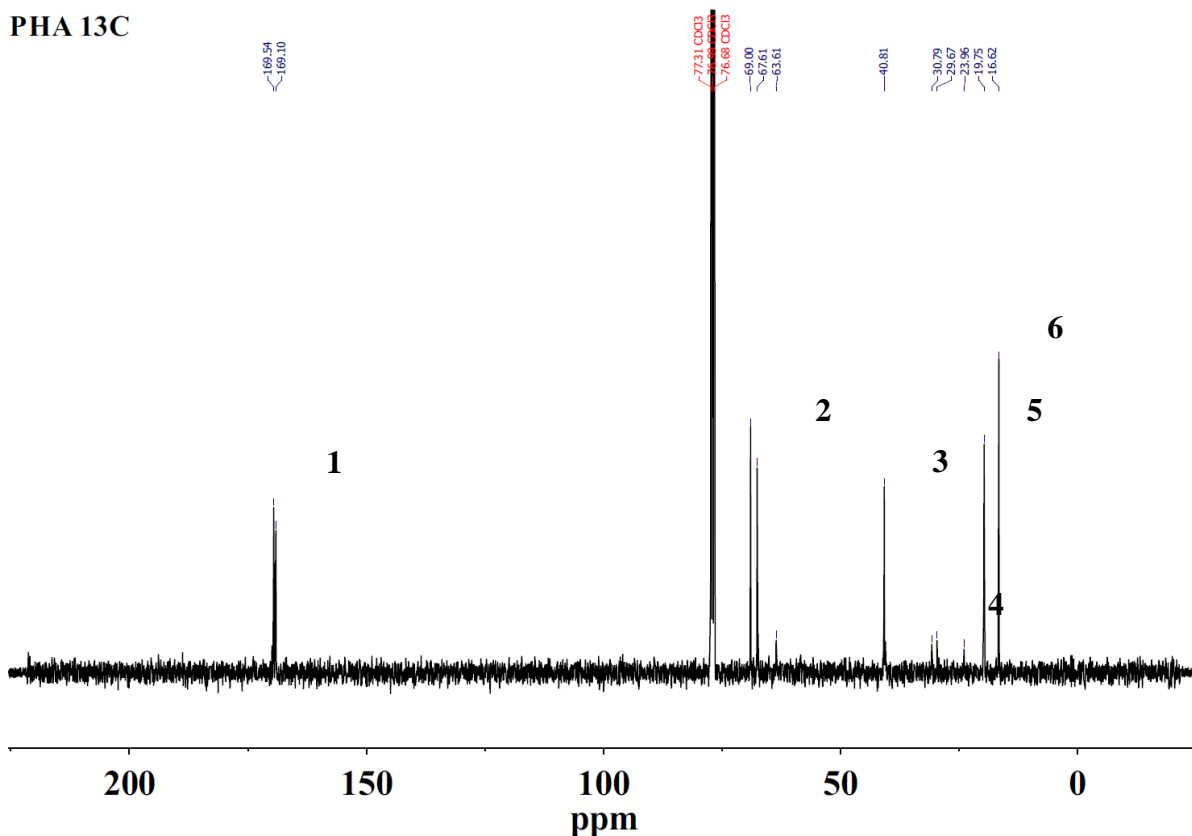
Figure 27 – ^{13}C-NMR spectra in liquid phase (CDCl$_3$) of ground PHBV_GF (see **Table 18**)

Table 18 – ^{13}C-NMR in liquid phase (CDCl$_3$) characterisation of ground PHBV_GF

REFERENCE SPECTRA NUMBER (FIGURE)	REFERENCE NUMBER IN MOLECULE STRUCTURE (FIGURE)	GROUP	δ (PPM)
1	1 - 5	-C=O	169.10 – 169.54
2	3 - 7	-CH	63.61 – 69.00
3	2	-CH$_2$	40.81
4	8 - 12	-CH$_2$	23.96 – 30.79
5	4	-CH$_3$	19.75
6	9	-CH$_3$	16.62

Thanks to the analysis of the two-dimensional spectra obtained for the PHBV_GF sample solubilized in CDCl$_3$ it was possible to observe the proton-carbon correlations in the 1H-^{13}C-HSQC NMR spectrum and the proton-proton correlations in the ^{1}H-^{1}H-COSY NMR spectrum within of the same molecule. Based on the analysis of the ^{1}H-^{13}C HSQC NMR spectrum (**Figure 28**) it is possible to identify the cross-peaks belonging to the PHB: the methine carbon (-CH) at δ 68.05 ppm is correlated with the proton resonance at δ 5.27 ppm,

the methylene carbon (-CH$_2$) at δ 41.21 ppm correlates with the proton resonance at δ 2.61 ppm, and methyl carbon (-CH$_3$) at δ 19.61 ppm correlates with the proton resonance at δ 1.30 ppm. The other cross-peaks are to be attributed to the -CH, -CH$_2$ and -CH$_3$ groups constituting the PHV polymer in its various forms. In detail, the identification of the correlation points observed in the ^{1}H-^{13}C HSQC NMR spectrum is shown in the table (**Table 19**).

PHA HSQC
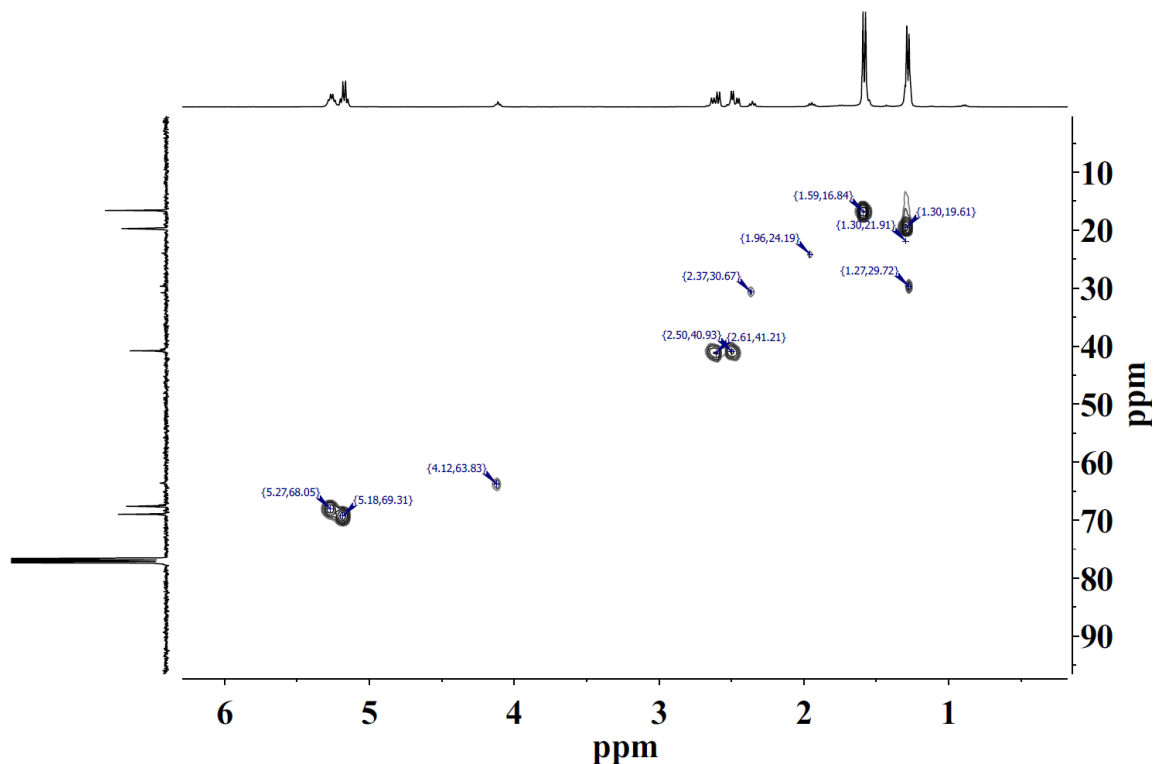
Figure 28 – ^{1}H-^{13}C HSQC NMR liquid phase (CDCl$_3$) spectra of ground PHBV_GF (see **Table 20**)

Table 19 - ^{1}H-^{13}C HSQC NMR liquid phase (CDCl$_3$) spectra characterisation of ground PHBV_GF

δ (PPM)	GROUP	MOLECULE
(5.27, 68.05)	-CH	PHB
(5.18, 69.31)	-CH	PHV
(4.12, 63,83)	-CH	PHV
(2.50, 40.93)	-CH$_2$	PHV
(2.61, 41.21)	-CH$_2$	PHB
(2.37, 30.67)	-CH$_2$	PHV
(1.96, 24.19)	-CH$_2$	PHV
(1.59, 16.84)	-CH$_3$	PHV
(1.27, 29.72)	-CH$_3$	PHV
(1.30, 21.91)	-CH$_3$	PHV
(1.30, 19.61)	-CH$_3$	PHB

The two-dimensional analysis of the correlations between the protons of the sample (^{1}H-^{1}H COZY NMR, **Figure 29**) further confirms the identification made by the two-dimensional analysis ^{1}H-^{13}C HSQC NMR. The protons belonging to the functional groups of the PHB polymer are thus identified, in particular, the proton at δ 5.26 ppm correlated with the proton resonance at δ 2.58 ppm belongs to the -CH group, while the proton at δ 5.27 ppm correlated with the proton resonance at δ 1.28 ppm they belong to the -CH$_3$ group. The remaining cross-peaks are to be attributed to the protons belonging to the -CH, -CH$_2$, and -CH$_3$ groups constituting the PHV polymer in its various forms. In detail, the identification of the correlation points observed in the ^{1}H-^{1}H COZY NMR spectrum is shown in the table (**Table 20**).

PHA COSY
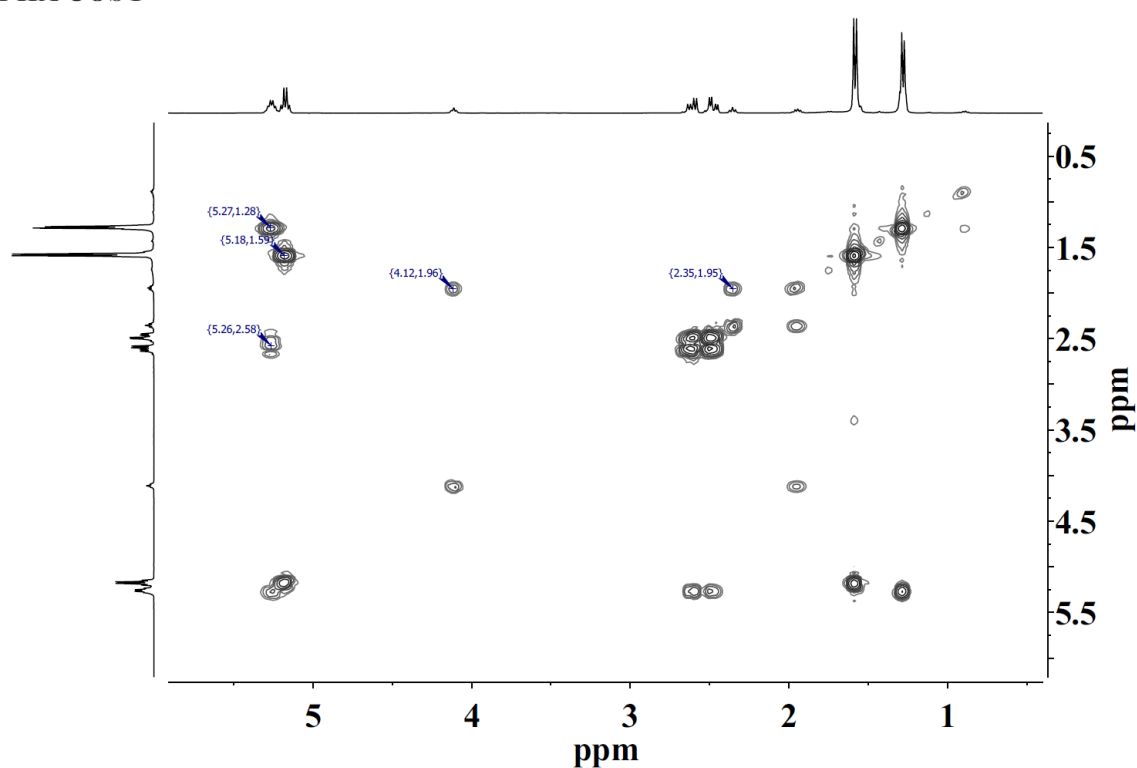
Figure 29 – ^{1}H-^{1}H COSY NMR liquid phase (CDCl$_3$) spectra of ground PHBV_GF (see **Table 18**)

Table 20- ^{1}H-^{1}H COSY NMR liquid phase (CDCl$_3$) spectra characterisation of PHBV_GF

δ (PPM)	GROUP	MOLECULE
(5.26, 2.58)	-CH	PHB
(5.27, 1.28)	-CH$_3$	PHB
(5.18, 1.59)	-CH$_2$	PHV
(4.12, 1.96)	-CH	PHV
(2.35, 1.95)	-CH$_2$	PHV

6 - Solubility test

The results obtained from the various polymer/solvent systems following the solubility tests are reported below (**Table 21**).

SOLVENT	EXPERIMENTAL TEMPERATURE (°C)	PHBV_GF	PHB_GF	PHB	PLA
CHCL$_3$	25	79%	19% [b]	16%	100%
DMSO	25	n.d.	-	n.d.	n.d.
CH$_3$COOC$_2$H$_5$	25	15%	-	19%	-
CH$_3$CN [a]	50	77%	-	42%	-
CH$_3$CN	50	50%	11%	n.d.	11%
ETOH [a]	50	7%	-	29%	-
ETOH	50	3%	-	n.d.	-

The results of the solubility tests show that all the polymers used for the tests have a higher solubility in solvents containing chlorine. As reported in the literature (Jacquel et al. 2007), this behavior of polyhydroxyalkanoates is explained as a polar interaction of the chlorine atom of the solvent with the carbonyl carbon of PHBV_GF which also interacts with the hydrogen atom of the solvent. Furthermore, as already observed from the results on the Crystallinity Index and the degree of Crystallinity of the polymers under study, reported in paragraph 4 of this appendix, the copolymerization also decreases the crystallinity and, consequently, increases the solubility of the polymer.

The ground PHBV_GF not solubilized in CHCl$_3$ was recovered following the separation from the solvent. The FT-IR analysis was carried out on the insoluble residual fraction and the spectrum obtained was compared with the PHBV_GF polymer as such. From the comparison (**Figure 30**, **Table 20**) the differences between the two spectra appear evident: this would confirm the occurred solubilization of the PHB and PHV constituting the sample. The signals present are therefore attributable to the wood flour used as filler in the PHBV_GF pellet, which would therefore be the main component of the non-solubilised fraction. In fact, it is possible to observe how the peaks of the stretching of the -CH groups, the peak of the carbonyl group, the peak of the bending of the -CH and the peak stretching of the -C-O group are not detected. Instead, there is one of the two peaks referable to the bending of the -CH group (*Reference* 6, **Figure 30**, **Table 20**) and the band referable to the

stretching of the alcoholic -C-O group (*Reference 7*, **Figure 30**, **Table 20**), this last detected with an intensity considerably higher than the reference sample. Also, there is a slight broadening of the peak of the -OH group (3400-3200 cm^{-1}) (*Reference 2*, **Figure 30**, **Table 22**).
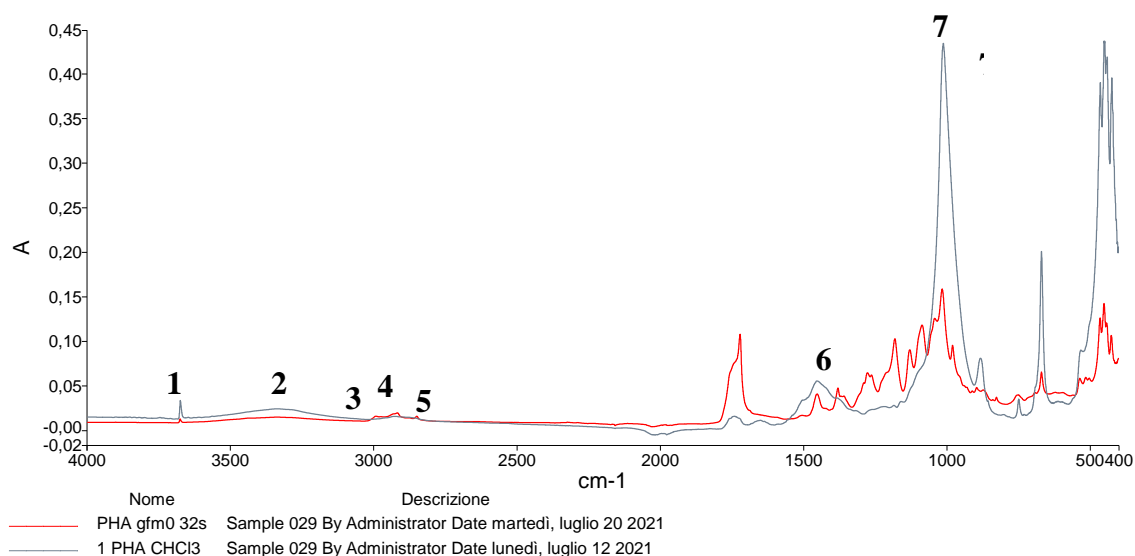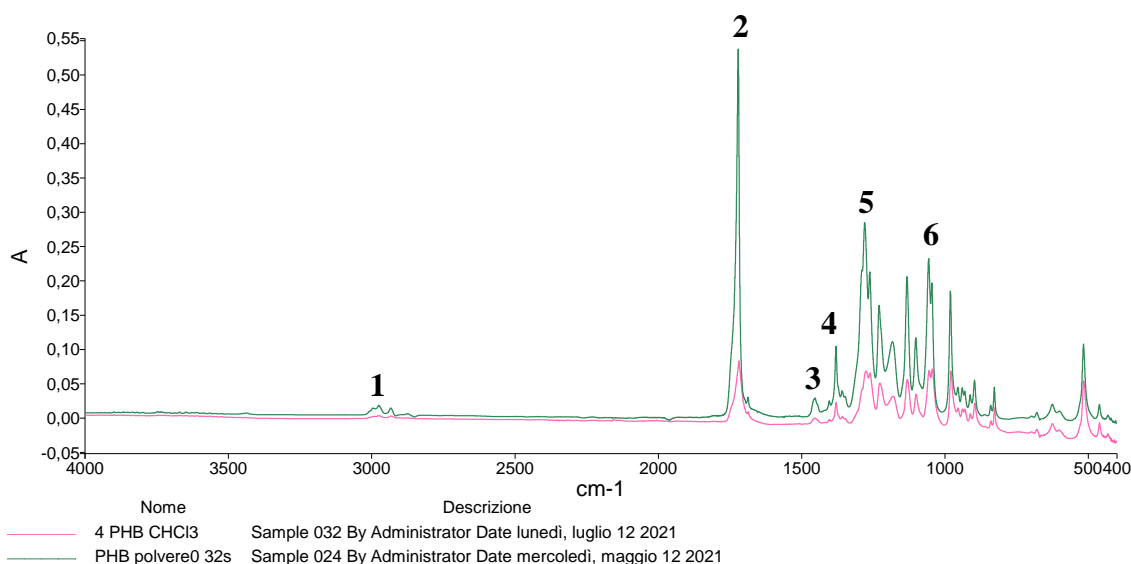

Figure 30 – FT-IR spectrum of ground PHBV_GF insoluble in chloroform (CHCl$_3$) (black spectrum), compared with FT-IR spectrum of PHBV_GF (red spectrum) (see **Table 22**)

Table 22 - Infra-Red characterisation values of ground PHBV_GF insoluble in chloroform (CHCl$_3$)

REFERENCE NUMBER	GROUP	WAVE NUMBER ν (CM^{-1})
1	ν OH	3675
2	ν OH	3400-3200
3-5	ν CH	2988-2920
6	δ CH	1452-1380
7	ν C-O (alcoholic)	1150-950

To confirm what was obtained from the results of the test just described, a further solubility test in chloroform (CHCl$_3$) was carried out to separate the polymeric component of the PHBV_GF sample from the wood flour. FT-IR analyses were carried out on the fraction insoluble in CHCl$_3$ and on the fraction solubilized in CHCl$_3$ of the PHBV_GF-WF sample, recovered after having dried all the fractions by placing them in an oven at a temperature of 55°C for 24h. The spectra obtained were compared with the reference spectrum of the PHBV_GF polymer and are reported below (**Figure 31**).

131
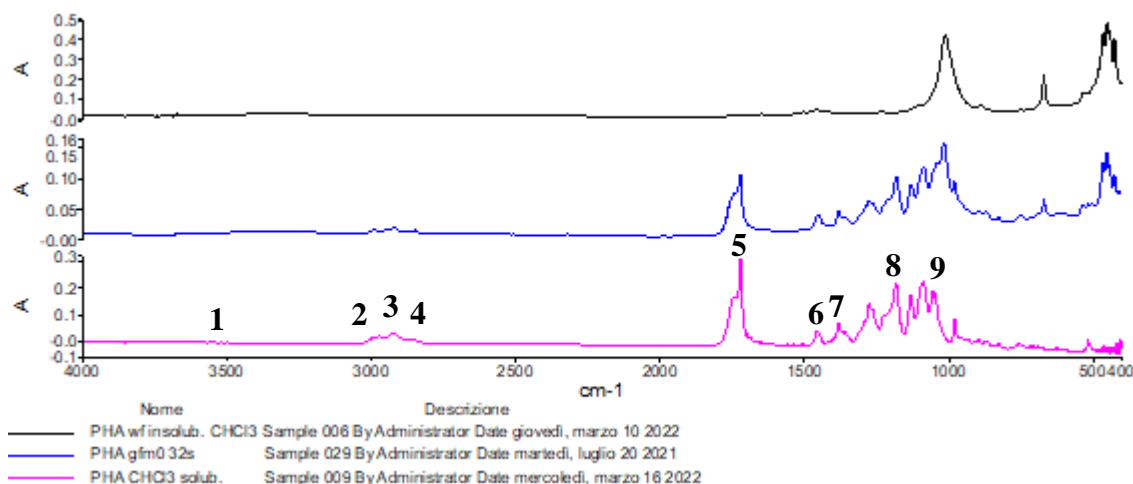
Figure 31 – FT-IR spectra of ground PHBV_GF insoluble in chloroform (CHCl₃) (black spectrum), compared with FT-IR spectra of PHBV_GF (blue spectrum) and of PHBV_GF solubilized in chloroform (CHCl₃) (pink spectrum) (see **Table 23**)
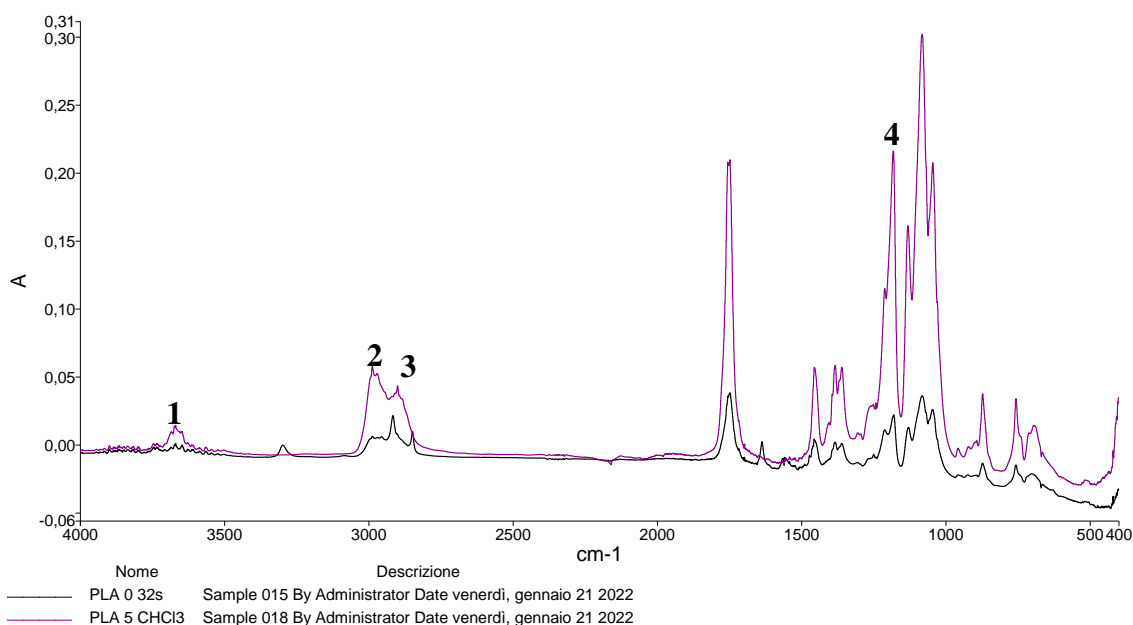
Table 23 - Infra-Red characterisation values of ground PHBV_GF solubilized in chloroform (CHCl₃)

REFERENCE NUMBER	GROUP	WAVE NUMBER ν (CM^{-1})
1	ν OH	3675
2 - 4	ν CH	2988 -2920
5	ν C=O	1725
6 - 7	δ CH	1452 - 1380
8	ν C-O (esters)	1300-1150
9	ν C-O (alcoholic)	1150-950

From the comparison between the spectra, it is possible to state that the solubilization test carried out led to the effective separation of the PHA polymer from the wood flour originally present in the sample and notoriously insoluble in chloroform. In fact, the characteristic peaks of the polymer are absent in the spectra of the insoluble fraction; it can be deduced that the peaks detected in these spectra are attributable exclusively to the wood flour. The characteristic peaks of the polymers constituting the PHBV_GF sample are instead present in the spectra referable to the fraction solubilized in chloroform.

We proceeded with the FT-IR analysis of the pure PHB powder samples subjected to CHCl₃ solubility tests. The spectrum obtained was compared with the reference spectrum of the same polymer (spectrum in pink, **Figure 32**). The peaks of the two spectra are perfectly superimposable: variations are found only on the intensity of the peaks. Indeed, the spectral analysis shows the stretching peaks of the -CH groups (*Reference 1*, **Figure 32, Table 24**), the carbonyl group peak (*Reference 2*, **Figure 32, Table 24**), the bending peaks of the - CH (*References 3 and 4*, **Figure 32, Table 24**), the -C-O group stretching peak (*Reference 5*, **Figure 32, Table 24**), and the alcoholic -C-O peaks (*Reference 6*, **Figure 32, Table 24**).

Figure 32- FT-IR spectrum of PHB pure powder insoluble in chloroform (CHCl$_3$) (pink spectrum), compared with FT-IR spectrum of PHB (green spectrum) (see

Table 24)

Table 24 - Infra-Red characterisation values of PHB pure powder insoluble in chloroform (CHCl$_3$)

REFERENCE NUMBER	GROUP	WAVE NUMBER ν (CM^{-1})
1	ν CH	2936
2	ν C=O	1721
3 - 4	δ CH	1452 - 1380
5	ν C-O (esters)	1300-1100
6	ν C-O (alcoholic)	1100-1000

Further considerations can be made following the analysis of the FT-IR spectra obtained from the solubilized portion and from the non-solubilized portion of the PHB_GF sample following the solubility test with CHCl$_3$. The solubilized portion (spectrum in green, **Figure 33**), shows a different spectrum compared to that of the reference (spectrum in red, **Figure 33**) and to the spectrum of the fraction insoluble in CHCl$_3$ (spectrum in black, **Figure 33**). In particular, a considerable variation in the proportions is observed due to an increase in the intensity of the peak at 1180 cm^{-1} (*Reference 6*, **Figure 33**, **Table 25**) relative to the amorphous state. From this, it is possible to deduce that the amorphous portion was mostly solubilised in CHCl$_3$.
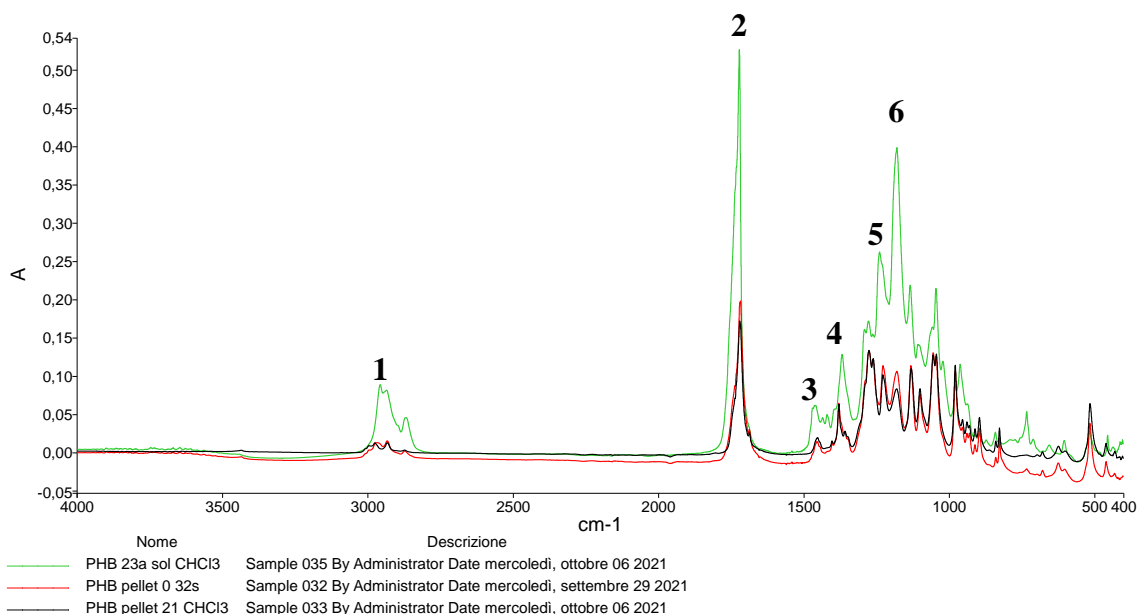
Figure 33 - FT-IR spectrum of PHB_GF solubilized in chloroform (CHCl$_3$) (green spectrum), compared with FT-IR spectra of PHB_GF insoluble in chloroform (CHCl$_3$) (black spectrum) and of PHB_GF (red spectrum) (see **Table 25**)

Table 25 - Infra-Red characterisation values of PHB_GF solubilized in chloroform (CHCl$_3$)

REFERENCE NUMBER	GROUP	WAVE NUMBER ν (CM^{-1})
1	ν CH	3000-2900
2	ν C=O	1721
3	δ CH	1452 - 1380
4	ν C-O (esters)	1300-1100
5	ν C-O (alcoholic)	1100-1000
6	ν C=O	1721

The variation of the ratios between the peaks also leads to a variation of the crystallinity index, calculated precisely on the basis of the ratio between the intensity of the bands of the FT-IR spectra at 1382 cm^{-1} (-CH), which is indicative of the crystalline state of the molecule, to that at 1185 cm^{-1} (-C–O–C-), index of the amorphous state.

This would confirm the effective decrease in the crystallinity of the PHB_GF polymer following the pelletisation processes, as deduced thanks to the DSC analyses. PLA is the only polymer that has completely solubilized in CHCl$_3$ therefore the FT-IR analysis was conducted on the solubilized fraction, recovered following the removal of the solvent. The analysis of the IR spectrum (spectrum in violet, **Figure 34**Figure) obtained shows a perfectly

superimposable trend with respect to the spectrum of the reference sample (spectrum in black), with the only difference found in the intensity of the peaks.

Figure 34 – FT-IR spectrum of PLA solubilized in chloroform (CHCl$_3$) (violet spectrum), compared with FT-IR spectrum of PLA (black spectrum) (see **Table 26**)

Table 26 - Infra-Red characterisation values of PLA solubilized in chloroform (CHCl$_3$)

REFERENCE NUMBER	GROUP	WAVE NUMBER ν (CM^{-1})
1	ν OH	3669
2 - 3	ν CH	2998 -2900
4	ν C-O (esters)	1211

The solubility tests conducted in DMSO gave a solubility percentage of less than 1% for all the samples analysed. In confirmation of this, the spectrum of the reference PHBV_GF sample and the fraction of PHBV_GF insoluble in DMSO show the same trend. The spectrum of the sample subjected to solubility tests in DMSO, however, presents a different peak intensity, in particular, that referring to the carbonyl group (*Reference 6*, **Figure 35**, **Table 27**), and those referring respectively to the stretching of the -C-O group ester (*Reference 9*, **Figure 35**, **Table 27**) and the alcoholic -C-O group (*Reference 10*, **Figure 35**, **Table 27**). Furthermore, a broadening of the peak of the -OH group (3500-3200 cm^{-1}) is observed (*Reference 2*, **Figure 35**, **Table 27**). These variations could be due to the possible coordination of the solvent (DMSO) with the polymer, with the consequent formation of a solute-solvent complex.
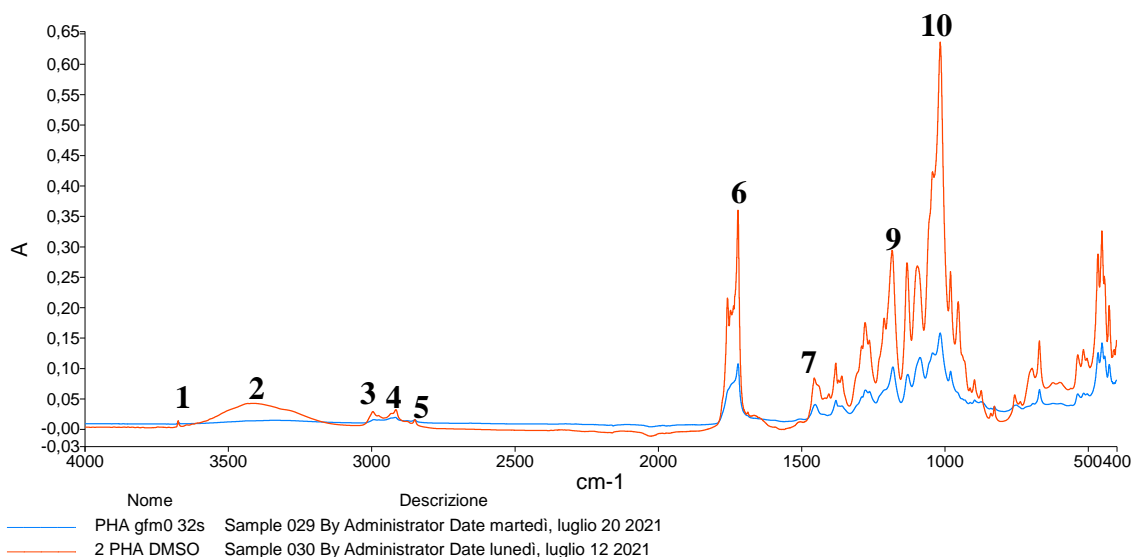
Figure 35 – FT-IR spectrum of ground PHBV_GF insoluble in Dimethyl sulfoxide (DMSO - C_2H_6OS) (red spectrum), compared with FT-IR spectrum of PHBV_GF (blue spectrum) (see **Table 27**)

Table 27 – Infra-Red characterisation values of ground PHBV_GF insoluble in Dimethyl sulfoxide (DMSO – C_2H_6OS)

REFERENCE NUMBER	GROUP	WAVE NUMBER ν (CM^{-1})
1	ν OH	3675
2	ν OH	3400-3200
3 – 5	ν CH	2988 -2920
6	ν C=O	1725
7 – 8	δ CH	1452 -1380
9	ν C-O (esters)	1300-1150
10	ν C-O (alcoholic)	1150-950

The solubility tests in Ethyl Acetate gave low and comparable solubility percentages both for the PHBV_GF sample and for the pure powdered PHB sample. From the FT-IR analysis of the insoluble fraction of PHBV_GF in ethyl acetate, a spectrum partially superimposable on the reference spectrum was obtained, albeit with a lower intensity of the bands present (**Figure 36**, **Table 28**). As a variation from the reference, a difference is observed in the peak relating to the carbonyl group (*Reference 5*, **Figure 36**, **Table 28**), and in those relating to the alcoholic -C-O (*Reference 9*, **Figure 36**, **Table 28**).
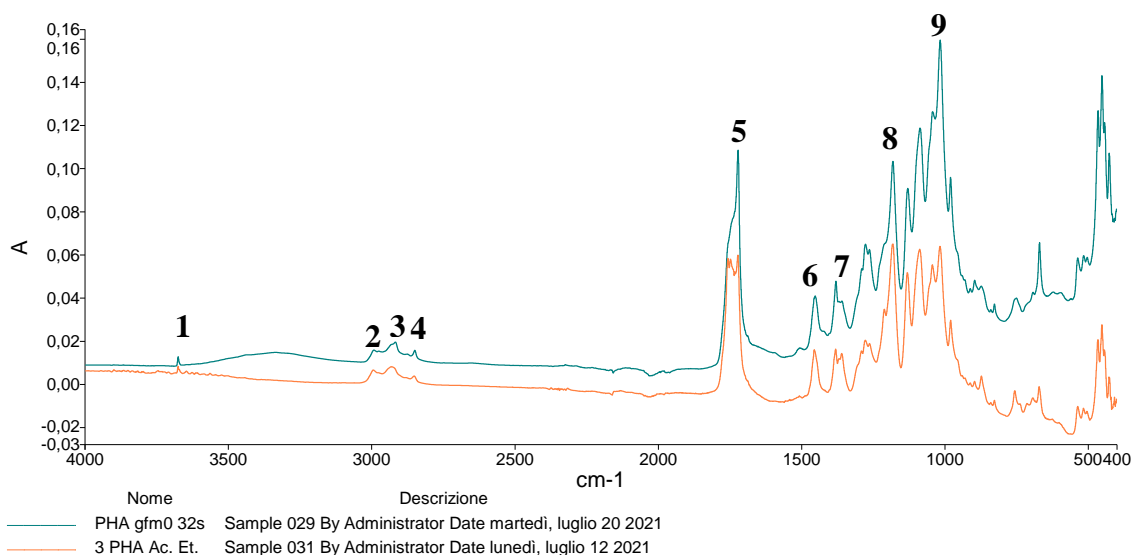
Figure 36 – FT-IR spectrum of ground PHBV_GF insoluble in Ethyl acetate ($CH_3COOC_2H_5$) (orange spectrum), compared with FT-IR spectrum of PHBV_GF (green spectrum) (see **Table 28**)

Table 28 - Infra-Red characterisation values of ground PHBV_GF insoluble in Ethyl acetate ($CH_3COOC_2H_5$)

REFERENCE NUMBER	GROUP	WAVE NUMBER ν (CM^{-1})
1	ν OH	3675
2 - 4	ν CH	2988 -2920
5	ν C=O	1725
6 – 7	δ CH	1452 -1380
8	ν C-O (esters)	1300-1150
9	ν C-O (alcoholic)	1150-950

The spectrum obtained from the analysis on the residue of the pure PHB sample in powder form (spectrum in red, **Figure 37**) recovered following the solubilization test in ethyl acetate, perfectly superimposable on the reference spectrum (spectrum in blue, **Figure 37**), also in the intensity of the peaks.
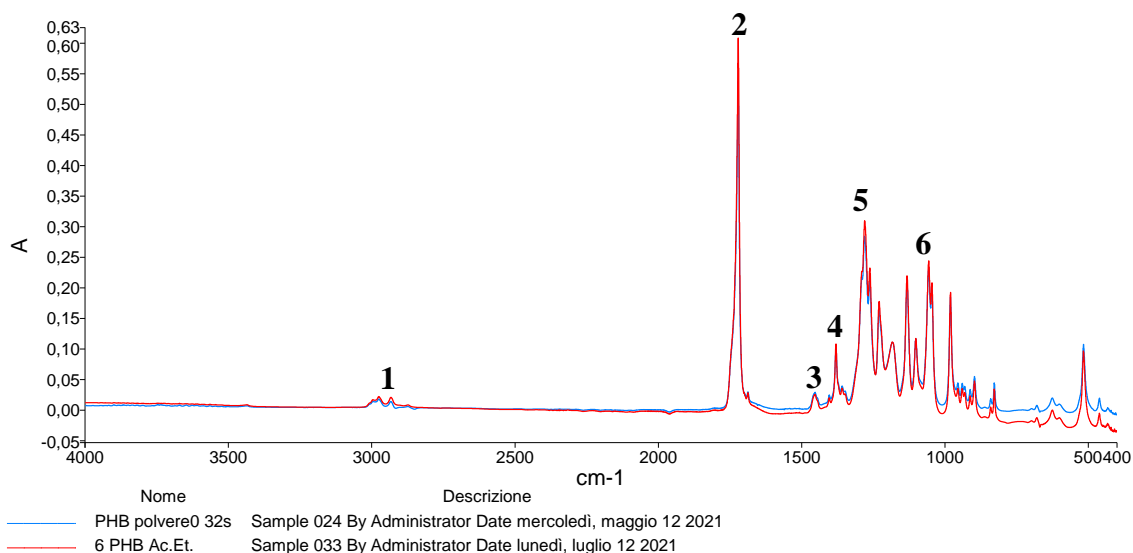
Figure 37 - FT-IR spectrum of PHB pure powder insoluble Ethyl acetate (CH$_3$COOC$_2$H$_5$) (red spectrum), compared with FT-IR spectrum of PHB (blue spectrum) (see

Table)

Table 29 - Infra-Red characterisation values of PHB pure powder insoluble in Ethyl acetate (CH$_3$COOC$_2$H$_5$)

REFERENCE NUMBER	GROUP	WAVE NUMBER ν (CM^{-1})
1	ν CH	2936
2	ν C=O	1721
3 - 4	δ CH	1452 - 1380
5	ν C-O (esters)	1300-1100
6	ν C-O (alcoholic)	1100-1000

Among the solubility tests in acetonitrile carried out, only the PHBV_GF sample showed greater solubility. Following the test in acetonitrile, both the soluble portion and the insoluble portion of the PHBV_GF sample were characterized by IR spectroscopy. A first comparison was made between the spectra obtained for both portions, with the reference spectrum of the same biopolymer.

The solubilized portion of the sample (Blue spectrum, **Figure 38**) shows a variation of the peaks referable to the stretching of the -C-O ester group (Blue spectrum, *Reference 7*, **Figure 38**, **Table 30**), whose intensity compared to the other peaks, considering the proportions detected in the other two spectra, is higher and almost comparable to the intensity of the peak attributable to stretching of the alcoholic -C-O group (*Reference 8*, **Figure 38**, **Table 30**). The spectrum of the non-solubilized portion (Pink spectrum, **Figure 38**, **Table 30**), on the other hand, presents a trend and proportions between the peaks more similar to the reference, except for the peak of the carbonyl group (Pink spectrum, *Reference*

4, **Figure 38**, **Table 30**) which is instead narrower, both with respect to the same peak present in the reference spectrum and in the spectrum of the solubilized sample.
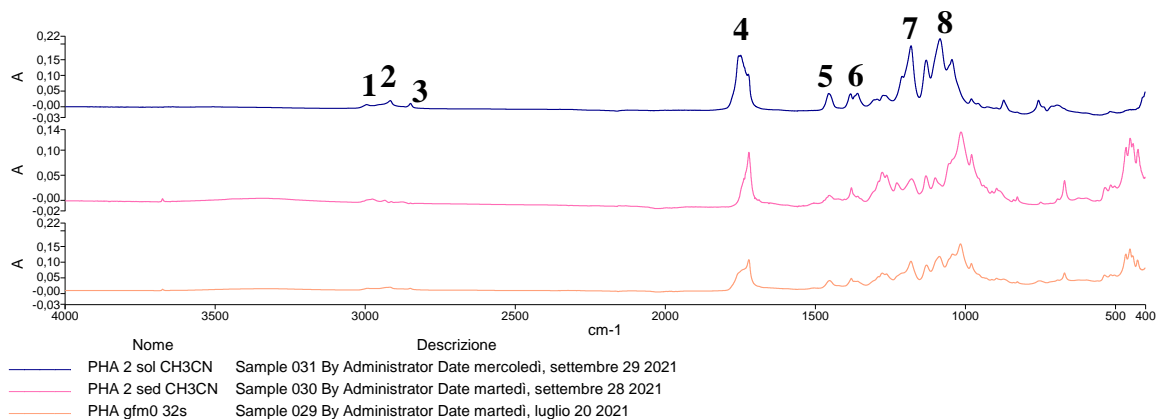
Figure 38 – FT-IR spectrum of ground PHBV_GF solubilized in Acetonitrile (CH$_3$CN) (blu spectrum), compared with FT-IR spectra of PHBV_GF insoluble in Acetonitrile (CH$_3$CN) (pink spectrum) and of PHBV_GF (orange spectrum) (see **Table 30**)

Table 30 - Infra-Red characterisation values of ground PHBV_GF solubilized in Acetonitrile (CH$_3$CN)

REFERENCE NUMBER	GROUP	WAVE NUMBER ν (CM^{-1})
1 - 3	ν CH	2988 - 28920
4	ν C=O	1725
5 - 6	δ CH	1452 -1380
7	ν C-O (esters)	1300-1150
8	ν C-O (alcoholic)	1150-950

Having known the polymeric composition of the PHBV_GF sample obtained from the NMR analyses previously conducted, we continued with the analysis of the FT-IR spectra obtained following the solubility test in CH$_3$CN by comparison with the spectrum obtained from the analysis of the reference sample PHB pure powder (Green spectrum, **Figure 39**Figure). Observing the trend of the spectra, it can be seen that the spectrum of the non-solubilized portion is more similar to the spectrum of the reference PHB polymer.
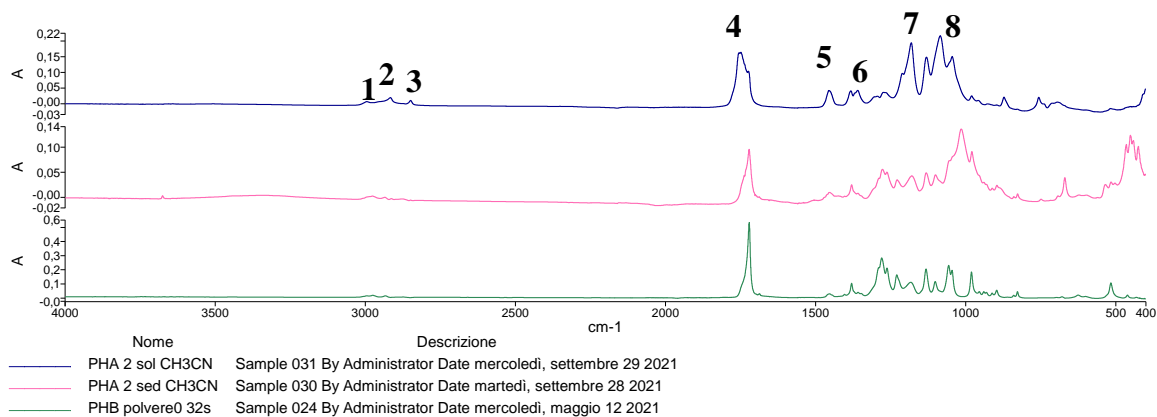
Figure 39 – FT-IR spectrum of ground PHBV_GF solubilized in Acetonitrile (CH$_3$CN) (blu spectrum), compared with FT-IR spectra of PHBV_GF insoluble in Acetonitrile (CH$_3$CN) (pink spectrum) and of PHB pure powder (green spectrum) (see **Table 31**)

Table 31 - Infra-Red characterisation values of PHBV_GF solubilized in Acetonitrile (CH$_3$CN)

REFERENCE NUMBER	GROUP	WAVE NUMBER ν (CM^{-1})
1 - 3	ν CH	2988 - 28920
4	ν C=O	1725
5 - 6	δ CH	1452 -1380
7	ν C-O (esters)	1300-1150
8	ν C-O (alcoholic)	1150-950

Knowing that the PHBV_GF sample consists of PHB and PHV, and having found only PHB in the spectrum of the insoluble portion in CH$_3$CN, we can assume that the solvent has solubilized the PHV present in the polymer. This could mean that the sample is not a PHB-PHV co-polymer, but a mixture to which the wood flour has been further added. This evaluation is made in consideration of the fact that a co-polymer condition would have led to a lower solubilization of the sample and a selective solubility for the PHV would not have been found. Since the analyses carried out have allowed us to observe how the regions most subject to solubilization are those corresponding to the amorphous portions of the polymer, it is assumed that these portions are degraded first and that, in the biodegradation processes, any enzymatic systems can use this portion as a site of the attack.

7 - Electrospray Mass Spectrometry (ESI – MS)

The first sample analysed by MS spectrometry was the pure PHB powder sample subjected to a solubilization test in acetonitrile without pre-solubilization in chloroform. From the observation of the spectrum obtained from this analysis (**Figure 40**), the typical

bell-shaped trend can be seen, with an m/z difference between one peak and the next equal to a monomeric unit of 86 and a maximum peak identified at 1141 m/z. The calculation of the molecular weights of the samples was carried out considering the value of the mass/charge ratio of the most intense peak of the spectrum (corresponding to the most representative ions of the sample) and the values of the m/z ratio of the immediately following peak (m+1). From these values we obtain, through **Equation (2)**, the number of protons (n):

$$n = \frac{(m+1) - H^+}{(m+1) - m} \qquad (2)$$

The number of protons is then entered into **Equation (3)** to derive the molecular weight of the sample:

$$(m+1) = \frac{MW + (n+1) * H^+}{(n+1)} \qquad (3)$$

Using **Equation (2)** and **Equation (3)**, the average molecular mass (Mw) of the sample was calculated, resulting in 1.594×10^4 Da.
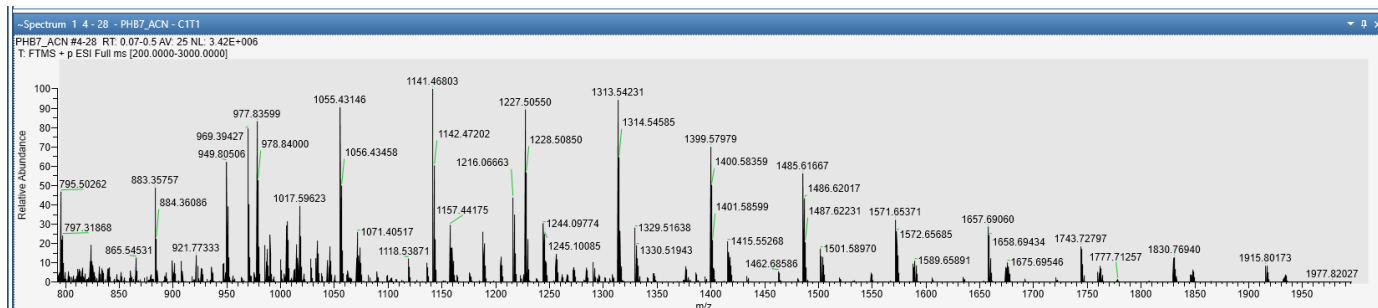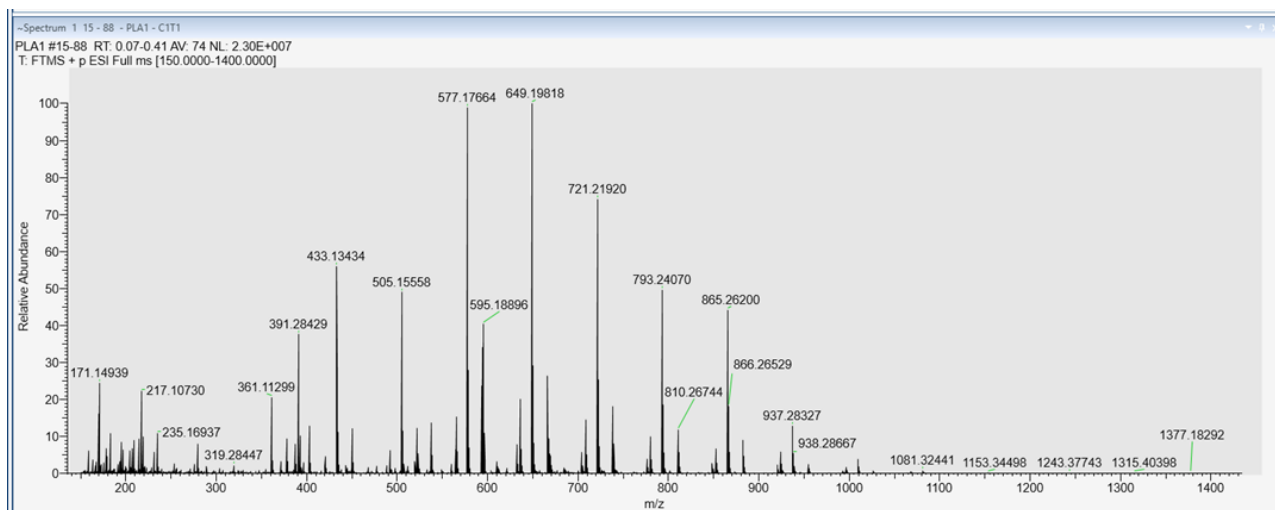

Figure 40 - Mass spectrum in FULL SCAN of the PHB pure powder sample diluted in acetonitrile (1/10): mass range 800-2000 m/z

The same considerations were made for the pure PHB sample in powder which had instead been subjected to pre-solubilization in chloroform and subsequently, after drying, solubilized again in acetonitrile. Also in this case (**Figure 41**) an m/z difference from the peaks equal to a monomeric unit of 86 was observed, which confirms that the sample has not undergone transformations. The maximum peak was identified at 1055 m/z. From the calculations carried out, the average molecular weight was equal to 1.627×10^4 Da.
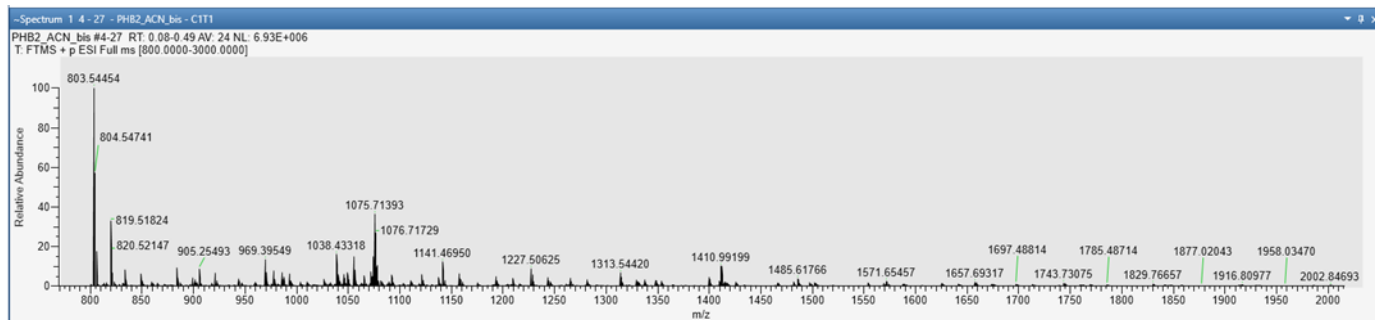
Figure 41 - Mass spectrum in FULL SCAN of the PHB pure powder sample diluted in acetonitrile (1/10): mass range 800-2000 m/z

Considering the difference of a monomeric unit of 86 detected in the spectra of both PHB samples, it was possible to identify the correspondence in the molecular weights of the repeating unit of the molecule (**Figure 42**). This incremental value, then, corresponds to the molar mass of the P-3HB repeating unit.
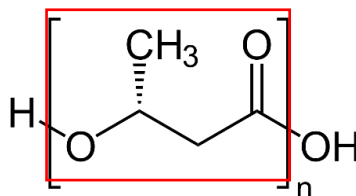
Figure 42 – Chemical structure of poly-3-hydroxybutyrate (P3HB); the repeating unit of the molecule is highlighted, corresponding to the molecular weight of 86 g/mol (or 86 u.m.a.)

The analysis continued by studying the spectra obtained on the PHBV_GF sample, subjected to solubilization tests directly in acetonitrile. It was necessary to add 0.1% formic acid to try to better ionize the polymer during the analysis. Unlike the PHB samples, in the PHBV_GF sample spectrum (**Figure 43**) the typical bell curve proceeds with an m/z difference between peaks of a monomeric unit of 72, with a maximum peak identified at 833 m/z (Sikorska et al., 2020). The calculation of the average molecular weight of this sample resulted in an equal to 1.046×10^4 Da.
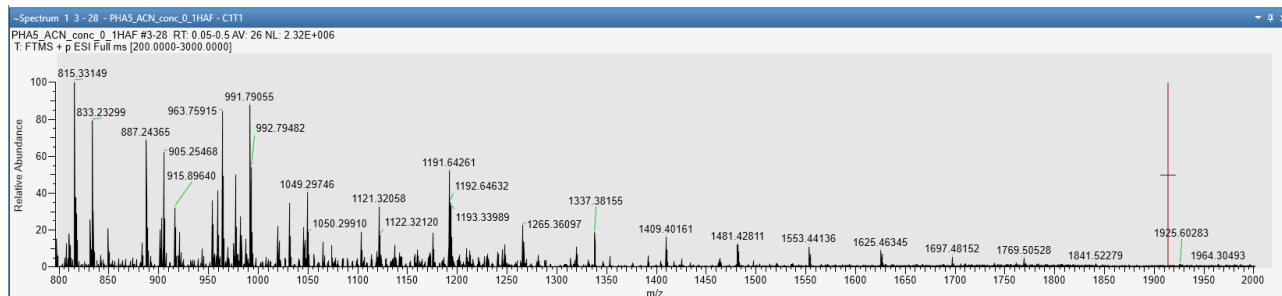
Figure 43 - Mass spectrum in FULL SCAN of the concentrated PHBV_GF sample (as it is) acidified with 0.1%HAF: mass range 800-2000 m/z

The analysis of the PHBV_GF sample, pre-solubilized in chloroform and subsequently solubilized in acetonitrile, always showed a trend with the difference between the peaks equal to a monomeric unit of 72, while the most intense peak of the bell curve was identified at 1121 m /z (**Figure 44**) (Sikorska et al., 2020). From the calculation carried out using **Equation (2)** and **Equation (3)**, the average molecular weight of the sample was obtained, resulting in equal to 2.086 x 10^4 Da.
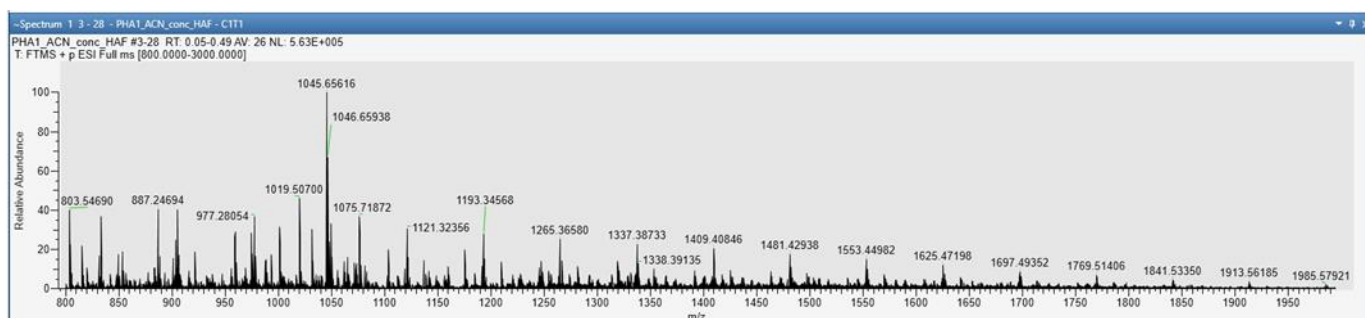
Figure 44 - Mass spectrum in FULL SCAN of the concentrated PHBV_GF sample (as it is): mass range 800-2000 m/z

Considering the difference of a monomeric unit of 72 detected in the spectra of both PHBV_GF samples, it was possible to identify the correspondence in the molecular weights of the repeating units of the hydroxyvalerate isomers (3HV and 5HV), from which the carboxyl group is excluded (**Figure 45**).
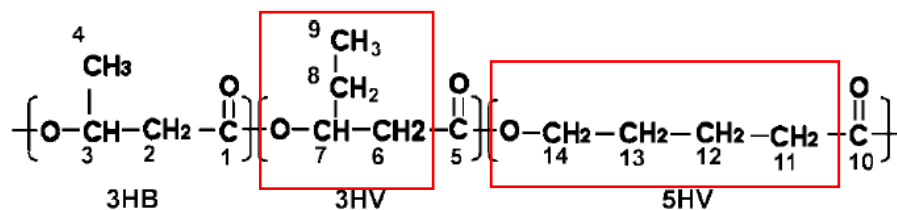
Figure 45 - Chemical structure of poly-3-hydroxybutyrate-co-3-hydroxyvalerate-co-5-hydroxyvalerate (P3HB3HV5HV); the repeating units of the two forms of hydroxyvalerate (3HV and 5HV) are highlighted, excluding the carboxyl group, each corresponding to the molecular weight of 72 g/mol (or 86 u.m.a.)

143

From this observation, it can be assumed that the PHV fraction in the PHBV_GF polymer is more easily soluble. For comparison with other biopolymers, mass spectrometry analyses were also conducted on PLA samples solubilized exclusively in acetonitrile. Two replicates were made for this test. The mass spectra of both replicates showed a peak-to-peak mass increment of a monomeric unit of 72 (Sikorska et al., 2020); one of the two replicas has a maximum peak of 649 m/z (**Figure 46**), while the other one has a maximum peak of 599 m/z (**Figure 47**).

Figure 46 - Mass spectrum in FULL SCAN of the first PLA sample: mass range 150-1400 m/z
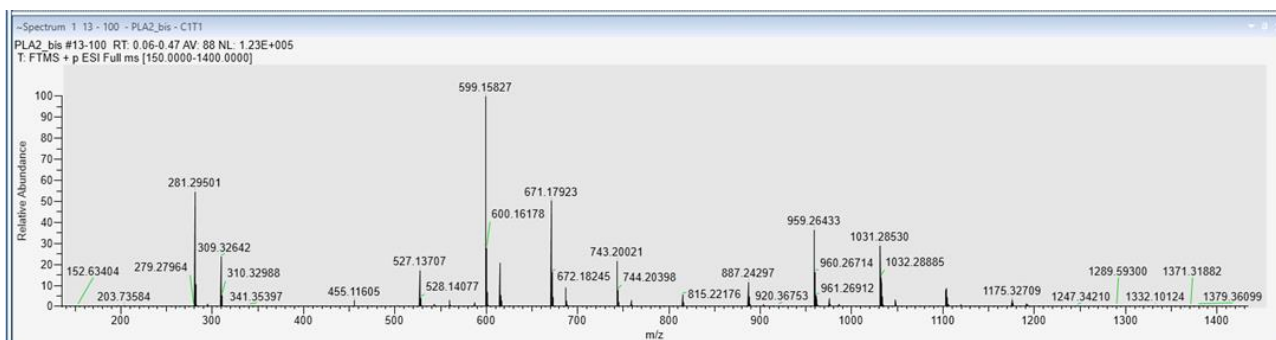
Figure 47 - Mass spectrum in FULL SCAN of the second PLA sample: mass range 150-1400 m/z

An important difference can be observed from the results of the calculation of the average molecular weights of the samples.

Through **Equation (2)** and **Equation (3)**, the average molecular weights of the two PDLA samples analysed were calculated. In fact, an average of 5.184×10^3 Da was obtained for one sample, while for the other the weight was calculated as equal to 1.339×10^4 Da. This difference could be due to the fact that the samples used for this analysis, i.e. polymers that already have a variable molecular weight distribution, may have been further reduced into

fragments of even more variable weight by their own production processes, such as pelletizing and mechanical extrusion. Recital a peak-to-peak mass increment of a monomer unit of 72 detected in the spectra of both PDLA samples, it was possible to identify the correspondence in the molecular weights of the repeating unit of the molecule (Figure).
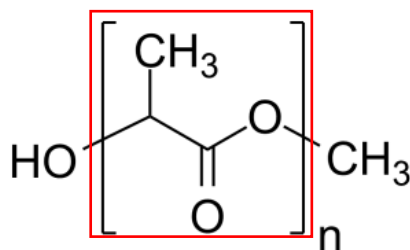
Figure 48 - Chemical structure of polylactic acid (PLA); the repeating unit of the molecule is highlighted, corresponding to the molecular weight of 72 g/mol (or 72 u.m.a.)

The obtained results in terms of the average molecular mass revealed that only low molecular mass fractions of each polymer were dissolved in the selected solvent (CH_3CN). Considering the insolubility of these polymers in water, our solubility results suggest the opportunity to use $CHCl_3$, immiscible in water, as an extraction solvent of micro or nanoparticles dispersed in the sample of water, allowing studying with the instruments above reported the chemical-physical characteristics of polymers (physical, chemical or biological degradation).

REFERENCE

Abd-El-Haleem D. A. M., Zaki, S. A., Abuelhamd, A. T., Amara, A., & Aboelreesh, G. M. S. (2007). Biosynthesis of polyhydroxyalkanotes in wildtype yeasts. Journal of Applied Sciences and Environmental Management, 11(3).

Abid, S., Raza, Z. A., & Hussain, T. (2016). Production kinetics of polyhydroxyalkanoates by using Pseudomonas aeruginosa gamma ray mutant strain EBN-8 cultured on soybean oil. 3 Biotech, 6, 1-10.

Aoyagi, Y., Yamashita, K., & Doi, Y. (2002). Thermal degradation of poly [(R)-3-hydroxybutyrate], poly [ε-caprolactone], and poly [(S)-lactide]. Polymer Degradation and Stability, 76(1), 53-59.

Badawi, H. M., Förner, W., & Ali, S. A. (2014). A study of the experimental and theoretical infrared, Raman, 1H and 13C NMR spectra of the biochemicals valeric and valproic acids. Journal of Molecular Structure, 1075, 494-503.

Barham, P. J., Keller, A., Otun, E. L., & Holmes, P. A. (1984). Crystallization and morphology of a bacterial thermoplastic: poly-3-hydroxybutyrate. Journal of Materials Science, 19, 2781-2794.

Bugnicourt, E., Cinelli, P., Lazzeri, A., & Alvarez, V. A. (2014). Polyhydroxyalkanoate (PHA): Review of synthesis, characteristics, processing and potential applications in packaging.

Cuiffo, M.A.; Snyder, J.; Elliott, A.M.; Romero, N.; Kannan, S.; Halada, G.P. Impact of the Fused Deposition (FDM) Printing Process on Polylactic Acid (PLA) Chemistry and Structure. Appl. Sci. 2017, 7, 579. https://doi.org/10.3390/app7060579

De Stefano, C., Foti, C., Gianguzza, A., Piazzese, D., Sammartano, S. (2002). Binding Ability of Inorganic Major Components of Sea Water towards some Classes of Ligands, Metal and Organometallic Cations. In: Gianguzza, A., Pelizzetti, E., Sammartano, S. (eds) Chemistry of Marine Water and Sediments. Environmental Science. Springer, Berlin, Heidelberg. https://doi.org/10.1007/978-3-662-04935-8_9

Galego, N., Rozsa, C., Sánchez, R., Fung, J., Vázquez, A., & Santo Tomás, J. (2000). Characterization and application of poly (β-hydroxyalkanoates) family as composite biomaterials. Polymer Testing, 19(5), 485-492.

Gumel, A. M., Annuar, M. S. M., & Heidelberg, T. (2012). Biosynthesis and characterization of polyhydroxyalkanoates copolymers produced by Pseudomonas putida Bet001 isolated from palm oil mill effluent.

Kolahchi, A. R., & Kontopoulou, M. (2015). Chain extended poly (3-hydroxybutyrate) with improved rheological properties and thermal stability, through reactive modification in the melt state. Polymer degradation and stability, 121, 222-229.

Mehrpouya, M., Vahabi, H., Barletta, M., Laheurte, P., & Langlois, V. (2021). Additive manufacturing of polyhydroxyalkanoates (PHAs) biopolymers: Materials, printing techniques, and applications. Materials Science and Engineering: C, 127, 112216.

Nishida, M., Tanaka, T., Hayakawa, Y., & Nishida, M. (2018). Solid-state nuclear magnetic resonance (NMR) and nuclear magnetic relaxation time analyses of molecular mobility and compatibility of plasticized polyhydroxyalkanoates (PHA) copolymers. Polymers, 10(5), 506.

Nygaard, D., Yashchuk, O., Noseda, D. G., Araoz, B., & Hermida, É. B. (2021). Improved fermentation strategies in a bioreactor for enhancing poly (3-hydroxybutyrate)(PHB) production by wild type Cupriavidus necator from fructose. Heliyon, 7(1).

Rebocho, A. T., Pereira, J. R., Torres, C. A., Freitas, F., & Reis, M. A. (2020). 9 Linking the Properties of. The Handbook of Polyhydroxyalkanoates: Postsynthetic Treatment, Processing and Application, 203.

Reis, K. C., Pereira, L., Melo, I. C. N. A., Marconcini, J. M., Trugilho, P. F., & Tonoli, G. H. D. (2015). Particles of coffee wastes as reinforcement in polyhydroxybutyrate (PHB) based composites. Materials Research, 18, 546-552.

Sabarinathan, D., Chandrika, S. P., Venkatraman, P., Easwaran, M., Sureka, C. S., & Preethi, K. (2018). Production of polyhydroxybutyrate (PHB) from Pseudomonas plecoglossicida and its application towards cancer detection. Informatics in Medicine Unlocked, 11, 61-67.

Salgaonkar, B. B., Mani, K., & Braganca, J. M. (2013). Characterization of polyhydroxyalkanoates accumulated by a moderately halophilic salt pan isolate Bacillus megaterium strain H16. Journal of applied microbiology, 114(5), 1347-1356.

Sathiyanarayanan, G., Bhatia, S. K., Song, H. S., Jeon, J. M., Kim, J., Lee, Y. K., ... & Yang, Y. H. (2017). Production and characterization of medium-chain-length polyhydroxyalkanoate copolymer from Arctic psychrotrophic bacterium Pseudomonas sp. PAMC 28620. International journal of biological macromolecules, 97, 710-720.

Sikorska, W.; Zięba, M.; Musioł, M.; Kowalczuk, M.; Janeczek, H.; Chaber, P.; Masiuchok, O., Demchenko, V.; Talanyuk, V.; Iurzhenko, M.; Puskas, J.E.; Adamus, G. Forensic Engineering of Advanced Polymeric Materials—Part VII: Degradation of Biopolymer Welded Joints. Polymers, 2020, 12, 1167. doi:10.3390/polym12051167

Sindhu, R., Ammu, B., Binod, P., Deepthi, S. K., Ramachandran, K. B., Soccol, C. R., & Pandey, A. (2011). Production and characterization of poly-3-hydroxybutyrate from crude glycerol by Bacillus sphaericus NII 0838 and improving its thermal properties by blending with other polymers. Brazilian archives of Biology and Technology, 54, 783-794.

Singla, P., Mehta, R., Berek, D., & Upadhyay, S. N. (2012). Microwave assisted synthesis of poly (lactic acid) and its characterization using size exclusion chromatography. Journal of Macromolecular Science, Part A, 49(11), 963-970. https://doi.org/10.1080/10601325.2012.722858

Tan, G. Y. A., Chen, C. L., Li, L., Ge, L., Wang, L., Razaad, I. M. N., ... & Wang, J. Y. (2014). Start a research on biopolymer polyhydroxyalkanoate (PHA): a review. Polymers, 6(3), 706-754.

Wei, L., & McDonald, A. G. (2015). Peroxide induced cross-linking by reactive melt processing of two biopolyesters: Poly (3-hydroxybutyrate) and poly (l-lactic acid) to improve their melting processability. Journal of Applied Polymer Science, 132(13).

LIST OF PUBBLICATIONS AND COMMUNICATIONS

Conference proceeding

Dara M., **Torregrossa N.**, La Corte C., Parisi M.G., Piazzese D., Cammarata M. (2023). *Bio-plastic recognition by mussels hemocytes*.

Invertebrate Survival Journal, 20(1), 34-34.

Dara M. 1#, **Torregrossa N.** 1#, Bisanti L., La Corte C., Bertini F., Parrinello D., Piazzese D., Cammarata M., Mohamed B., Parisi M.G (2023). *In vivo and in vitro effects of bioplastic materials on immune functions of mussels (Mytilus galloprovincialis)*.

Poster communication

Censi V., Saiano F., Bocini P., Giraldi D., **Torregrossa N.**, Cammarata M., Dara M., Parisi M.G., Indelicato S., Bongiorno D., Piazzese D. (2022). *Systematic study of bio-based plastic materials properties. Physical Chemical Aspects and Immunobiological Interaction.*

Poster exhibited at XXIX Congresso della Divisione di Chimica Analitica.

Dara M., **Torregrossa N.**, Bisanti L., La Corte C., Bertini F., Parrinello D., Parisi M.G., Piazzese D., Cammarata M. (2023). *Mediterranean mussel (Mytilus galloprovincialis) as sentinel for to assess the effect of bio-plastic materials.*

Poster exhibited at LXXXII Congresso Nazionale dell'Unione Zoologica Italiana.

In submission

Dara M. 1#, **Torregrossa N.** 1#, Bisanti L., La Corte C., Bertini F., Parrinello D., Piazzese D., Cammarata M., Mohamed B., Parisi M.G (2023). *In vivo and in vitro effects of bioplastic materials on immune functions of mussels (Mytilus galloprovincialis)*.

Paper submitted to the journal "Chemosphere"

singolarmente - ma anche voi come gruppo - siete stati dei tasselli fondamentali per la mia serenità, anche quando le emozioni rischiavano di sopraffarmi.

Ringrazio il prof. Filippo Saiano, che oltre ad insegnarmi a leggere spettri IR ed NMR e a ragionare sui dati ottenuti, mi ha anche indotta a pormi delle domande per raddrizzare la strada quando perdevo la rotta, e Marcella La Barbera e Valentina Censi, per avermi aiutata nell'ambito delle analisi chimiche, dei dati ottenuti e nella revisione di tesi e relazioni, ma anche per aver condiviso con me la stanza in via Archirafi 26, la cioccolata fondente, i caffè e momenti di chiacchiere che alleggerivano la pressione di impegni e scadenze.

Ringrazio il gruppo del Laboratorio di Scienza e Tecnologia dei Materiali del Dipartimento di Ingegneria Chimica del prof. La Carrubba, ed in particolare ringrazio il dott. Francesco Lopresti, il dott. Francesco Carfì-Pavia e Camilla Carbone per tutto l'aiuto ed i suggerimenti che mi hanno dato per migliorare la realizzazione dei miei scaffold durante i mesi che ho trascorso nei loro laboratori.

Ringrazio gli amici: il gruppo "Super_Colleganza" (che fin dai tempi della laurea magistrale mi sono sempre rimasti accanto e mi hanno regalato momenti di spensieratezza unici e preziosi, tra pause pranzo condivise, incontri fugaci tra i corridoi e cene - matrimoni compresi - divertenti e serene passate insieme), il gruppo "Super Zii per scelta" (per le serate, le arrustute, per i mille messaggi, i balletti, le costellazioni e le rimpatriate che danno sempre brio alla pesantezza di tutti i giorni), ed il gruppo "Capodanno" (perché questa grande e bella famiglia di amici mi ha sempre dato forza, sostegno e affetto, anche e soprattutto in questi tre anni durante i quali abbiamo vissuto momenti davvero difficili).

Ringrazio i miei amati genitori, i miei preziosi nonni - chi c'è e chi ci sarà per sempre -, le mie sorelle e i miei cognati, i miei super nipoti e la mia famiglia acquisita, perché non hanno smesso nemmeno per un istante di fare il tifo per me e di credere nelle mie capacità più di quanto potessi arrivare a fare io.

Ringrazio la mia piccola Miru per la sua preziosa compagnia, acciambellata sulle mie gambe mentre lavoravo alla scrivania, in prima fila durante riunioni o lezioni in telematica passando ripetutamente passata davanti la webcam, per non avermi mai abbandonata di giorno o di notte, standomi vicina sempre con le sue dolci fusa.

Ringrazio Giancarlo, mio amato compagno di vita, con il quale proprio in questi ultimi tre anni ho vissuto momenti belli, altri strabelli, ma anche di difficili e alcuni terrificanti. Sempre accanto e sempre uniti e sempre guardando a ciò che insieme stiamo costruendo, passo dopo passo.

Ringrazio Andrea, il mio marmocchietto meraviglioso, che nei suoi primi tre anni di vita ha sopportato la mamma troppo spesso impegnata a sbrigare cose per il dottorato, che

aspettava a casa il mio ritorno e che ha sempre accolto il mio rientro con sorrisi e abbracci, che per emulazione si è messo a "lavorare" al suo computer, che ha curiosamente chiesto di batteri e di cozze e di università e di scienza e che mi ricorda ogni giorno che il mio meraviglioso piccolo grande sogno è sempre stato lui.

Mamma. Biologa. Prof. E ora anche PhD.

Grazie alla mia vita, perché mi sento ricca.